

# Analysis of the TREAT LEU Conceptual Design

---

Nuclear Engineering Division

### **About Argonne National Laboratory**

Argonne is a U.S. Department of Energy laboratory managed by UChicago Argonne, LLC under contract DE-AC02-06CH11357. The Laboratory's main facility is outside Chicago, at 9700 South Cass Avenue, Argonne, Illinois 60439. For information about Argonne and its pioneering science and technology programs, see [www.anl.gov](http://www.anl.gov).

### **DOCUMENT AVAILABILITY**

**Online Access:** U.S. Department of Energy (DOE) reports produced after 1991 and a growing number of pre-1991 documents are available free via DOE's SciTech Connect (<http://www.osti.gov/scitech/>)

### **Reports not in digital format may be purchased by the public from the National Technical Information Service (NTIS):**

U.S. Department of Commerce  
National Technical Information  
Service 5301 Shawnee Rd  
Alexandria, VA 22312  
**[www.ntis.gov](http://www.ntis.gov)**  
Phone: (800) 553-NTIS (6847) or (703) 605-6000  
Fax: (703) 605-6900  
Email: [orders@ntis.gov](mailto:orders@ntis.gov)

### **Reports not in digital format are available to DOE and DOE contractors from the Office of Scientific and Technical Information (OSTI):**

U.S. Department of Energy  
Office of Scientific and Technical Information  
P.O. Box 62  
Oak Ridge, TN 37831-0062  
**[www.osti.gov](http://www.osti.gov)**  
Phone: (865) 576-8401  
Fax: (865) 576-5728  
Email: [reports@osti.gov](mailto:reports@osti.gov)

### **Disclaimer**

This report was prepared as an account of work sponsored by an agency of the United States Government. Neither the United States Government nor any agency thereof, nor UChicago Argonne, LLC, nor any of their employees or officers, makes any warranty, express or implied, or assumes any legal liability or responsibility for the accuracy, completeness, or usefulness of any information, apparatus, product, or process disclosed, or represents that its use would not infringe privately owned rights. Reference herein to any specific commercial product, process, or service by trade name, trademark, manufacturer, or otherwise, does not necessarily constitute or imply its endorsement, recommendation, or favoring by the United States Government or any agency thereof. The views and opinions of document authors expressed herein do not necessarily state or reflect those of the United States Government or any agency thereof, Argonne National Laboratory, or UChicago Argonne, LLC.

## Analysis of the TREAT LEU Conceptual Design

---

prepared by

H. M. Connaway, D. C. Kontogeorgakos, D. D. Papadimas, A. J. Brunett, K. Mo, P. S. Strons, T. Fei, and A. E. Wright

Nuclear Engineering Division, Argonne National Laboratory

sponsored by

U. S. Department of Energy, National Nuclear Security Administration  
Office of Material Management and Minimization

March 2016

## Executive Summary

Analyses were performed to evaluate the performance of the low enriched uranium (LEU) conceptual design fuel for the conversion of the Transient Reactor Test Facility (TREAT) from its current highly enriched uranium (HEU) fuel. TREAT is an experimental nuclear reactor designed to produce high neutron flux transients for the testing of reactor fuels and other materials. TREAT is currently in non-operational standby, but is being restarted under the U.S. Department of Energy's Resumption of Transient Testing Program. The conversion of TREAT is being pursued in keeping with the mission of the Department of Energy National Nuclear Security Administration's Material Management and Minimization (M<sup>3</sup>) Reactor Conversion Program.

The focus of this study was to demonstrate that the converted LEU core is capable of maintaining the performance of the existing HEU core, while continuing to operate safely. Neutronic and thermal hydraulic simulations have been performed to evaluate the performance of the LEU conceptual-design core under both steady-state and transient conditions, for both normal operation and reactivity insertion accident scenarios. In addition, ancillary safety analyses which were performed for previous LEU design concepts have been reviewed and updated as-needed, in order to evaluate if the converted LEU core will function safely with all existing facility systems. Simulations were also performed to evaluate the detailed behavior of the UO<sub>2</sub>-graphite fuel, to support future fuel manufacturing decisions regarding particle size specifications. The results of these analyses will be used in conjunction with work being performed at Idaho National Laboratory and Los Alamos National Laboratory, in order to develop the Conceptual Design Report project deliverable.

# Table of Contents

	<u>Page</u>
Executive Summary .....	i
Table of Contents .....	ii
List of Figures .....	iv
List of Tables .....	vii
1 Introduction .....	1
1.1 Summary of TREAT Design and Operation .....	1
1.2 Core Conversion Requirements .....	3
1.3 Current Methodology .....	5
1.4 LEU Conceptual Design Description .....	6
2 Neutronic Analyses .....	8
2.1 Steady-state Analysis with MCNP .....	8
2.1.1 Fuel Carbon-to-Uranium Search .....	8
2.1.2 Excess Reactivity and Control Rod Worth .....	9
2.1.3 Power Coupling Factor Calculations .....	10
2.1.4 Neutron Energy Spectrum .....	18
2.2 TREKIN Transient Analyses – Normal and Accident Conditions .....	20
2.2.1 TREKIN Input Tables .....	20
2.2.2 Transient Calculations - Matching the HEU Performance .....	27
2.2.3 Full Width at Half Maximum (FWHM) .....	30
3 Thermal Hydraulic Analyses .....	31
3.1 Model Description .....	32
3.2 Analyses Assumptions and Parameters .....	33
3.2.1 Cooling .....	33
3.2.2 Thermal Properties .....	33
3.2.3 Peak Fuel Temperatures .....	34
3.2.4 Corrosion Kinetics .....	35
3.3 Results .....	37
3.3.1 Normal Operation .....	37
3.3.2 Accident Scenario .....	41
3.4 Summary .....	43
4 Additional Safety-related Analyses .....	44
4.1 Previously-performed Bounding Analyses .....	44
4.2 Updated Analysis: Thermal Hydraulic Analysis of Core Support .....	45
4.2.1 Core Support Model and Assumptions .....	45
4.2.2 Maximum Grid plate Temperatures .....	47
4.3 Grid Plate Thermal Distortion Analysis .....	48
4.3.1 Assumptions .....	48
4.3.2 Non-uniform Thermal Loading .....	49
4.3.3 Maximum Uniform Temperature .....	53
4.4 Updated Analysis: Effect of Effluent Air Temperature on Filtration/Cooling System .....	55

4.5	Ongoing and Future Analyses .....	56
4.5.1	<i>Heat Transfer from the Experiment to the TREAT Fuel</i> .....	56
4.5.2	<i>Source Term Evaluation</i> .....	56
4.5.3	<i>Additional Future Ancillary Analyses</i> .....	58
5	UO <sub>2</sub> -graphite Behavior and Fuel Particle Size .....	59
5.1	Determination of the Upper Limit of UO <sub>2</sub> Particle Size in LEU TREAT Fuel .....	59
5.2	Determination of the Lower Limit of UO <sub>2</sub> Particle Size in LEU TREAT Fuel .....	60
6	Conclusions .....	61
	References .....	63
Appendix A.	Comparison of Temperature-dependent Cross Section Generation with MAKXSf and NJOY201265 .....	
Appendix B.	Steady-state Thermal Hydraulic Analysis .....	72

## List of Figures

	<u>Page</u>
Figure 1-1. TREAT Core Layout with Example Half-slotted Core Loading; plotted at ~23 cm above Core Centerline to Illustrate a Portion of the Instrumentation Holes .....	2
Figure 1-2. Locations of the Control Rod Banks in the Current (Upgraded) TREAT Core .....	2
Figure 1-3. Side View of TREAT Fuel Assembly Axial Surfaces, Grid Plate – to – Top Fitting; From INL Analysis Guide [17]. .....	7
Figure 2-1. Core loadings A, B, and C Used to Further Evaluate LEU and HEU ARO Reactivity. ....	10
Figure 2-2. Radial Dimensions of the M8CAL Test Pins [8]. .....	11
Figure 2-3. M8CAL Half-slotted Core Loading.....	12
Figure 2-4. M8CAL Experiment Configuration. ....	12
Figure 2-5. MCNP Model of LO3-like Experiment Configuration.....	13
Figure 2-6. LO3 Experiment Region within the MCNP Core Model. ....	14
Figure 2-7. Modeled STEP Experiment Configuration. ....	15
Figure 2-8. Core Loadings Used to Evaluate STEP Experiment. ....	16
Figure 2-9. Neutron Spectrum at the M8CAL Test Sample Location, Inside M8CAL Vehicle. ....	18
Figure 2-10. Neutron Spectrum at the M8CAL Test Sample Location, Without the M8CAL Vehicle. ....	19
Figure 2-11. Ratio of the Fuel Element Power Density to the Core Average Power Density for LEU M8CAL Half-slotted Core.....	22
Figure 2-12. Ratio of the Fuel Element Power Density to the Core Average Power Density for HEU M8CAL Half-slotted Core.....	23
Figure 2-13. Ratio of the Axial Segment Power Density to the Fuel Element Average Power Density for the Hottest Fuel Element for the HEU and LEU Cores.....	23
Figure 2-14. HEU and the Scaled LEU Power-Time History Curves for the Different Relative-to-HEU PCF Values.....	28
Figure 2-15. Power Pulse Created after Accidental Step Insertion of the Pre-Transient Available Reactivity for the HEU and the LEU Core and for the Different Relative-to-HEU PCF.....	29
Figure 2-16. Power Pulse after Step Reactivity Insertion for the HEU and the LEU for the Different Relative-to-HEU PCF Matching the Test Fuel Energy Deposition. ....	31
Figure 3-1. COMSOL® geometry and dimensions of a single TREAT LEU fuel assembly. A) Cross-sectional view, B) Axial view showing reflector and fuel block region. ....	32
Figure 3-2. Contact Resistance Measured at LANL [21] using two B&W Compacts with no Pressure; measurements Performed for as-formed Surfaces as well as Machined Surfaces. ....	34
Figure 3-3. LEU Axial Power Profile and Peak Fuel Temperatures as a Function of Total Core Energy; peak Fuel Temperatures Established from the Energy Deposited to the Hottest Assembly. ....	35
Figure 3-4. Post-transition Corrosion Rates in Air as Function of Temperature, HEU FSAR Zircaloy 2 Rates Compared with Corrosion Rates for Zircaloy-4 (open symbols); Line Corresponds to the Rates as Calculated Using Expression (3.1).....	36
Figure 3-5. Cooling Time Histories for Normal Operation with 6000 cfm of Cooling, a) Peak Fuel Temperatures as function of Cooling Time, Initial Peak Fuel Temperatures of 600 (red), 500 (green) and 400°C (blue), and b) Temperature of the Cladding at Three Different Locations as function of Cooling Time (for 600°C Peak Fuel case).....	37

Figure 3-6. Effect of Contact Resistance and Air Flow through the Reactor on Cooling Time Histories; Case Above Shown for a Peak Fuel Temperature of 600 °C. ....	38
Figure 3-7. Axial Variation of Cladding (T-S) Metal Loss as Function of Peak Fuel Temperature and Contact Resistance; Cooling to Ambient Conditions was Achieved with One Blower in Operation (3000 cfm). ....	39
Figure 3-8. Axial Temperature Profiles of the Side Section of the Cladding (T-S) as function of Time, Initial Peak Fuel Temperature = 600 °C, 3000 cfm of Air Cooling through the Reactor. ....	39
Figure 3-9. Cross-sectional Metal Loss of the Cladding Near the Fuel Mid-plane. Total Metal Loss shown as a function of Initial Peak Fuel Temperature and Cladding Distance, Results Shown when using 3000 cfm of Air Cooling through the Reactor. ....	40
Figure 3-10. Cooling Time Histories for the Accident Case Scenario Assuming No Air Flow, Peak Fuel Temperatures Investigated in the Range of 700-820 °C; Left Panel shows Peak Fuel Temperatures as function of Time Assuming No Contact Resistance, Right Panel shows the Effect of Contact Resistance on Cooling Times to Below 600°C. ....	41
Figure 3-11. Contact Resistance Translated to an Equivalent Effective Axial Conductivity of the Fuel ....	42
Figure 3-12. Metal Loss of the Cladding Near the Fuel Mid-plane after an Accident (No Air Flow assumed through the Reactor); Total Metal Loss is shown as Function of Initial Peak Fuel Temperature and Contact Resistance. ....	43
Figure 4-1. Current Grid Plate Configuration for TREAT (without Fuel Alignment Pins) ....	46
Figure 4-2. M8CAL Half-slotted Core Loading and Corresponding LEU Core Accident Scenario Fuel Temperature Distribution; Peak Temperatures are Highest in South-East (Q3) Region. ....	47
Figure 4-3. Maximum Grid Plate Temperatures After ~2 hours of Cooling after an Accident; Grid Plate Temperature is Nearly the Same for both HEU and LEU Cores. ....	47
Figure 4-4. Drawing of Grid Plate and Seal Assemblies ....	49
Figure 4-5. Cross-Sectional View of Control Rod Assembly Showing Graphite Bearings (Red). ....	50
Figure 4-6. Non-thermal Grid Plate Loads in the Quarter Symmetry Model. ....	51
Figure 4-7. Contour Plot of Non-uniform Thermal Loading of the Grid Plate in the LEU Core Design Basis Accident ....	51
Figure 4-8.. Contour Plots Showing Total (a) and Radial (b) Deformation of the Grid Plate Due to Non-Uniform Thermal Loading ....	52
Figure 4-9. Deflection of Control Rod Positions. ....	52
Figure 4-10. Control Rod Deflection (in inches) Resulting from 0.30° Angular Displacement at Middle Bearing ....	53
Figure 4-11. Radial Deformation (a) and Total Deflection (b) Resulting From Uniform Thermal Load of 320°C. ....	54
Figure 4-12. Control Rod Deflection Resulting from 0.443° Angular Displacement at Middle Bearing ....	54
Figure 4-13. Reactor Effluent Air Temperature to the Exhaust Filtration System. ....	56
Figure 5-1. Determination of the Upper Limit of the Fuel Particle Size in LEU TREAT Fuel: (a) The Peak Temperatures of Differently-sized Particles, at the Particle Center, during a 4.63% Reactivity Step Transient (HEU Core), and (b) Calculated Time-lag in HEU and LEU Fuels for Various Sized UO <sub>2</sub> particles based on Hetrick's Model [3]. ....	60

Figure 5-2. The Thermal Conductivity Degradation of LEU TREAT Fuels with Different-sized UO <sub>2</sub> Particles after 1, 3, 10, and 40 Years; Thermal Conductivity Degradation of the HEU Fuel was calculated to provide a Comparison with the LEU Fuel .....	61
Figure A-1. Carbon S( $\alpha,\beta$ ) Total Cross Section at 400K and 500K from ENDF/B-VII (grph.11t and grph.12t) and at 450K produced by MAKXSf (grph.95t). .....	65
Figure A-2. Carbon S( $\alpha,\beta$ ) Elastic Cross Section at 400K and 500K from ENDF/B-VII (grph.11t and grph.12t) and at 450K produced by MAKXSf (grph.95t). .....	66
Figure A-3. Carbon S( $\alpha,\beta$ ) Inelastic Cross Section at 400K and 500K from ENDF/B-VII (grph.11t and grph.12t) and at 450K produced by MAKXSf (grph.95t). .....	66
Figure A-4. Carbon S( $\alpha,\beta$ ) Total Cross Section at 400K and 500K from ENDF/B-VII (grph.11t and grph.12t) and at 450K produced by NJOY2012 (p70grp.05t). .....	67
Figure A-5. Carbon S( $\alpha,\beta$ ) Elastic Cross Section at 400K and 500K from ENDF/B-VII (grph.11t and grph.12t) and at 450K produced by NJOY2012 (p70grp.05t). .....	68
Figure A-6. Carbon S( $\alpha,\beta$ ) Inelastic Cross Section at 400K and 500K from ENDF/B-VII (grph.11t and grph.12t) and at 450K produced by NJOY2012 (p70grp.05t). .....	68
Figure B-1. Constant power operation (120 kW) as function of time followed by cooling to near ambient temperature. Cases shown with 3000 cfm air cooling through the reactor. Left plot: no contact resistance. Right plot: contact resistance (CR) between graphite blocks of 5e-3 m <sup>2</sup> K W <sup>-1</sup> .....	73
Figure B-2. Axial Variation of Cladding (T-S) Metal loss as Function of Peak Fuel Temperature and Contact Resistance (as Indicated above Axis, Numerical Values of Metal Loss are Multiplied by 1E-6; Cooling to Ambient Conditions Achieved with One Blower in Operation (3000 cfm). .....	73
Figure B-3. Cross-sectional Metal Loss of the cladding near the fuel mid-plane. Total metal loss is shown as a function of time during constant power operation. Results shown when using 3000 cfm of air cooling through the reactor. ....	74
Figure B-4. Maximum metal loss of the cladding during constant power operation. Effect of air flow through the reactor and contact resistance. ....	74

## List of Tables

	<u>Page</u>
Table 1-1. General Experiment Parameter Categories for LEU Core Analysis and Assessment.....	4
Table 2-1. LEU M8CAL Half-Slotted Core ARO Reactivity Values with C/U=2470, for Different Zircaloy-4 Specifications .....	8
Table 2-2. LEU M8CAL Half-slotted Core ARO Reactivity Values with Different C/U Ratios .....	9
Table 2-3. Reference LEU Fuel Composition Used in MCNP Analysis for C/U = 2370 .....	9
Table 2-4. Control Rod Bank Worths in LEU M8CAL Half-slotted Core .....	9
Table 2-5. Calculated M8CAL ARO Reactivity and Experiment Vehicle Worth.....	10
Table 2-6. ARO Reactivity, Core Loadings A, B, and C.....	10
Table 2-7. M8CAL Test Pin and Monitor Wire Compositions Used in MCNP Simulations.....	11
Table 2-8. PCF Results, M8CAL Test Pin and Monitor Wire.....	12
Table 2-9. LO3 Fuel Pin Composition .....	14
Table 2-10. PCF Results, LO3 Experiment Pins.....	14
Table 2-11. STEP Experiment Pin Composition.....	15
Table 2-12. Comparison of HEU and LEU PCF Values for STEP Pins .....	16
Table 2-13. Increase in PCF Values of STEP Pins Due to Reflectors near the Test Region, Increase = (With – Without)/Without.....	16
Table 2-14. PCF Results for Cylindrical Sample in M8CAL Experiment Vehicle, .....	17
Table 2-15. PCF Results for Low-enriched UO <sub>2</sub> Sample, M8CAL Vehicle, Stainless-steel Components Replaced with Zircaloy .....	17
Table 2-16. PCF Results for Pin T-462 Sample, M8CAL Vehicle, Perturbations in Stainless-steel Density .	17
Table 2-17. PCF Results for Pin T-462 Sample, M8CAL Vehicle, Perturbations in Sample Diameter .....	17
Table 2-18. Thermal (E < 0.625 eV) – to – Total Neutron Flux Ratio .....	19
Table 2-19. Fast (E > 0.625 eV) – to – Thermal (E < 0.625 eV) Neutron Flux Ratio.....	19
Table 2-20. MCNP Calculated Transient Rod Bank Worth for the HEU and LEU Cores. ....	20
Table 2-21. Delayed Neutron Fraction and the Delayed Neutron Precursor Decay Constant for the Six Delayed Neutron Groups for the HEU Core Calculated with MCNP. ....	21
Table 2-22. Delayed Neutron Fraction and the Delayed Neutron Precursor Decay Constant for the Six Delayed Neutron Groups for the LEU Core Calculated with MCNP.....	21
Table 2-23. Effective Delayed Neutron Fraction and Prompt Neutron Generation Lifetime .....	21
Table 2-24. Temperature Reactivity Feedback as a Function of Total Core Energy used in TREKIN for the HEU and LEU Cores. ....	24
Table 2-25. Temperature Reactivity Feedback as a Function of Core Average Temperature for the HEU and LEU Cores. ....	25
Table 2-26. Hot to Cold PCF for the HEU Core as a Function of Total Core Energy and Peak Core Temperature. ....	26
Table 2-27. Hot to Cold PCF for the LEU Core as a Function of Total Core Energy and Peak Core Temperature. ....	26
Table 2-28. LEU-to-HEU PCF Ratio for Equal Energy Deposition in the Test Sample for a 10% Decrease in the Cold-Core Performance of the LEU Core .....	27

Table 2-29. Operational and Accident Peak Temperatures for the Total Core Energies Calculated with TREKIN in Power-Driven and Temperature-Limited Transient Simulations respectively,, for Multiple LEU-to-HEU PCF Scenarios. ....	29
Table 2-30. Full Width at Half Maximum (FWHM) for Step Reactivity Insertion to Match the Test Fuel Energy Deposition for Different Relative-to-HEU Power Coupling Factors (PCF).....	30
Table 4-1: Material Properties for A36 Steel .....	49
Table 4-2. Operating Power History Used to Evaluate TREAT Core Source Term .....	57
Table 4-3. Photon Emission Rate (photons/second) For TREAT Core with HEU and LEU Fuel.....	58
Table A-1. Effective Multiplication Factor ( $k_{eff}$ ) Calculation using Temperature-Dependent Cross Sections Produced with MAKXSf and NJOY2012; $k_{eff}$ was calculated with MCNP with a Standard Deviation of 5pcm. ....	69
Table A-2. Temperature Reactivity Feedback ( $\Delta k/k$ ) with Temperature Dependent Cross Sections.....	70
Table A-3. TREKIN-calculated Peak Core Power, Total Core Energy and Peak Core Temperature using the Temperature Reactivity Feedback with MAKXSf- and NJOY2012-Produced Cross-Sections.....	71

# 1 Introduction

The Transient Reactor Test Facility (TREAT) is an experimental reactor designed for transient testing of reactor fuels and other materials. TREAT is located at the Idaho National Laboratory (INL) and was operated from 1959 until 1994, when it was placed on non-operational standby. TREAT is now being restarted under the U.S. Department of Energy's (DOE) Resumption of Transient Testing Program. In addition, work is ongoing for the conversion of TREAT from its current highly enriched uranium (HEU) fuel to low enriched uranium (LEU), in keeping with the mission of the DOE National Nuclear Security Administration (NNSA) Material Management and Minimization (M<sup>3</sup>) Reactor Conversion Program.

Initial evaluation of an LEU core for TREAT was presented in June 2013 [1], with additional fuel design options evaluated in subsequent reports [2, 3]. Following these studies, a baseline conceptual design was established and evaluated in collaboration with the design team at INL and Los Alamos National Laboratory (LANL). Neutronic and thermal hydraulic simulations have been performed in order to assess the LEU conceptual design performance under both steady-state and transient conditions, for both normal operation and reactivity insertion accident scenarios. In addition, the ancillary safety analyses which were performed for previous LEU designs [4] have been reviewed, and the calculations have been updated as needed. To support the fuel manufacturing studies being performed by INL and LANL, analysis of heat transfer from the fuel UO<sub>2</sub> to the fuel's graphite matrix and of changes in fuel conductivity with burnup have also been performed. This report documents the full set of analysis results produced by Argonne National Laboratory for the LEU conceptual design. The content of this report is intended to serve as input to the conversion project's Conceptual Design Report deliverable.

## 1.1 Summary of TREAT Design and Operation

TREAT is a homogenous, air-cooled, graphite-moderated and graphite-reflected reactor currently fueled with 93% enriched UO<sub>2</sub> dispersed in graphite, with a fuel carbon-to-<sup>235</sup>U (C/<sup>235</sup>U) ratio of approximately 10000:1. The fuel elements are approximately four-inch x four-inch square, with an active ~four-foot long Zircaloy-clad fuel region and ~two-foot long aluminum-clad graphite reflectors above and below the fuel region. The reactor cavity can accommodate a maximum of 361 assemblies in a 19x19 array. The fuel assemblies feature chamfered corners, which form square passageways for forced flow of cooling air (provided by two blowers) which travels downward axially from the top of the core. During irradiation experiments, a small number of fuel assemblies (typically two to four) near the center of the core are replaced with an experiment vehicle containing the test sample(s). Graphite dummies are utilized in corner locations as needed to provide the core loading size required for appropriate excess reactivity. In addition, a central row (or half row) of fuel assemblies is frequently removed in order to provide an unimpeded path for neutron travel between the test sample and an ex-core collimator and detector system called the hodoscope. The TREAT core is surrounded by a radial graphite reflector, which is in turn enclosed in a concrete bioshield. Both the reflector and bioshield feature a variety of holes to allow for instrumentation use. An illustration of an example half-slotted core loading, including the reflector and bioshield, is provided in Figure 1-1. Detailed descriptions of the current HEU fuel assembly design and TREAT facility can be found in previous reports [1, 5] and in the facility's design summary report [6].

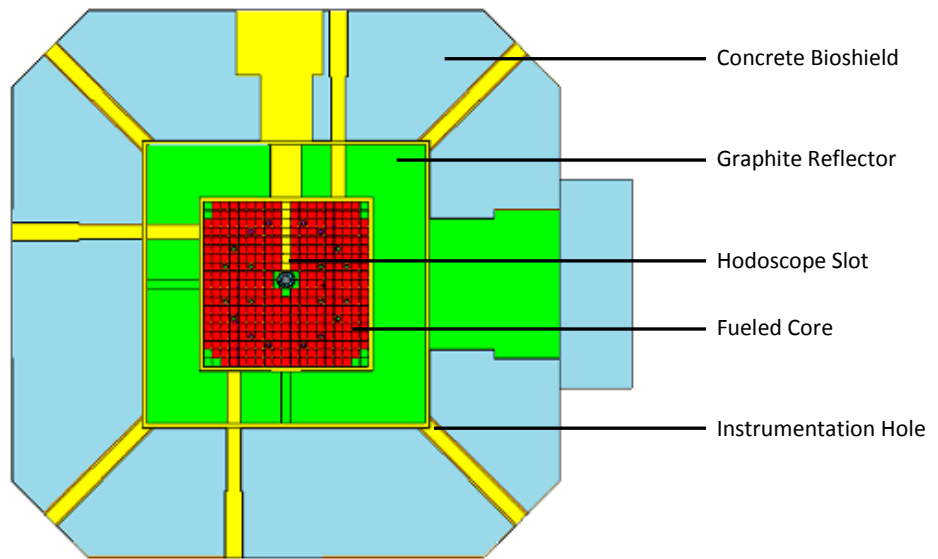


Figure 1-1. TREAT Core Layout with Example Half-slotted Core Loading; plotted at ~23 cm above Core Centerline to Illustrate a Portion of the Instrumentation Holes

TREAT is controlled by a set of twenty  $B_4C$ -bearing control rods, arranged in three banks: (1) four pairs of control/shutdown rods, used to set the reactor to a critical state, (2) four pairs of transient rods, used to introduce the reactivity changes which drive TREAT transients, and (3) four compensation rods used for reactivity compensation when an experiment vehicle is removed. The current layout of these rods within the TREAT core is shown in Figure 1-2. The control rods were re-located in the late 1980's; the current layout is referred to as the "upgraded core", while the previous configuration is identified as the "pre-upgrade core".

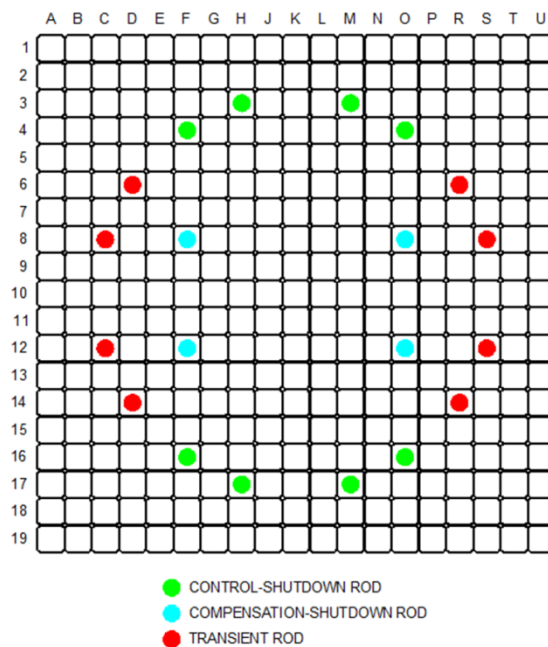


Figure 1-2. Locations of the Control Rod Banks in the Current (Upgraded) TREAT Core

TREAT transients are performed through the withdrawal of the transient rods from a pre-transient critical configuration (which has the control/shutdown and transient rod banks partially inserted and the compensation rods fully withdrawn). The transients typically fall into one of two categories: (1) shaped transients, in which a specific desired core power-time history is produced using complex motions of the transient rods, and (2) temperature-limited (or “burst”) transients, in which a step insertion of reactivity is performed by withdrawing the transient rods at their maximum speed, causing a bell-shaped burst in power. The burst is constrained by the large, prompt, negative temperature reactivity feedback provided by the heating of the fuel graphite.

## 1.2 Core Conversion Requirements

The converted LEU core must maintain the current HEU core’s full set of experimental capabilities, while continuing to operate safely. The LEU core must also be able to function with the existing facility support systems (reactor trip system, filtration/cooling system, etc.) and must be demonstrated to satisfy acceptable safety limits for all items addressed in the existing HEU core’s FSAR [7].

To maintain the HEU core’s experimental performance capabilities, the LEU core must be able to match the test-sample total energy deposition (TED) achievable in the HEU core for the full range of feasible experiment vehicle and test sample combinations. The TED is related to core operation through a parameter called the power coupling factor (PCF). The PCF represents the ratio of test sample power (or energy) per unit sample mass to total reactor core power (or energy) and is typically expressed in units of W/g/MW or J/g/MJ. The PCF is dependent upon a number of variables, including the neutron energy spectrum in the core and the composition and geometry of the test samples and experiment vehicle. A lower PCF means that more core energy is needed to achieve the same test sample TED.

In order to ensure that a complete range of possible experiment scenarios is addressed, a set of general experiment categories was established for the LEU core analysis, as outlined in Table 1-1. For a realistic assessment of LEU performance against HEU performance, experiment types with low attenuation by the experiment vehicle were generally only considered for tests with both low test-fuel fissile density and low test-fuel sample size. This is because in-pile test vehicles which contain large amounts of fissile material must be more robust, so that they are able to withstand the high energy releases and high temperatures which could be generated in either the planned test or a reactivity insertion accident scenario. In the context of this analysis, a small sample or bundle size is considered to be an experiment configuration which has a self-shielding of neutrons comparable to that of a single fuel pin (such as two or three pins which do not shield one another appreciably), while a large sample or bundle has significantly more self-shielding than that of a single fuel pin (such as pin bundles with several closely-spaced pins). Historically-performed TREAT experiments have been identified which match the characteristics of categories A, B, C, and D. Category E has little or no historical information available (and thus no historic test name is cited); however analysis of a concept test of this kind may be relevant to future irradiations (e.g., low-enriched LWR fuel pins in a Zircaloy test vehicle)

**Table 1-1. General Experiment Parameter Categories for LEU Core Analysis and Assessment**

Experiment Type	Test-fuel Fissile Density*	Test-fuel Sample/ Bundle Size	Neutron Attenuation by the In-pile Test Vehicle	Example Test in Each Category
A	High	Small	High	M8CAL
B	High	Large	High	LO-Series
C	Low	Small	High	S-11/S-12
D	Low	Large	High	STEP-Series
E	Low	Small	Low	LWR Low-pressure Test

\* Includes weighing of all fissile isotopes relative to fission density of <sup>235</sup>U

The TREAT LEU fuel must also provide an appropriate amount of reactivity. There must be sufficient core excess reactivity to compensate for the highest negative-worth experiment vehicles and to ensure that the most-demanding transients can be performed. On the other hand, the reactivity must be limited such that the control rod banks are still able to make the core subcritical with sufficient margin.

A key parameter in evaluating the safety of the LEU core is the peak temperature experienced by the TREAT fuel assembly cladding. Temperature limits are placed on the cladding to minimize oxidation (which accelerates rapidly above certain temperatures) and to prevent material phase change. In the current HEU core, there is a temperature limit during normal operation (Limiting Safety System Setting, or LSSS) of 600°C and an accident scenario temperature limit (Safety Limit, or SL) of 820°C. To provide additional margin given the potential uncertainties in thermocouple measurements, the 600°C limit is imposed as a 575°C limit during actual operation (as prescribed by the HEU core FSAR [7]). The LEU core therefore must be able to safely match HEU core performance for any experiment that the HEU core can perform within its temperature limits. Operationally, the temperature limits translate into limits on core energy and reactivity insertion. Both normal operation and reactivity insertion accident temperatures are considered in this study. During normal operation, cooling air flow is assumed, while in the accident scenario there is assumed to be zero air flow. The LEU conceptual design fuel elements feature a different cladding material from the HEU (Zircaloy-4 rather than Zircaloy-3) and are analyzed accordingly. Detailed evaluation of the LEU cladding material is ongoing within the fuel design work coordinated by INL, and the full set of properties and temperature limits have not yet been finalized. Therefore, for the purposes of this study the LEU fuel was evaluated for multiple temperature values up to the temperature limits of the existing HEU core.

In addition to operating within safe temperature margins for cladding integrity, the LEU core must also be demonstrated to function within the requirements of the existing facility support systems and components.

### 1.3 Current Methodology

The historic M8CAL experiment series [8] has been used as the reference case for LEU-to-HEU core comparisons throughout the conversion analysis over the past several years. M8CAL is one of the latest, best-documented, experiments. It was performed in the upgraded core and utilized the same core loading that is in TREAT today. M8CAL required a large core loading and a highly-absorbing experiment vehicle, which is consistent with the anticipated near-term future needs of TREAT. Additional discussion of the selection of M8CAL as the reference experiment can be found in the June 2013 conversion study [1]. In addition to M8CAL, the LEU conceptual design fuel was evaluated for several other TREAT core loadings and experiments.

Steady-state neutronic simulations were performed using the Monte Carlo Code MCNP5 with ENDF/B-VII.0 cross-section data [9]. Transient simulations were performed with TREKIN, a point kinetics code historically used during TREAT operations to evaluate transient behavior and support the design of experiments. TREKIN has been resurrected and updated for use in an Excel-based environment [10]. Its use requires a set of core-specific parameters: delayed neutron fraction and prompt generation lifetime, temperature reactivity feedback and core average and peak temperature values as a function of core energy, and transient rod bank available reactivity as a function of axial position. Historically this information came from measurements made in the HEU core, but a method of generating the information with MCNP has been developed and evaluated against the reported data available from the M8CAL and ANCAL historic experiments [8, 11-13]. Temperature reactivity feedback was evaluated using temperature-dependent neutron cross-sections for a series of hot-core temperature zones corresponding to increasing core energy steps. Previously these cross-sections were generated using the MAKXSFC MCNP utility program [14], but a method using NJOY2012 [15] has now been implemented, as discussed below.

Benchmarking work was also performed for the steady-state MCNP models using data from the M8CAL and Minimum Critical Core experiments [1, 2]. Thermal hydraulic analysis of the LEU fuel was performed using COMSOL®, a multiphysics finite element software package [16]. In order to verify the model and methodology, a 3D single assembly model for the HEU core was developed and benchmarked against historic TREAT analyses [3].

The key focus of the neutronic and thermal hydraulic analyses was the TREAT design basis accident, a zero-flow reactivity-insertion accident. The SL of 820°C discussed above represents the peak cladding temperature which can be experienced by any HEU fuel assembly during this accident, in which there is a step insertion of reactivity and the cooling blowers fail. Therefore, allowable transients under normal operation are limited to those which require a reactivity insertion value less than that which could cause the core to reach the 820°C limit in the accident scenario. Operationally, this is a constraint on the allowable pre-transient position of the transient rod bank.

To evaluate the accident scenario in the LEU core, the first step taken was to calculate an HEU shaped transient using the HEU core's maximum allowed reactivity. This transient represents the HEU core under normal operation. The HEU accident scenario was then evaluated by performing a step reactivity insertion (i.e., maximum-speed rod withdrawal) of this same reactivity. To meet the conversion requirement, the LEU core must be able to match the test-sample TED achievable in the HEU planned

transient. The LEU core transient necessary for equivalent TED to the HEU core was therefore evaluated by scaling the HEU transient power-time history by a multiplying factor equal to the ratio of the PCF values in the two cores. The resultant LEU power-time history was then evaluated using the TREKIN power-driven mode to determine the pre-transient reactivity needed. Finally, the LEU accident scenario was evaluated assuming a step insertion of this same reactivity.

As discussed previously, for the same LEU TREAT fuel, the PCF can vary between different experiments due to a number of factors. Therefore, the accident analysis considered multiple LEU-to-HEU PCF ratio cases to ensure that all feasible experiment scenarios were addressed. Similarly, the thermal hydraulic analysis did not evaluate only one accident scenario core energy but instead considered multiple core energy and corresponding peak fuel temperature scenarios within the range of anticipated LEU core operation.

#### 1.4 LEU Conceptual Design Description

The LEU conceptual design baseline parameters and key assumptions have been outlined in the Analysis Guide developed by INL [17]. These specifications were selected based on lessons learned in the previous work performed by the multi-lab team. The conceptual design LEU fuel element is similar in geometry to the existing HEU fuel element and is designed to fit into the existing core layout and grid plate.

The LEU assemblies are square with chamfered corners, with a 25-mil-thick Zircaloy-4 cladding and a 15-mil fuel-to-clad gap. As in the HEU fuel assembly, the LEU fuel is comprised of  $\text{UO}_2$  dispersed in graphite. The fuel reference C/U ratio was not specified as an initial parameter but instead has been selected following initial MCNP simulations, as described below. It should be noted that in the context of the LEU, C/U refers to carbon-to-total uranium, rather than just  $^{235}\text{U}$ . The reference LEU conceptual fuel design has a total density of  $1.85 \text{ g/cm}^3$  with an impurity concentration of 2 ppm (parts per million) boron equivalent and 85% graphitization of the fuel carbon (i.e., the atomic ratio of graphite-to-total carbon in the fuel = 0.85).

The fuel region in a fuel assembly is composed of 12 stacked four-inch tall blocks for a total length of four feet. Above and below the fuel region are graphite reflectors, each of which has a length of approximately two feet. The fuel region and reflectors are enclosed by a continuous Zircaloy-4 can. Unlike the HEU fuel assembly, the LEU fuel assembly does not have axial spacers between the fuel and axial reflectors, in order to improve axial heat transfer. Axial spacers were utilized in the HEU to prevent excessive heating of the aluminum-clad axial reflectors; this is not a concern in the LEU design because Zircaloy cladding is used everywhere. The axial dimensions of the upper and lower reflectors were selected such that the fuel axial mid-height location is similar to that of the HEU core (Figure 1-3). A more-detailed description of the LEU assembly design and properties can be found in the Analysis Guide.

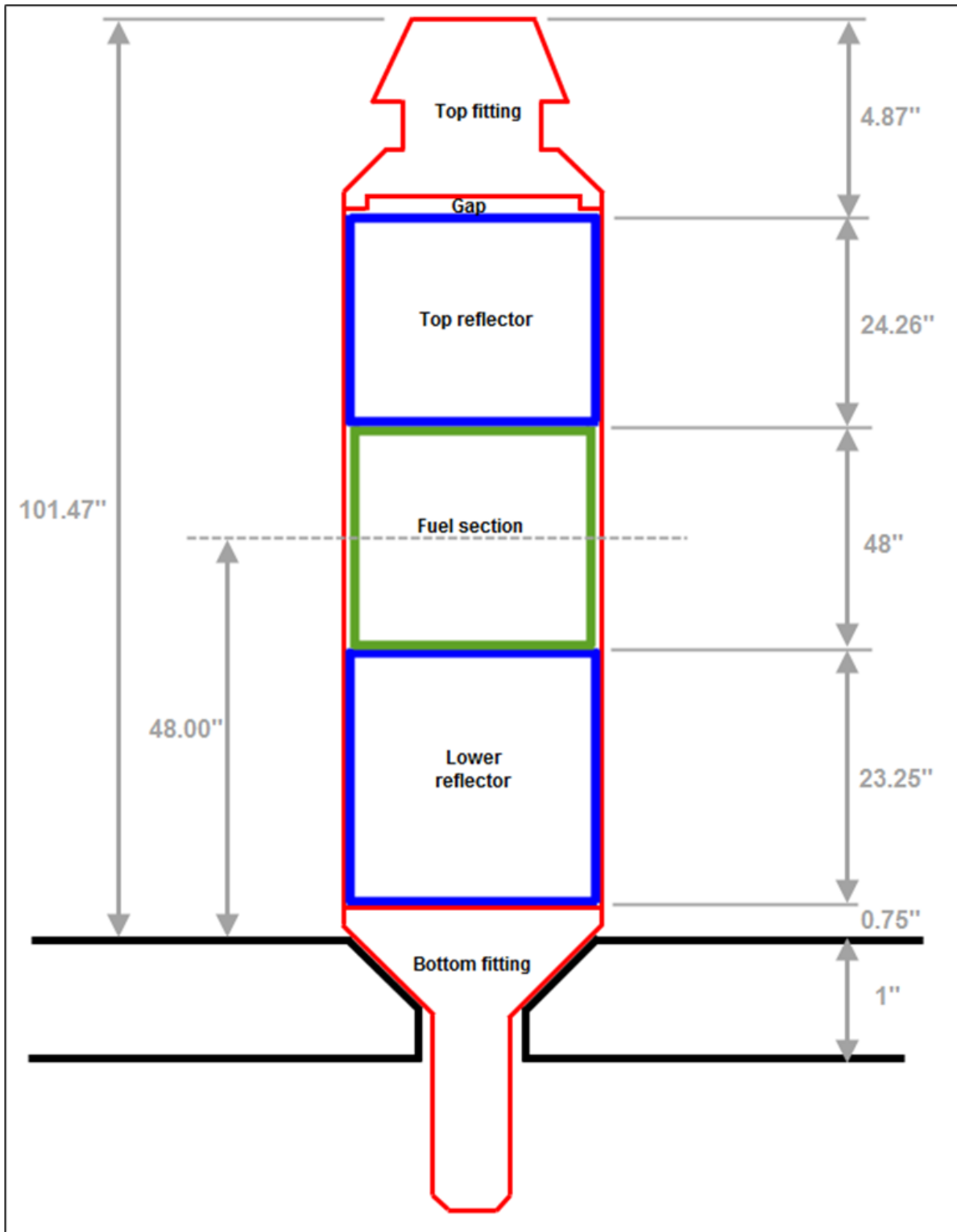


Figure 1-3. Side View of TREAT Fuel Assembly Axial Surfaces, Grid Plate – to – Top Fitting; From INL Analysis Guide [17].

## 2 Neutronic Analyses

Neutronic analyses were performed to characterize and evaluate the performance of the LEU core. MCNP-calculated parameters include all-rods-out reactivity, control rod bank worth, PCF values, and core properties needed by TREKIN. TREKIN was then utilized to evaluate core transient behavior.

### 2.1 Steady-state Analysis with MCNP

A detailed 3D model of the TREAT core has been developed for MCNP, including the fuel assemblies, control rods, slotted assemblies, experiment vehicle, and surrounding reflector and bioshield. The core grid plate and subpile room have also been modeled, to support safety analyses related to those areas. The MCNP models of the HEU and LEU cores assume that the details of the control rods, non-fueled assemblies (slotted, graphite dummies), and overall facility will not be altered in the conversion, with changes to the fuel assemblies only. The HEU MCNP model was developed and evaluated using best-available data [1, 5, 18], while the LEU MCNP model was established using the specifications of the Analysis Guide (building upon the models developed in the previous LEU analysis work [1, 2]).

#### 2.1.1 Fuel Carbon-to-Uranium Search

After the appropriate changes were made to the MCNP model of the LEU core to accommodate the parameters specified in the Analysis Guide, the fuel C/U was adjusted as needed in order to identify a composition which yielded a calculated all-rods-out (ARO) reactivity similar to the HEU core, using the M8CAL half-slotted core loading. As indicated above, C/U in the context of the LEU refers to carbon-to-total uranium, rather than just carbon-to-<sup>235</sup>U. Compared to previous draft information on fuel assembly properties, the recent Analysis Guide provides a more detailed definition of the anticipated Zircaloy-4 cladding composition. An initial set of runs were performed using C/U=2470, which was the value used in the most-recent previous analysis of an LEU design with an HEU-like geometry, in order to evaluate ARO reactivity for the LEU core with different fuel element Zircaloy-4 specifications (Table 2-1).

Table 2-1. LEU M8CAL Half-Slotted Core ARO Reactivity Values with C/U=2470, for Different Zircaloy-4 Specifications

Cladding Composition Summary		ARO Reactivity %Δk/k
<b>Case 1</b>	<ul style="list-style-type: none"> <li>Previous Zircaloy-4 Definition</li> </ul>	7.47%
<b>Case 2</b>	<ul style="list-style-type: none"> <li>Zircaloy-4 from Analysis Guide</li> <li>All isotopes explicitly modeled</li> </ul>	7.00%
<b>Case 3</b>	<ul style="list-style-type: none"> <li>Zircaloy-4 from Analysis Guide</li> <li>Zircaloy &amp; alloying elements modeled</li> <li>All other isotopes modeled as an equivalent boron content (with Zircaloy mass fraction evaluated as = 1 - (alloys) - (B) )</li> </ul>	7.16%

\* k-eff σ values = 0.0002-0.0003

For conservatism, it was decided to use the full detailed Zircaloy-4 definition (as in Case 2) in all subsequent analyses. A search was then performed to determine the C/U which yields a calculated reactivity similar to the value calculated with the current HEU core MCNP model (7.73 %Δk/k), as indicated in Table 2-2. In this analysis, the relative fractions of the isotopes in the fuel were adjusted

such that the boron impurity, oxygen-to-uranium ratio, and total fuel mass density were maintained. From this study, a new (lower) reference value of C/U=2370 was selected. The detailed isotopic composition of the fuel is provided in Table 2-3.

**Table 2-2. LEU M8CAL Half-slotted Core ARO Reactivity Values with Different C/U Ratios**

C/U	ARO Reactivity %Δk/k
2300	8.29%
2360	7.86%
2370	7.70%
2380	7.64%
2470	7.00%

\* k-eff σ values = 0.0002-0.0003

**Table 2-3. Reference LEU Fuel Composition Used in MCNP Analysis for C/U = 2370**

Isotope	Mass Fraction	Atom Fraction
<b>U-232</b>	1.65274E-11	8.62405E-13
<b>U-234</b>	2.14857E-05	1.11153E-06
<b>U-235</b>	1.63209E-03	8.40731E-05
<b>U-236</b>	3.80132E-05	1.94985E-06
<b>U-238</b>	6.57214E-03	3.34272E-04
<b>O</b>	1.11340E-03	8.42813E-04
<b>C (un-graphitized)</b>	1.48477E-01	1.49810E-01
<b>C (graphitized)</b>	8.42144E-01	8.48924E-01
<b>B-10</b>	3.68659E-07	4.45786E-07
<b>B-11</b>	1.63155E-06	1.79434E-06

### 2.1.2 Excess Reactivity and Control Rod Worth

The worth of each control rod bank was evaluated for the reference M8CAL half-slotted LEU core, which has a calculated ARO reactivity of 7.70 %Δk//k, as presented in Table 2-4. The rod bank worth is the reactivity decrease that occurs upon fully inserting the particular rod bank from an ARO configuration.

**Table 2-4. Control Rod Bank Worths in LEU M8CAL Half-slotted Core**

Bank	(ARO) - (Bank In) %Δk/k
<b>Transient</b>	8.66%
<b>Compensation/Shutdown</b>	8.41%
<b>Control/Shutdown</b>	9.18%

\* k-eff σ values = 0.0002-0.0003

Using the reference LEU assembly design, additional core loadings were evaluated. It was found that in the LEU core, the worth of the M8CAL vehicle is greater than in the HEU core (due to differences in the neutron energy spectrum, as discussed below). Therefore, the LEU core has a similar reactivity to the

HEU core with the vehicle but a slightly higher reactivity with the vehicle replaced by air (Table 2-5). Three additional loadings without an experiment or slot were also simulated (Figure 2-1). These core loadings similarly demonstrated slightly higher reactivity with the LEU fuel (Table 2-6). However, since the most demanding use of TREAT is high-energy transients with high-absorbing experiment vehicles, it is a better basis to establish the fuel composition as needed for a core with an experiment vehicle rather than one without. In practice, the core loading is chosen for each experiment in order to meet the particular experiment demands and safety requirements.

**Table 2-5. Calculated M8CAL ARO Reactivity and Experiment Vehicle Worth**

	HEU	LEU
Vehicle Present	7.73%	7.70%
Vehicle Replaced with Air	10.55%	10.85%
Vehicle Worth	-2.82%	-3.15%

\* k-eff  $\sigma$  values = 0.00004-0.00007

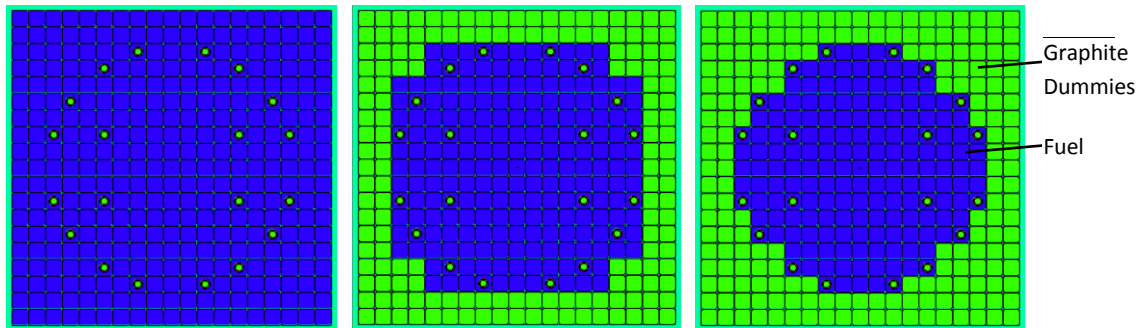


**Figure 2-1. Core loadings A, B, and C Used to Further Evaluate LEU and HEU ARO Reactivity.**

**Table 2-6. ARO Reactivity, Core Loadings A, B, and C**

	HEU	LEU
<b>Core A</b>	14.14%	14.28%
<b>Core B</b>	8.48%	8.89%
<b>Core C</b>	5.63%	6.36%

\* k-eff  $\sigma$  values = 0.0002-0.0003

### 2.1.3 Power Coupling Factor Calculations

MCNP was used to evaluate the PCF for several different experiment cases. LEU PCF values are reported relative to the PCF results for the HEU core, as the ratio  $\frac{PCF_{LEU}}{PCF_{HEU}}$ . A brief description of each experiment is provided in this discussion. For this work, models were developed which represent conditions similar to (but not exactly the same as) the actual historic experiment designs (per current best-available data). This approach was taken because the focus of this work was an LEU to HEU comparison (rather than validation of HEU core experiment details), assuming the same experiment conditions in each core. In this analysis, the PCF was evaluated as the ratio of the fission density of the test sample to the core average energy deposition in the TREAT fuel meat.

The relative differences in the PCF values (as compared to the HEU core) were used to estimate the LEU core energies needed to match the sample energy depositions achievable in the HEU core, as outlined in greater detail in the transient analysis discussion below. The goal of the analyses presented in this section was to estimate an upper bound on the increase in core power and energy anticipated for the LEU core. The impact of core temperature on the  $\frac{PCF_{LEU}}{PCF_{HEU}}$  ratio was also evaluated to support bounding the analysis, as discussed in Section 2.2.1.4.

### 2.1.3.1 PCF: M8CAL Experiment

The M8CAL experiment was a series of steady-state and transient calibration irradiations performed in TREAT to evaluate the power coupling between the core and test samples [8]. The experiment featured two test pins, T-462 and T-433 (Figure 2-2), placed at the core center in a stainless-steel vehicle. In addition to the pins, irradiations were also performed with U-Zr monitor wires (also referred to as “flux wires”), which helped to support the calibration work. Both low- and high-enriched wires were used in the actual experiment, and a low-enriched wire (19.8 wt%  $^{235}\text{U}$ ) was evaluated in this analysis. This wire was eight-inches long, with a 0.040-inch diameter. The compositions, as used in the analysis, of the test samples are summarized in Table 2-7. The M8CAL half-slotted core was used in this analysis (Figure 2-3). A closer view of the experiment configuration is provided in Figure 2-4. The PCF ratios, presented in Table 2-8, demonstrate that LEU core PCF values for this experiment are similar to those in the HEU core.

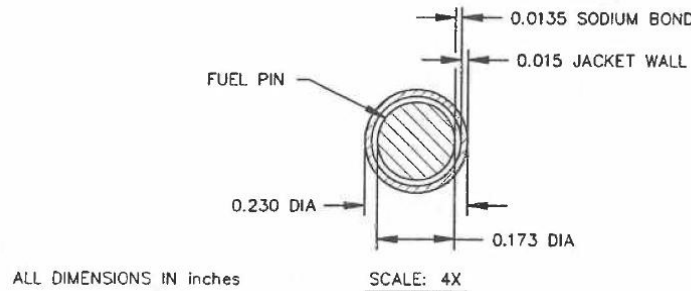


Figure 2-2. Radial Dimensions of the M8CAL Test Pins [8].

Table 2-7. M8CAL Test Pin and Monitor Wire Compositions Used in MCNP Simulations

Isotopic Composition		T-462	T-433	Flux Wire
Mass Fractions	Zr	9.823E-02	9.761E-02	9.400E-01
	$^{233}\text{U}$			3.000E-07
	$^{234}\text{U}$	3.980E-03	5.670E-03	6.684E-05
	$^{235}\text{U}$	4.040E-01	6.182E-01	1.190E-02
	$^{236}\text{U}$	2.310E-03	3.350E-03	8.274E-05
	$^{238}\text{U}$	3.000E-01	2.752E-01	4.795E-02
	$^{239}\text{Pu}$	1.798E-01		
	$^{240}\text{Pu}$	1.117E-02		
	$^{241}\text{Pu}$	5.100E-04		
	$^{242}\text{Pu}$	9.000E-05		
Total Density, g/cm <sup>3</sup>		14.91	14.9	8.16167542

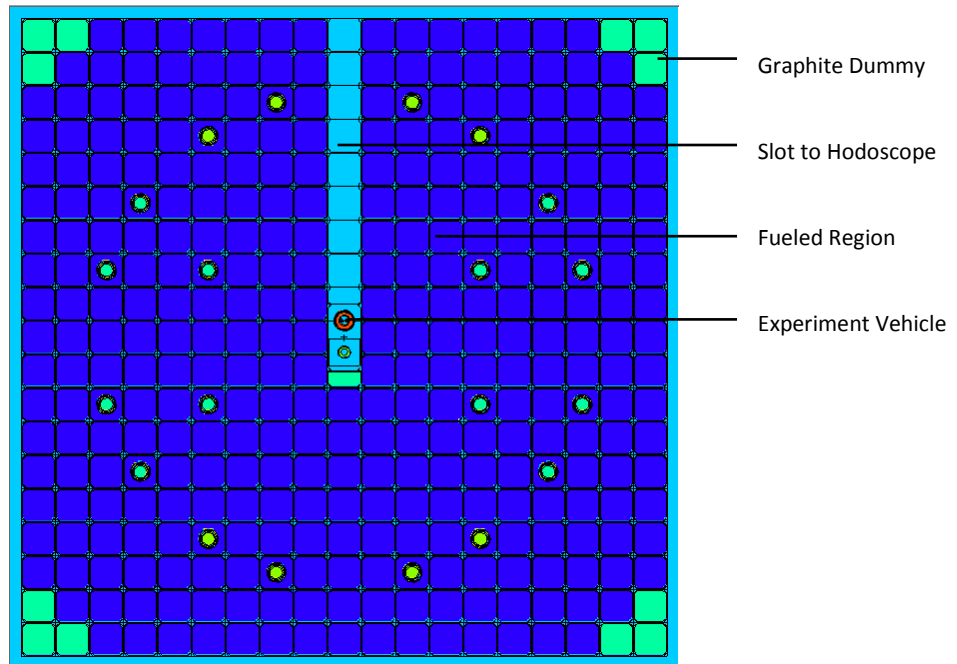


Figure 2-3. M8CAL Half-slotted Core Loading.

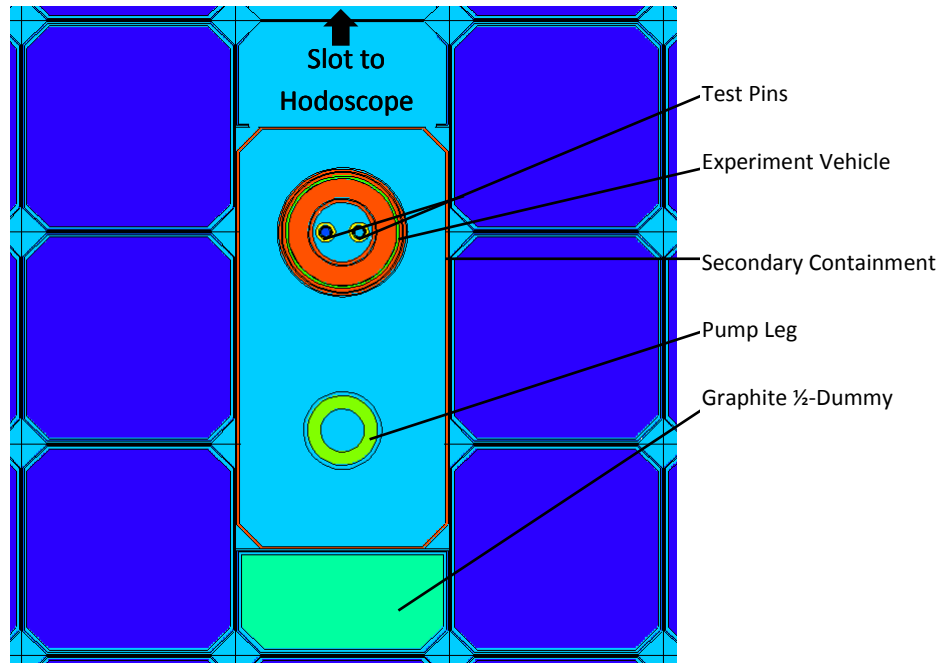


Figure 2-4. M8CAL Experiment Configuration.

Table 2-8. PCF Results, M8CAL Test Pin and Monitor Wire

Test Sample	$\frac{PCF_{LEU}}{PCF_{HEU}}$
Pin T-462	97.5%
Pin T-433	97.4%
Low-enriched Monitor Wire	100.6%

\* Statistical relative error in PCF values = 0.5% for pins; 1.4% for wire

### 2.1.3.2 PCF: LO3 Experiment

LEU core PCF values were also evaluated for an experiment setup similar to that of the historic LO3 calibration experiments. The LO3 calibration featured a seven-pin test bundle of PFR-type pins with a Mark-III loop (with a dummy sodium pump filled with silicon oil) and dysprosium shaping collars. The test samples were annular  $\text{PuO}_2\text{-UO}_2$  pins, with upper and lower breeder regions of depleted  $\text{UO}_2$ . The test fuel composition used in this analysis is documented in Table 2-9. The annular fuel region in each pin had an outer diameter of 4.98 mm and an inner diameter of 1.90 mm. Within the experiment vehicle, six pins were arranged in a circle, with the seventh pin in the center. The as-modeled experiment configuration is shown in Figure 2-5.

The actual experiment was performed in the pre-upgrade core. For comparison with LEU, the current simulations were performed using the upgraded HEU core. A core loading was selected with a half slot, three dummy elements in each corner, and half-dummy element behind the experiment location, similar to the loading used to evaluate M8CAL (Figure 2-3). An illustration of the experiment region is provided in Figure 2-6. The ratios presented in Table 2-10 show that the LEU core PCFs for this experiment are similar to those of the HEU core.

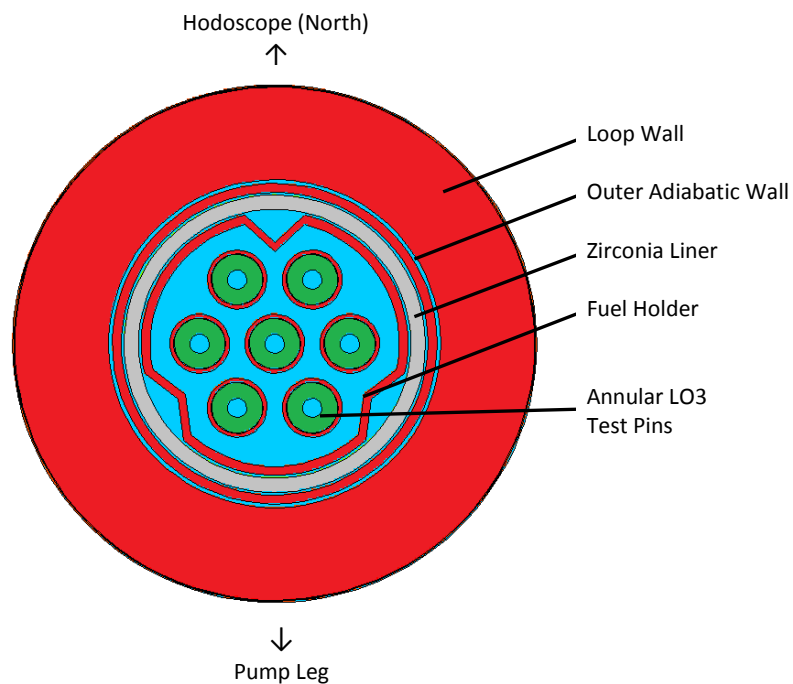


Figure 2-5. MCNP Model of LO3-like Experiment Configuration.

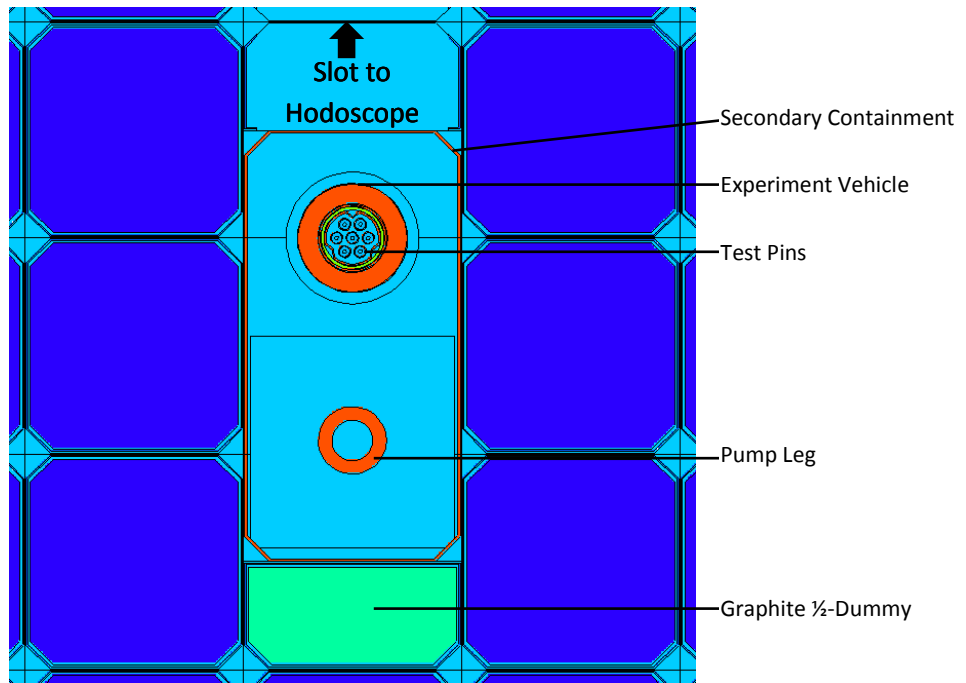


Figure 2-6. LO3 Experiment Region within the MCNP Core Model.

Table 2-9. LO3 Fuel Pin Composition

Isotope	Mass Fraction in Fuel Mixture	U and Pu Isotopics (Mass %)	
		$^{235}\text{U}$	4.260E-03
$^{238}\text{U}$	6.044E-01	$^{238}\text{U}$	99.3%
$^{239}\text{Pu}$	2.027E-01	$^{239}\text{Pu}$	74.0%
$^{240}\text{Pu}$	5.751E-02	$^{240}\text{Pu}$	21.0%
$^{241}\text{Pu}$	1.096E-02	$^{241}\text{Pu}$	4.0%
$^{242}\text{Pu}$	2.739E-03	$^{242}\text{Pu}$	1.0%
O	1.175E-01		

Table 2-10. PCF Results, LO3 Experiment Pins

	Pin 1	Pin 2	Pin 3	Pin 4	Pin 5	Pin 6	Pin 7
$\text{PCF}_{\text{LEU}} / \text{PCF}_{\text{HEU}}$	100.5%	100.8%	102.0%	102.7%	101.3%	100.4%	99.6%

\* Statistical relative error in PCF values = 0.41%-0.47%

### 2.1.3.3 PCF: STEP Experiment

PCF values were also evaluated for an estimated model of the STEP calibration experiment. This experiment utilized four low-enriched  $\text{UO}_2$  pins. The pin fuel region had a diameter of 0.804 cm, with the composition provided in Table 2-11. The experiment vehicle featured two concentric zirconia tubes and an Inconel 625 primary vessel (Figure 2-7). As with LO3, STEP was performed in the pre-upgrade core but has been evaluated in a half-slotted upgraded core for this analysis. The historic experiment utilized graphite dummy reflector elements near the test vehicle. LEU vs. HEU comparisons have been made both with and without the reflectors (Figure 2-8, Table 2-12). The LEU and HEU cores had similar PCFs

both with and without the reflectors (indicating that the impact of the reflectors is roughly the same in both cores, as confirmed in Table 2-13). An additional test case was also simulated with the primary containment material replaced with Zircaloy-4. This hypothetical lower-absorbing vehicle demonstrated a slightly greater increase in LEU PCF relative to HEU.

Table 2-11. STEP Experiment Pin Composition

	Isotope	Fraction
<b>Mass Fractions</b>	<b>O</b>	1.18552E-01
	<sup>234</sup> U	3.86313E-03
	<sup>235</sup> U	5.05562E-02
	<sup>236</sup> U	3.18678E-04
	<sup>238</sup> U	8.26710E-01
<b>Total Density (g/cm<sup>3</sup>)</b>		10.202

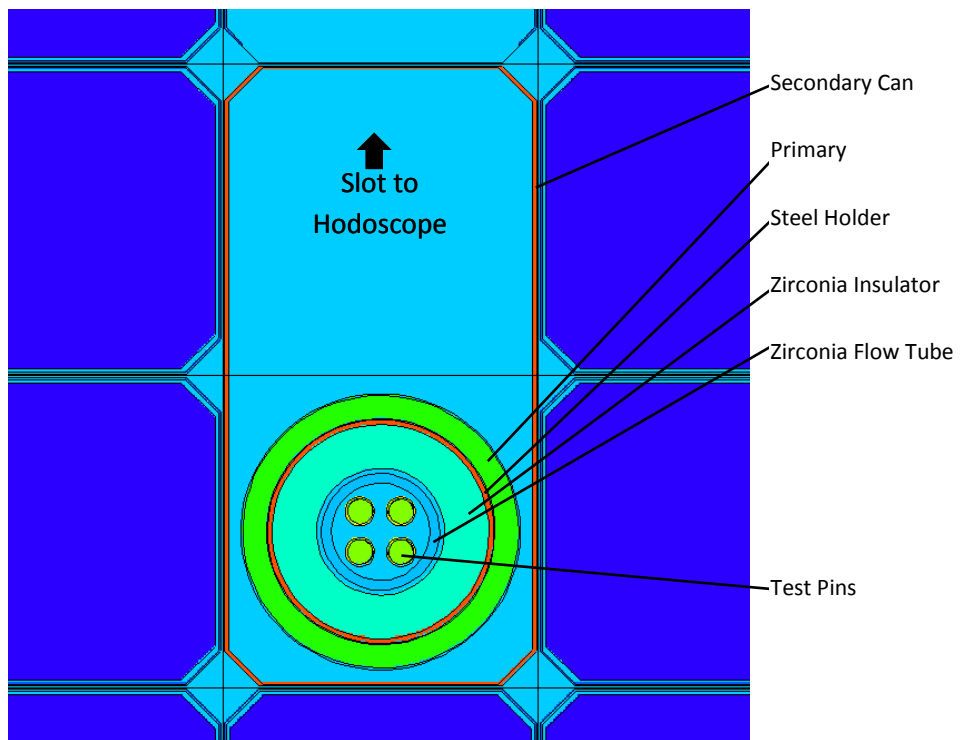


Figure 2-7. Modeled STEP Experiment Configuration.

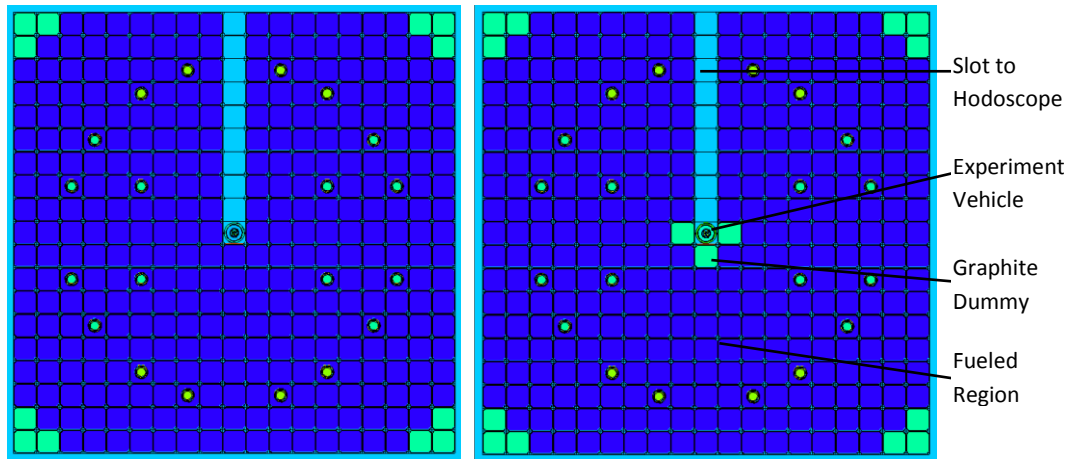


Figure 2-8. Core Loadings Used to Evaluate STEP Experiment.

Table 2-12. Comparison of HEU and LEU PCF Values for STEP Pins

	PCF <sub>LEU</sub> / PCF <sub>HEU</sub>			
	pin 1	pin 2	pin 3	pin 4
<b>Without Reflectors, Inconel primary</b>	102.3%	102.1%	102.2%	102.2%
<b>With Reflectors, Inconel primary</b>	102.5%	102.2%	102.4%	101.8%
<b>With Reflectors, Zr Primary</b>	105.3%	105.9%	105.6%	105.8%

\* Statistical relative error in PCF values = 0.17%-0.18%

Table 2-13. Increase in PCF Values of STEP Pins Due to Reflectors near the Test Region, Increase = (With – Without)/Without

	% Increase in PCF			
	pin 1	pin 2	pin 3	pin 4
<b>HEU core</b>	5.6%	5.2%	6.2%	6.7%
<b>LEU core</b>	5.7%	5.2%	6.4%	6.2%

#### 2.1.3.4 PCF: M8CAL Vehicle and Sample Perturbations

For further investigation of LEU core performance, additional cases were evaluated using perturbations on the M8CAL sample and experiment vehicle. These simulations were performed with the test sample represented as a cylinder placed at the center of the experiment vehicle, with a test-sample diameter equal to that of the M8CAL test pins. Using the reference M8CAL experiment vehicle, the PCF of this sample was evaluated with both the low-enriched wire and Pin T-462 compositions, along with low- and high-enriched UO<sub>2</sub>. The results, presented in Table 2-14, demonstrate that the LEU core PCFs are again similar to those of the HEU core. The low-enriched UO<sub>2</sub> pin was also evaluated for a case with the stainless-steel components of the experiment vehicle replaced with Zircaloy-4 (Table 2-15). Consistent with the results of the STEP analysis, this change to a lower absorbing vehicle material caused a slight increase in the PCF ratio.

**Table 2-14. PCF Results for Cylindrical Sample in M8CAL Experiment Vehicle, for Different Sample Compositions**

Test Sample Composition	PCF <sub>LEU</sub> / PCF <sub>HEU</sub>
Low-enriched Monitor Wire	100.0%
Pin T-462	97.5%
UO <sub>2</sub> – 5% <sup>235</sup> U, 95% <sup>238</sup> U	100.3%
UO <sub>2</sub> – 90% <sup>235</sup> U, 10% <sup>238</sup> U	97.9%

\* Statistical relative error in PCF values = 0.5%-0.6%

**Table 2-15. PCF Results for Low-enriched UO<sub>2</sub> Sample, M8CAL Vehicle, Stainless-steel Components Replaced with Zircaloy**

Experiment Vehicle Composition	PCF <sub>LEU</sub> / PCF <sub>HEU</sub>
Reference (Stainless-steel)	100.3%
Replaced with Zircaloy	102.2%

\* Statistical relative error in PCF values = 0.5%

To further investigate the impact of the vehicle on the PCF, the Pin T-462 and low-enriched UO<sub>2</sub> composition cases were simulated with the density of the stainless-steel components of the experiment vehicle hypothetically increased by a factor of five (from 7.944 g/cm<sup>3</sup> to 39.73 g/cm<sup>3</sup>) in order to simulate a very (unrealistically) high-absorbing vehicle (Table 2-16). The PCF ratios of both samples decrease when the more absorbing vehicle is used. This is due to the more thermal spectrum in the LEU core (as compared to the HEU core), which is discussed in greater detail below. The optimization studies which will take place during the upcoming preliminary design phase will include further analysis of the relationship between fuel design parameters, core neutron spectrum, and PCF values for different experiment conditions.

**Table 2-16. PCF Results for Pin T-462 Sample, M8CAL Vehicle, Perturbations in Stainless-steel Density**

Sample Composition	Change in Density of the Stainless-steel Vehicle Components	PCF <sub>LEU</sub> / PCF <sub>HEU</sub>
Pin T-462	Reference – No Change	97.5%
	Increase x5	91.1%
Low-enriched UO <sub>2</sub>	Reference – No Change	100.3%
	Increase x5	91.0%

\* Statistical relative error in PCF values = 0.5%-0.7%

As a final perturbation, the diameter of the sample was increased by a factor of four, and the PCF was re-evaluated using the T-462 composition and reference M8CAL experiment vehicle. The results are presented in Table 2-17.

**Table 2-17. PCF Results for Pin T-462 Sample, M8CAL Vehicle, Perturbations in Sample Diameter**

Sample Diameter	PCF <sub>LEU</sub> / PCF <sub>HEU</sub>
Reference	97.5%
Increase x4	95.3%

\* Statistical relative error in PCF values = 0.2%-0.5%

### 2.1.4 Neutron Energy Spectrum

The neutron energy spectrum in the LEU core was calculated with MCNP for the M8CAL half-slotted core, and the results were compared to the HEU core. The spectrum was evaluated in an air-filled cylinder placed at the location of the M8CAL test sample. Calculations were performed both with the M8CAL vehicle present and with the vehicle replaced with air, as shown in Figure 2-9 and Figure 2-10, respectively. The data is plotted as the relative fraction of the flux in each energy bin. The LEU core was found to have a more thermal spectrum both with and without the vehicle. The impact of this more thermal spectrum can be observed in the PCF studies above, where changes such as increasing the vehicle density, which causes a larger increase in neutron loss via absorption (and corresponding larger decrease in PCF) in the more thermal LEU core, causes a decrease in the  $\frac{PCF_{LEU}}{PCF_{HEU}}$  ratio.

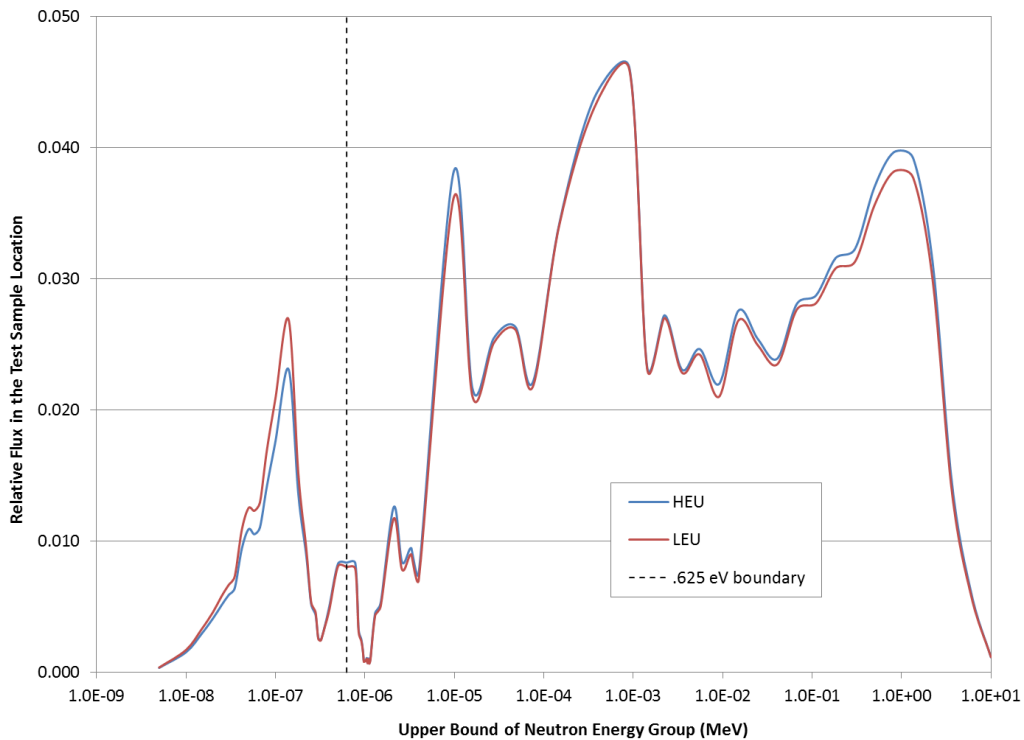


Figure 2-9. Neutron Spectrum at the M8CAL Test Sample Location, Inside M8CAL Vehicle.

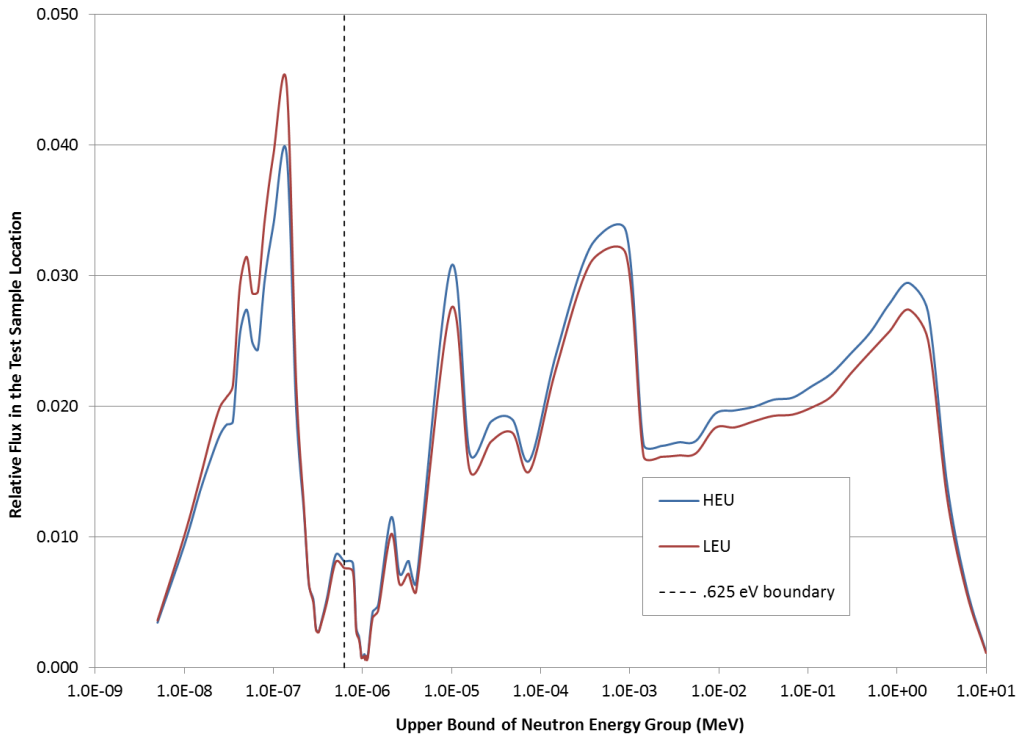


Figure 2-10. Neutron Spectrum at the M8CAL Test Sample Location, Without the M8CAL Vehicle.

To further characterize the spectrum differences, Table 2-18 and Table 2-19 present the thermal-to-total and fast-to-thermal fluxes for both cases. In addition, results are provided for the neutron flux spectrum in the TREAT fuel (that is, the average spectrum evaluated across the TREAT fuel rather than in the air “sample” at the experiment location).

Table 2-18. Thermal ( $E < 0.625$  eV) – to – Total Neutron Flux Ratio

	HEU	LEU	LEU/HEU
<b>Sample Location, With Vehicle</b>	0.19	0.21	1.12
<b>Sample Location, Without Vehicle</b>	0.38	0.42	1.11
<b>In TREAT Fuel</b>	0.38	0.42	1.11

Table 2-19. Fast ( $E > 0.625$  eV) – to – Thermal ( $E < 0.625$  eV) Neutron Flux Ratio

	HEU	LEU	LEU/HEU
<b>Sample Location, With Vehicle</b>	4.39	3.83	0.87
<b>Sample Location, Without Vehicle</b>	1.65	1.38	0.84
<b>In TREAT Fuel</b>	1.67	1.40	0.84

## 2.2 TREKIN Transient Analyses – Normal and Accident Conditions

The point kinetics code TREKIN was used for the transient analysis of the LEU core. The input tables required for the TREKIN calculations were produced with MCNP and were as follows: a) the transient rod bank worth as a function of rod bank withdrawal, b) the temperature reactivity feedback as a function of total core energy and c) the peak and average core temperatures as a function of total core energy, as well as the prompt neutron generation lifetime and the effective fraction of the six delayed neutron groups. The TREKIN computations do not include any thermal-hydraulic modelling, and the peak core temperature value reported for a given transient is based on the user-provided lookup table. This table contains peak core temperature as a function of the total energy deposition, and was calculated using the relative power distribution provided by MCNP assuming adiabatic heating. More detailed analysis of the core’s thermal behavior was performed separately using COMSOL®, as discussed below. Additional detail on the transient analysis methods, including benchmarking against historic HEU data, can be found in previous studies [11, 13].

With core energy generation and corresponding core temperature rise, the LEU-to-HEU PCF ratio may change. Therefore the hot-core simulations used to evaluate temperature reactivity feedback were also used to further bound the PCF ratio by evaluating its change with core energy and temperature.

### 2.2.1 TREKIN Input Tables

#### 2.2.1.1 Transient Rod Bank Worth

The transient rod bank worth was calculated for cold core conditions for the HEU and the LEU cores as a function of rod bank withdrawal. For each step in the analysis, the worth was evaluated as the reactivity change from the given rod position to full withdrawal. The control/shutdown bank was positioned as needed for approximately critical conditions with the transient bank inserted. The calculated worth values were then multiplied by 0.95, the average ratio of the measured-to-calculated transient rod bank worth for the HEU core, for use in TREKIN (consistent with the approach taken in the previous studies [12]). The values used in the TREKIN calculations are shown in Table 2-20.

Table 2-20. MCNP Calculated Transient Rod Bank Worth for the HEU and LEU Cores.

Rod Bank Withdrawal		Transient Rod Bank Worth, % $\Delta k/k$		LEU/HEU
Control/Shutdown	Transient	HEU	LEU	
100%	0%	8.64%	8.27%	0.96
100%	13%	7.57%	7.28%	0.96
91%	25%	6.27%	5.91%	0.94
71%	38%	4.73%	4.52%	0.96
60%	50%	3.29%	3.12%	0.95
51%	63%	2.08%	2.05%	0.98
44%	75%	1.10%	1.16%	1.05
40%	88%	0.42%	0.48%	1.15

\* k-eff  $\sigma$  value = 0.00017

### 2.2.1.2 Effective Delayed Neutron Fraction and Prompt Neutron Generation Lifetime

The prompt generation lifetime and the effective delayed neutron fraction as well as the six-group delayed neutron precursors were calculated with MCNP using the *kopts* card for a cold and critical core (using the same rod configuration for both cores). The delayed neutron and the delayed neutron precursor decay constant for the HEU and LEU cores are shown in Table 2-21 and Table 2-22, respectively. The effective delayed neutron fraction and the prompt neutron generation lifetime for the HEU and the LEU cores are summarized in Table 2-23.

Table 2-21. Delayed Neutron Fraction and the Delayed Neutron Precursor Decay Constant for the Six Delayed Neutron Groups for the HEU Core Calculated with MCNP.

HEU				
Delayed Neutron Group	Delayed Neutron Fraction ( $\beta_i$ )	Standard Deviation	Decay Constant ( $\lambda_i$ )	Standard Deviation
1	0.00023	0.00001	0.01249	<1E-5
2	0.00115	0.00002	0.03182	<1E-5
3	0.00111	0.00002	0.10938	<1E-5
4	0.00322	0.00004	0.31699	<1E-5
5	0.00093	0.00002	1.35398	<1E-5
6	0.00034	0.00001	8.63652	0.00004

Table 2-22. Delayed Neutron Fraction and the Delayed Neutron Precursor Decay Constant for the Six Delayed Neutron Groups for the LEU Core Calculated with MCNP.

LEU				
Delayed Neutron Group	Delayed Neutron Fraction ( $\beta_i$ )	Standard Deviation	Decay Constant ( $\lambda_i$ )	Standard Deviation
1	0.00021	0.00001	0.01249	<1E-5
2	0.00114	0.00002	0.03182	<1E-5
3	0.00110	0.00002	0.10938	<1E-5
4	0.00324	0.00004	0.31702	<1E-5
5	0.00089	0.00002	1.35389	<1E-5
6	0.00033	0.00001	8.63893	0.00015

Table 2-23. Effective Delayed Neutron Fraction and Prompt Neutron Generation Lifetime Calculated with MCNP for the HEU and the LEU Cores.

Core Energy (MJ)	HEU	LEU
Effective Delayed Neutron Fraction, $\beta_{\text{eff}}$	$0.00697 \pm 0.00006$	$0.00692 \pm 0.00006$
Prompt Neutron Generation Lifetime, $\lambda_p$ ( $\mu\text{s}$ )	$867.6 \pm 0.8$	$956.0 \pm 0.8$

### 2.2.1.3 Temperature Reactivity Feedback

The analysis of the core temperature reactivity feedback was performed using hot core temperature distributions evaluated based on the MCNP-calculated power distribution in the M8CAL half-slotted core. The ratio of fuel element power density to the core average power density is shown for the LEU and HEU cores in Figure 2-11 and Figure 2-12, respectively<sup>1</sup>. The location of the maximum power fuel element in each core is indicated with a white box (location N12 in both cores, with peaking factors of 1.52 and 1.47 in the LEU and HEU cores, respectively) The axial variation of the ratio of the local power density to the fuel element average power density, evaluated in the hottest fuel element in each core, is presented in Figure 2-13. The HEU and LEU cores demonstrate different profiles at the ends of the fuel region because in the LEU the fuel is in direct contact with the axial reflector graphite, while in the HEU there are spacers between the fuel and graphite. The profiles are non-symmetric axially because the control rods are partially inserted into the top of the core, thereby suppressing power somewhat in that region.

	A	B	C	D	E	F	G	H	J	K	L	M	N	O	P	R	S	T	U
1			0.52	0.52	0.52	0.50	0.47	0.43	0.41		0.41	0.43	0.47	0.49	0.51	0.51	0.52		
2		0.57	0.57	0.58	0.58	0.55	0.52	0.48	0.49		0.49	0.48	0.52	0.55	0.58	0.59	0.59	0.59	
3	0.60	0.62	0.65	0.67	0.65	0.61	0.58	0.52	0.57		0.57	0.52	0.58	0.61	0.66	0.69	0.68	0.65	0.65
4	0.65	0.69	0.75	0.78	0.75	0.65	0.70	0.70	0.70		0.70	0.71	0.71	0.66	0.76	0.80	0.78	0.73	0.71
5	0.72	0.78	0.85	0.90	0.90	0.88	0.89	0.88	0.82		0.83	0.89	0.90	0.90	0.92	0.93	0.89	0.82	0.78
6	0.80	0.86	0.95	1.01	1.06	1.07	1.06	1.01	0.92		0.92	1.02	1.08	1.09	1.08	1.04	0.99	0.91	0.86
7	0.87	0.94	1.04	1.12	1.19	1.21	1.18	1.11	0.98		0.98	1.12	1.20	1.23	1.21	1.16	1.08	0.99	0.92
8	0.92	1.01	1.11	1.22	1.29	1.30	1.27	1.17	0.98		0.98	1.18	1.29	1.32	1.32	1.25	1.14	1.05	0.98
9	0.96	1.06	1.18	1.29	1.37	1.39	1.35	1.21	0.92		0.92	1.23	1.37	1.42	1.40	1.33	1.22	1.10	1.02
10	0.99	1.09	1.22	1.34	1.43	1.46	1.42	1.27	0.93		0.94	1.29	1.44	1.48	1.46	1.38	1.26	1.13	1.04
11	1.00	1.10	1.23	1.35	1.45	1.48	1.47	1.36	1.12		1.12	1.38	1.49	1.51	1.48	1.39	1.27	1.14	1.05
12	0.99	1.08	1.20	1.33	1.43	1.47	1.49	1.46	1.36	1.30	1.37	1.47	1.52	1.50	1.46	1.37	1.24	1.12	1.04
13	0.96	1.05	1.17	1.28	1.38	1.44	1.48	1.49	1.47	1.46	1.48	1.51	1.50	1.47	1.41	1.32	1.21	1.09	1.01
14	0.92	1.00	1.11	1.19	1.28	1.34	1.40	1.44	1.46	1.47	1.47	1.45	1.42	1.37	1.31	1.23	1.15	1.04	0.96
15	0.86	0.93	1.03	1.10	1.13	1.15	1.23	1.30	1.35	1.37	1.36	1.32	1.25	1.18	1.17	1.14	1.07	0.97	0.91
16	0.80	0.85	0.93	0.99	0.97	0.89	1.01	1.08	1.17	1.21	1.18	1.10	1.03	0.91	1.00	1.02	0.97	0.89	0.84
17	0.75	0.78	0.83	0.87	0.88	0.86	0.87	0.84	0.98	1.04	0.99	0.85	0.89	0.89	0.91	0.91	0.87	0.82	0.79
18		0.73	0.74	0.77	0.80	0.81	0.82	0.82	0.88	0.92	0.89	0.84	0.84	0.84	0.84	0.82	0.79	0.77	
19			0.69	0.70	0.73	0.76	0.79	0.81	0.84	0.85	0.85	0.83	0.82	0.80	0.78	0.76	0.74		

Figure 2-11. Ratio of the Fuel Element Power Density to the Core Average Power Density for LEU M8CAL Half-slotted Core.

<sup>1</sup> The HEU and LEU core power profiles are not symmetric about the core centerline, as there is asymmetry in the surrounding reflector and bioshield (see Figure 1-1).

	A	B	C	D	E	F	G	H	J	K	L	M	N	O	P	R	S	T	U
1			0.58	0.56	0.56	0.54	0.50	0.46	0.44		0.44	0.46	0.50	0.53	0.55	0.55	0.58		
2		0.62	0.61	0.61	0.60	0.57	0.54	0.50	0.51		0.51	0.50	0.54	0.58	0.60	0.61	0.62	0.64	
3	0.65	0.65	0.67	0.68	0.66	0.62	0.59	0.53	0.58		0.58	0.53	0.59	0.63	0.67	0.70	0.69	0.69	0.70
4	0.69	0.71	0.76	0.78	0.75	0.65	0.70	0.71	0.70		0.70	0.71	0.71	0.66	0.76	0.80	0.79	0.76	0.76
5	0.76	0.79	0.85	0.89	0.89	0.87	0.88	0.87	0.82		0.82	0.88	0.89	0.89	0.92	0.92	0.89	0.84	0.83
6	0.84	0.87	0.94	0.99	1.04	1.05	1.04	1.00	0.91		0.92	1.01	1.06	1.07	1.07	1.03	0.98	0.92	0.90
7	0.91	0.95	1.03	1.10	1.16	1.18	1.16	1.10	0.97		0.97	1.10	1.18	1.20	1.19	1.14	1.07	1.00	0.97
8	0.96	1.01	1.09	1.19	1.25	1.27	1.25	1.15	0.98		0.98	1.17	1.26	1.29	1.29	1.23	1.13	1.06	1.02
9	1.01	1.06	1.16	1.26	1.33	1.35	1.31	1.19	0.92		0.93	1.21	1.34	1.38	1.36	1.30	1.20	1.11	1.06
10	1.03	1.09	1.20	1.30	1.38	1.41	1.38	1.25	0.94		0.94	1.26	1.40	1.44	1.41	1.34	1.24	1.14	1.09
11	1.04	1.10	1.21	1.32	1.40	1.44	1.42	1.34	1.11		1.12	1.35	1.45	1.47	1.43	1.35	1.25	1.15	1.09
12	1.03	1.09	1.18	1.30	1.38	1.43	1.45	1.42	1.34	1.28	1.34	1.43	1.47	1.46	1.42	1.34	1.22	1.13	1.08
13	1.00	1.06	1.15	1.25	1.34	1.40	1.43	1.44	1.43	1.43	1.44	1.46	1.46	1.43	1.37	1.29	1.19	1.10	1.05
14	0.96	1.01	1.09	1.17	1.25	1.31	1.35	1.39	1.42	1.42	1.42	1.41	1.38	1.33	1.28	1.21	1.13	1.05	1.01
15	0.91	0.94	1.02	1.08	1.11	1.13	1.20	1.27	1.31	1.33	1.32	1.28	1.22	1.15	1.15	1.12	1.06	0.99	0.96
16	0.85	0.87	0.93	0.98	0.96	0.88	1.00	1.07	1.15	1.19	1.15	1.08	1.02	0.90	0.99	1.01	0.97	0.92	0.90
17	0.81	0.81	0.85	0.88	0.88	0.86	0.87	0.84	0.98	1.04	0.98	0.85	0.89	0.89	0.91	0.92	0.89	0.86	0.86
18		0.78	0.78	0.80	0.82	0.83	0.84	0.84	0.90	0.94	0.91	0.86	0.86	0.86	0.86	0.84	0.83	0.83	
19			0.75	0.75	0.78	0.81	0.84	0.86	0.89	0.91	0.90	0.88	0.87	0.85	0.84	0.81	0.81		

Figure 2-12. Ratio of the Fuel Element Power Density to the Core Average Power Density for HEU M8CAL Half-slotted Core.

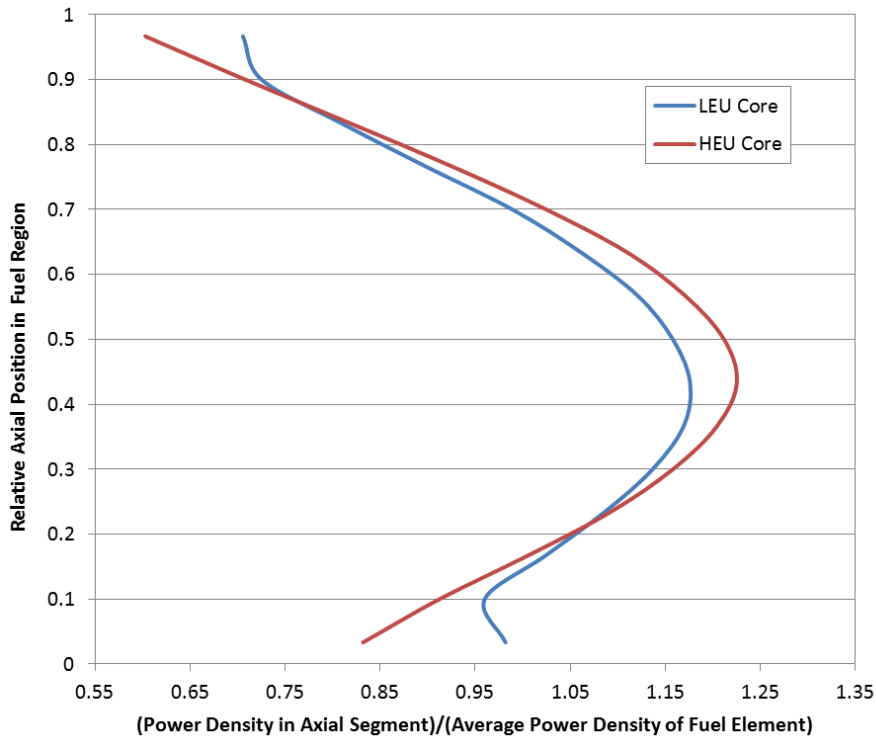


Figure 2-13. Ratio of the Axial Segment Power Density to the Fuel Element Average Power Density for the Hottest Fuel Element for the HEU and LEU Cores

The evaluation of the temperature reactivity feedback of the LEU core (as a function of core energy) requires the simulation of the core using temperature-dependent cross sections. In previous analysis these cross sections were generated using the MCNP utility program MAKXSf, but in the current analysis cross sections produced with NJOY2012 were used. To support this change, the temperature-dependent cross sections developed with MAKXSf and NJOY2012 were first compared, as documented in Appendix A. TREKIN reports 2% higher peak core temperatures with the NJOY2012 method.

The temperature reactivity feedback as a function of core energy dataset provided to TREKIN was generated using the temperature-dependent cross section sets produced with NJOY2012. Using the temperature distributions calculated for every total core energy for the HEU and LEU cores, the temperature reactivity feedback was calculated as the reactivity change from room temperature,  $\frac{1}{k_{COLD}} - \frac{1}{k_{HOT}} \left( = \frac{k_{hot}-k_{cold}}{k_{hot}*k_{cold}} \right)$ . The temperature reactivity feedback as a function of total core energy is summarized in Table 2-24. The total core energy for a peak core temperature of 820°C was reported to be 4677 MJ for the HEU M8CAL core. This value was determined by the TREAT operators as the energy limit for the historic HEU core, by extrapolating the measured energy values for the three experimentally-performed temperature-limited transients. Based on this value, the TREKIN tables were produced for total core energy values ranging from 100 to 5000 MJ.

**Table 2-24. Temperature Reactivity Feedback as a Function of Total Core Energy used in TREKIN for the HEU and LEU Cores.**

Total Core Energy (MJ)	Temperature Reactivity Feedback $\left( \frac{1}{k_{COLD}} - \frac{1}{k_{HOT}} \right), \% \Delta k/k$		LEU / HEU
	HEU	LEU	
100	-0.608%	-0.445%	0.731
200	-1.036%	-0.831%	0.802
300	-1.335%	-1.182%	0.886
400	-1.827%	-1.523%	0.834
500	-2.196%	-1.837%	0.836
1000	-3.741%	-3.275%	0.875
2000	-6.137%	-5.626%	0.917
3000	-8.048%	-7.555%	0.939
4000	-9.679%	-9.211%	0.952
5000	-10.678%	-10.650%	0.997

\* k-eff  $\sigma$  value = 0.00007

For the same total core energy as the HEU core, the LEU core demonstrates a lower temperature reactivity feedback due to its lower core temperature (the higher LEU fuel density results in lower temperature for equal core energy). For equal core-average temperature, the temperature reactivity feedback of the LEU core is higher than that of the HEU core. This is because in the HEU core the temperature reactivity feedback is provided almost entirely by the fuel graphite, while in the LEU core the temperature reactivity feedback has contributions from both the fuel graphite and the Doppler feedback provided by the higher  $^{238}\text{U}$  content. Table 2-25 presents the temperature reactivity feedback for both cores for equal core-average temperature.

Table 2-25. Temperature Reactivity Feedback as a Function of Core Average Temperature for the HEU and LEU Cores.

Core Average Temperature (°C)	Temperature Reactivity Feedback $(\frac{1}{k_{COLD}} - \frac{1}{k_{HOT}}), \% \Delta k/k$		LEU / HEU
	HEU	LEU	
100	-1.713%	-1.725%	1.007
200	-3.852%	-3.910%	1.015
300	-5.806%	-5.986%	1.031
400	-7.600%	-7.938%	1.044
500	-9.330%	-9.738%	1.044
600	-10.518%	11.415%	1.085

\* k-eff  $\sigma$  values = 0.00007

#### 2.2.1.4 Impact of Core Temperature on M8CAL PCF

As the temperature of the TREAT core changes, the ratio of the number of fissions occurring in the test sample per fission neutron produced in the core changes, resulting in a different PCF. An initial study of this behavior was previously performed for the HEU core [19]. In the current analysis, simulations were performed to calculate how the PCF changes in the HEU and LEU cores with increasing core energy (and consequently core temperature), to evaluate the changes of the LEU PCF relative to the HEU. These simulations were performed using the same energy steps and temperature distributions as the temperature reactivity feedback analysis.

As in the previously-discussed analyses, the test-sample PCF values in the HEU and LEU cores were calculated as the ratio of the fission rate in the test sample to the core fuel average energy deposition, with simulations performed for increasing core temperatures. These simulations were performed with the control/shutdown rod bank inserted at the pre-transient position (~50% withdrawal in this case) and the transient and compensation/shutdown rod banks fully withdrawn. The temperature distribution was calculated for total core energy values ranging from 100 to 5000 MJ, starting from a cold core and using the MCNP-calculated relative power distribution. The TREAT fuel fission energy was assumed to all be absorbed locally (the F7 tally was used in MCNP), and the heating of the fuel was approximated as adiabatic without considering heat transfer mechanisms. A single test pin was modeled at the center of the M8CAL vehicle, filled with the T-462 pin composition. It should be noted that the increasing energy steps assumed a fixed composition and location of the test sample.

The ratio of the ‘hot’ to ‘cold’ PCF calculated for the HEU and the LEU cores is presented in Table 2-26 and Table 2-27, respectively. As the temperature of the core increases, more neutrons are “leaking” towards the test sample, causing an increase in the PCF. Due to the differences between the neutron spectrum of the HEU and LEU cores, the behavior of the PCF with core temperature is not the same. Therefore, the PCF performance of the LEU core relative to the HEU core also depends on the core temperature.

Table 2-26. Hot to Cold PCF for the HEU Core as a Function of Total Core Energy and Peak Core Temperature.

Total Core Energy (MJ)	HEU Peak Core Temperature (°C)	PCF <sub>HOT</sub> / PCF <sub>COLD</sub>
0	26.0	1.00
100	63.8	1.02
200	96.9	1.04
300	126.9	1.05
400	154.7	1.08
500	180.8	1.09
1000	295.1	1.15
2000	484.9	1.27
3000	652.4	1.36
4000	808.9	1.45
5000	957.7	1.49

\* Statistical relative error in PCF values = 0.49%

Table 2-27. Hot to Cold PCF for the LEU Core as a Function of Total Core Energy and Peak Core Temperature.

Total Core Energy (MJ)	LEU Peak Core Temperature (°C)	PCF <sub>HOT</sub> / PCF <sub>COLD</sub>
0	26.0	1.00
100	56.5	1.02
200	84.8	1.03
300	110.9	1.06
400	135.4	1.07
500	158.7	1.07
1000	262.2	1.14
2000	435.5	1.24
3000	587.9	1.33
4000	730.1	1.41
5000	866.4	1.46

\* k-eff  $\sigma$  values =

To demonstrate the temperature-dependence of the LEU core performance relative to the HEU, the LEU-to-HEU PCF ratio was calculated as a function of core energy, assuming that the initial cold-core PCF of the LEU core was 90% of the corresponding HEU core PCF (a 10% decrease in performance,  $\frac{PCF_{LEU}}{PCF_{HEU}} = 0.9$ ). This case was selected as it bounds the worst PCF ratio observed in this study (the unrealistic factor of 5 increase in the experiment vehicle density, which produced a ratio of ~91%). In order to achieve equal energy deposition in the test sample, the LEU core would need to produce higher core energy, and based on the ratio of the PCF for the cold core condition, the necessary LEU core energy would be  $\frac{Core\ Energy_{HEU}}{90\%}$  (i.e., the LEU core would need to produce 1/0.9=1.111 times higher energy). Following this scheme, the energy production by the LEU core was calculated, along with the peak core temperature and the PCF.

Table 2-28 shows the change of the LEU-to-HEU PCF ratio as a function of equal test-sample energy deposition assuming a fixed 1.11 LEU-to-HEU core energy ratio. Relative to the assumed LEU-to-HEU PCF ratio of 90%, which was used in determining the required core energy, the last column in the table indicates that there will be an additional 2-3% decrease in the core performance (PCF ratio) as the core temperature increases which should be taken into account (although the peak core temperature would still be lower in the LEU core than in the HEU core).

**Table 2-28. LEU-to-HEU PCF Ratio for Equal Energy Deposition in the Test Sample for a 10% Decrease in the Cold-Core Performance of the LEU Core**

HEU Total Core Energy (MJ)	LEU Total Core Energy (MJ)	HEU Peak Core Temperature (°C)	LEU Peak Core Temperature (°C)	PCF <sub>LEU</sub> / PCF <sub>HEU</sub>
100	111	64	60	88%
200	222	98	91	87%
300	333	128	119	88%
400	444	156	146	87%
500	556	182	171	86%
1000	1111	297	283	87%
2000	2222	489	471	87%
3000	3333	658	636	87%
4000	4444	816	791	87%
5000	5556	966	942	87%

## 2.2.2 Transient Calculations - Matching the HEU Performance

The historic HEU core shaped transient #2874, which was performed in the M8CAL experiment series, was chosen as the reference case for evaluating the performance of the LEU core. This transient used the maximum allowed reactivity value. The performance requirement for the LEU core is to produce the same test-sample TED that can be produced in the HEU core, while at the same time satisfying all operational safety requirements. As previously indicated, the HEU core has 600°C and 820°C peak core temperature limits under normal and accident conditions, respectively. Those limits, which were established for the Zircaloy-3 cladding in the HEU core, have been retained for evaluation of the LEU conceptual design with Zircaloy-4 cladding. The LEU power-time history needed to match the TED achievable in the #2874 transient was evaluated using equation 2.1.

$$\begin{aligned}
 \text{TED}_{\text{HEU}} = \text{TED}_{\text{LEU}} &\Rightarrow \text{Power}_{\text{HEU}} \times \text{PCF}_{\text{HEU}} = \text{Power}_{\text{LEU}} \times \text{PCF}_{\text{LEU}} \Rightarrow \\
 &\Rightarrow \text{Power}_{\text{LEU}} = \text{Power}_{\text{HEU}} \times \frac{\text{PCF}_{\text{HEU}}}{\text{PCF}_{\text{LEU}}} \quad (2.1)
 \end{aligned}$$

This approach conservatively assumes that the LEU core's test sample power-time history (rather than just the TED) must be the same as that of the planned HEU experiment (and therefore it is not sufficient to just operate the LEU core at the same power level as the HEU core for a longer period of time). To ensure that the analysis encompassed the full range of feasible experiments and their associated power coupling factors, a series of computations were performed to evaluate the power-time history and total core energy in the LEU core as a function of PCF, using for this purpose  $\frac{\text{PCF}_{\text{LEU}}}{\text{PCF}_{\text{HEU}}}$  ratios of 80%, 85%, 90%,

95% and 100%. The corresponding calculated LEU power-time histories needed to match the HEU shaped transient test-sample TED are shown in Figure 2-14. It should be noted that the lower bound of this analysis included PCF ratios which are below the lower limit of the range of PCF ratios calculated for the set of experiments evaluated in the conceptual design analysis. These lower PCF cases were included to support bounding the analysis and to provide further characterization of the LEU core behavior.

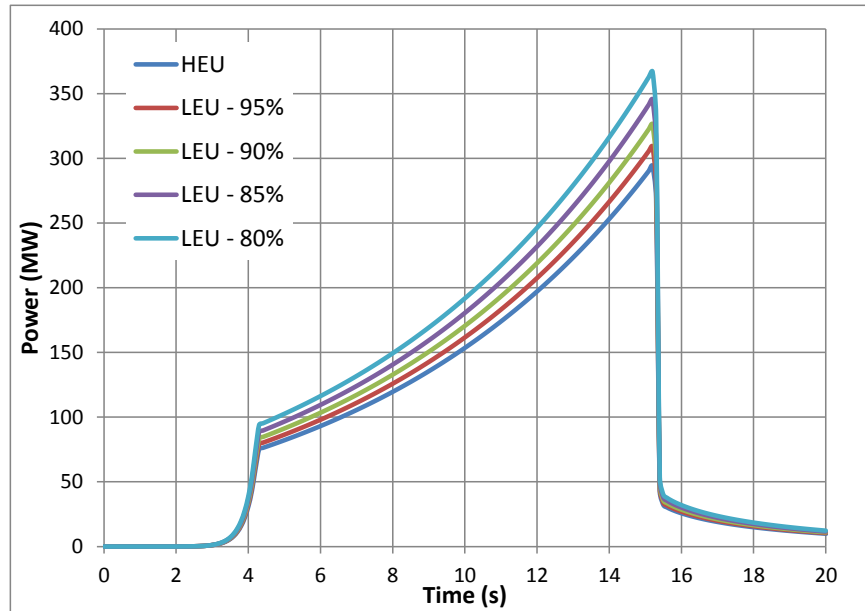


Figure 2-14. HEU and the Scaled LEU Power-Time History Curves for the Different Relative-to-HEU PCF Values

Using the scaled power-time histories as an input, the reactivity needed in the LEU core for each PCF ratio was calculated with TREKIN power-driven simulations. For each of these normal operation scenarios, the peak fuel temperature values were also noted (representing the peak core temperature under normal conditions, for which the 600°C limit would apply in the HEU core).

The next step taken was to evaluate the reactivity accident scenario corresponding to each case. In the accident scenario simulations, all of the available reactivity before performing the shaped transient is assumed to be inserted as a step, producing a temperature-limited transient (that is, instead of withdrawing the transient rod bank as planned to achieve the required power-time history, the bank is withdrawn at its maximum speed). Table 2-29 shows the peak core temperature under normal (“operational”) and accident conditions for the different  $\frac{PCF_{LEU}}{PCF_{HEU}}$  ratio scenarios. Figure 2-15 shows the accident scenario power pulses. Due to the longer prompt generation lifetime, the LEU core has wider pulses with longer reactor periods, as compared to the HEU core.

Table 2-29. Operational and Accident Peak Temperatures for the Total Core Energies Calculated with TREKIN in Power-Driven and Temperature-Limited Transient Simulations respectively,, for Multiple LEU-to-HEU PCF Scenarios.

Core	PCF <sub>LEU</sub> /PCF <sub>HEU</sub>	Pre-Transient Available Reactivity %Δk/k	Operational Conditions		Accident Conditions	
			Peak Temperature (°C)	Total Energy (MJ)	Peak Temperature (°C)	Total Energy (MJ)
HEU	100%	5.950%	471	1898	839	4149
LEU	100%	5.370%	419	1899	733	4018
	95%	5.570%	435	1999	761	4226
	90%	5.787%	453	2109	793	4458
	85%	6.025%	472	2233	828	4718
	80%	6.288%	494	2372	868	5014

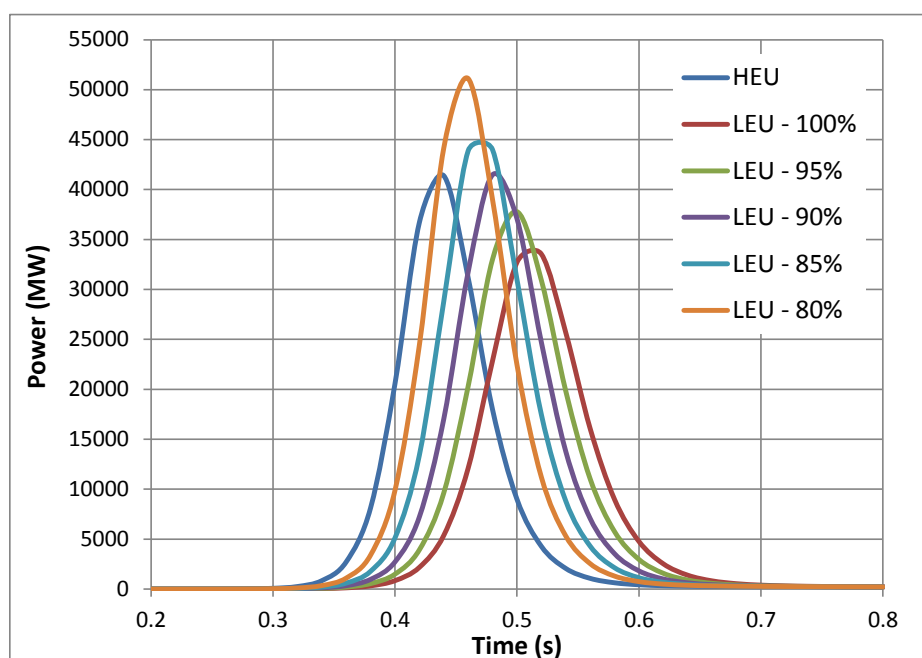


Figure 2-15. Power Pulse Created after Accidental Step Insertion of the Pre-Transient Available Reactivity for the HEU and the LEU Core and for the Different Relative-to-HEU PCF.

For the  $\frac{PCF_{LEU}}{PCF_{HEU}}$  ratios determined in the current analysis for a range of experiments (Section 2.1.3), the accident scenario temperatures are below the 820°C temperature limit. The evaluated experiments all had cold-core LEU-to-HEU PCFs which were 95% and above, with the exception of the scenario of an unrealistically high-absorbing experiment vehicle, which had a PCF ratio of 91%. However, it was also observed that the PCF increases with temperature, with a slightly greater PCF increase in the HEU core (for the particular evaluated experiment) than in the LEU core. The PCF ratio therefore may worsen by with increasing core energy generation (but this effect was shown to be very small (2-3%) for the evaluated experiment). More detailed analysis of the PCF for a wider range of experiments and core conditions will be performed in the upcoming Preliminary Phase of the conversion. The operational peak core temperatures for all of the evaluated LEU cases were well below the 600°C limit and were comparable to the HEU core.

### 2.2.3 Full Width at Half Maximum (FWHM)

In order to further characterize the LEU core, the properties of a planned temperature-limited transient, including the FWHM, were evaluated. The minimum FWHM achievable in TREAT is of interest because some experiments need a narrow pulse in order to replicate as closely as possible the conditions a sample might experience in a power reactor accident (in particular, reactivity-initiated accident (RIA) conditions).

The FWHM was first calculated for the HEU core temperature-limited transient that approaches the HEU core LSSS temperature limit of 600°C. This represents the maximum-energy planned transient that could be performed in the HEU core. Using the LEU-to-HEU PCF ratio, the reactivity step insertion in the LEU core was calculated with TREKIN as the value needed to match the HEU core TED in a test sample. For this analysis, the reactivity insertion value was varied until the LEU total core energy became equal to the value needed to match the test-sample TED, as determined by the ratio of the PCF values. As in the previous analysis, the LEU energy needed was evaluated as the HEU total core energy divided by the LEU-to-HEU PCF ratio. Again PCF ratios of 80%, 85%, 90%, 95% and 100% were considered in the analysis, although all current experiment analyses yield ratios greater than 90%. The TREKIN results are summarized in Table 2-30. It should be noted that for planned temperature-limited transients, the core-accident transient is the same as the operational transient.

**Table 2-30. Full Width at Half Maximum (FWHM) for Step Reactivity Insertion to Match the Test Fuel Energy Deposition for Different Relative-to-HEU Power Coupling Factors (PCF).**

Core	$\frac{PCF_{LEU}}{PCF_{HEU}}$	Step Reactivity Insertion	Total Core Energy (MJ)	Peak Core Power (MW)	Peak Core Temperature (°C)	FWHM (s)
HEU	100%	4.190%	2497	16360	575	0.108
LEU	100%	3.763%	2497	13671	513	0.129
	95%	3.915%	2629	14926	533	0.125
	90%	4.080%	2776	16868	555	0.118
	85%	4.260%	2939	18986	579	0.112
	80%	4.459%	3123	21286	606	0.107

The LEU core produces wider pulses (higher FWHM) due to the longer prompt neutron generation lifetime, which corresponds to longer reactor periods. The lower the LEU PCF, the higher the reactivity step insertion required to provide an equal TED in the test fuel sample, resulting in shorter FWHM values. The power pulses corresponding to the cases documented in Table 2-30 are shown in Figure 2-16.

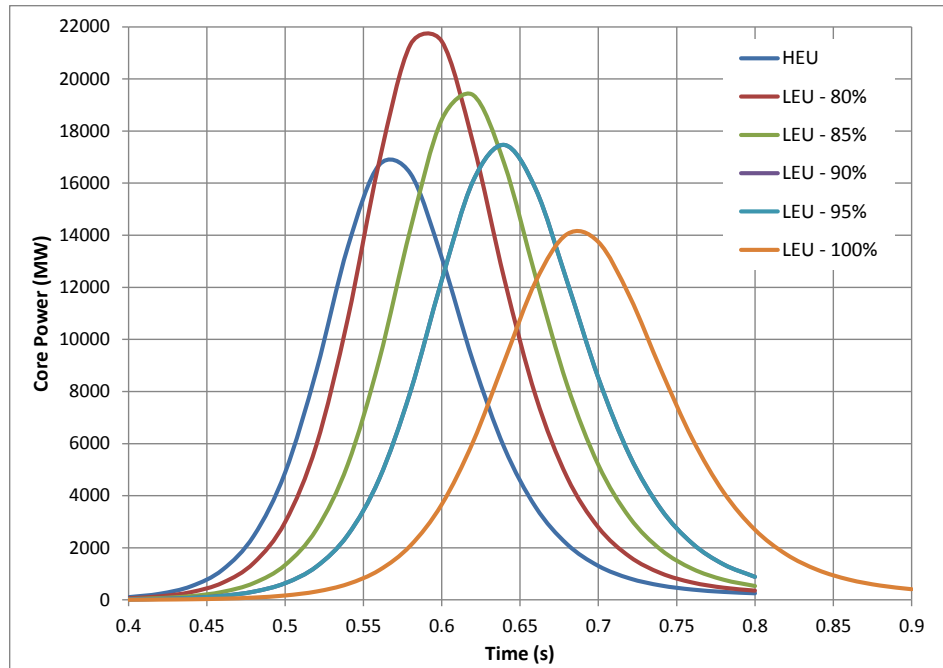


Figure 2-16. Power Pulse after Step Reactivity Insertion for the HEU and the LEU for the Different Relative-to-HEU PCF Matching the Test Fuel Energy Deposition.

### 3 Thermal Hydraulic Analyses

The following thermal-hydraulic analysis focuses on studies intended to examine the impact of thermal and mechanical properties on metal loss (by oxidation) and peak fuel and cladding temperatures for various scenarios. In the current LEU design, the compaction process planned for the fuel manufacture limits the length of the individual fuel blocks to approximately four inches. The effect of axial thermal contact resistance, both between adjacent fuel blocks and between the fuel and axial graphite reflectors, on cooling times was evaluated for normal operation and accident case scenarios.

Normal operation encompasses peak fuel temperatures ranging from ~250°C during constant power operation up to 600°C, which reflects the current administrative limit for the HEU core. Operational peak fuel temperatures ranging from 400°C to 600°C were considered in this study. During normal operation, the reactor is always assumed to be convectively cooled by air at flow-rates up to 6000 cfm. The accident scenario assumes no flow conditions and that all of the reactivity available at the beginning of the planned bounding shaped transient is inserted as a step. As in the TREKIN analysis, multiple LEU core accident energies and corresponding temperatures were considered. Peak fuel temperatures between 700°C and 820°C were investigated in the accident analyses. For each cooling time history, the cumulative metal loss of the cladding was evaluated based on post-transition corrosion kinetics. The work presented in this study evaluates the oxidation which occurs in a single experiment or accident, but lifetime oxidation analysis (assuming a given multi-year operating history) is being performed by the fuel design team at INL.

### 3.1 Model Description

Cooling time histories evaluated for a single fuel assembly have been analyzed with a 3D transient thermal-hydraulic (TH) model using the COMSOL® code [16]. Details of the model used to analyze HEU and previous LEU designs can be found in earlier reports [2, 3]. This prior work included benchmarking of the HEU fuel element model against historic SINDA/G models and (these SINDA/G models in turn were validated by previous TREAT analysts against measurements taken in a small core loading during the early stages of TREAT operation) [3]. The model has been adapted to reflect the current LEU design dimensions and parameters for the conceptual design phase and is briefly described in the following sections.

Figure 3-1 below shows a schematic of a fuel assembly and its cross section including some key dimensions of the modeled geometry. Assuming negligible heat transfer between neighboring fuel assemblies, symmetry is utilized for the geometrical domain (a 1/8<sup>th</sup> section of the fuel assembly is modeled). The central section of the fuel assembly consists of twelve vertically stacked four-inch tall blocks to generate a four-foot fuel section. In direct contact, above and below the fuel section, are two ~24 inch long blocks of graphite reflector.

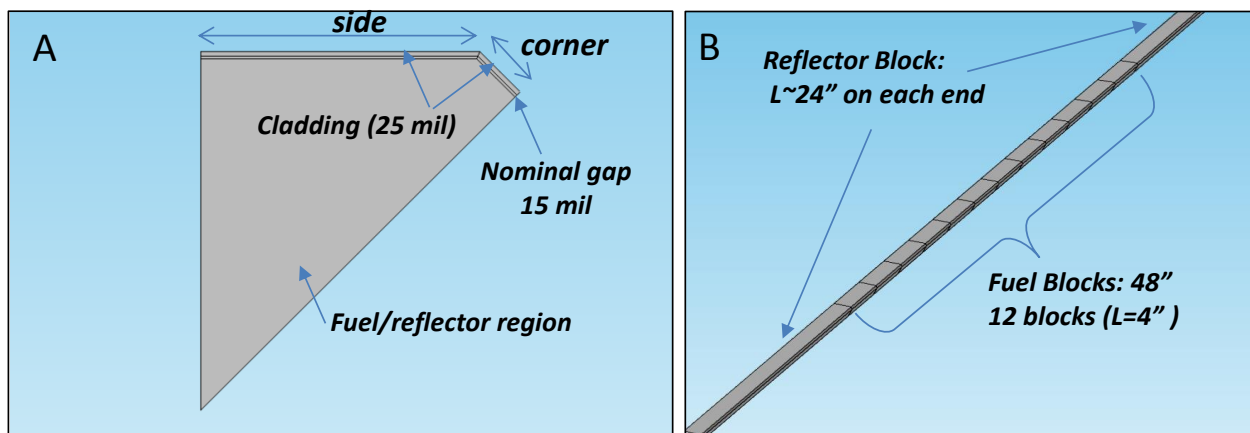


Figure 3-1. COMSOL® geometry and dimensions of a single TREAT LEU fuel assembly. A) Cross-sectional view, B) Axial view showing reflector and fuel block region.

A single 25-mil thick can of Zircaloy-4 is used for the cladding material for the entire fuel assembly and is separated by a 15 mil nominal gap around the entire fuel and reflector block circumference. For the current LEU design, the total cross-sectional areas of both the fuel and reflector blocks respectively have been increased (relative to the HEU fuel) to a nominal area of 14.699 sq-in.

Three-dimensional conduction heat transfer is modeled within the fuel, reflector, and cladding regions. The model also includes thermal contact resistance between regions of direct contact, i.e., between individual fuel blocks, between fuel and reflector regions, between the fuel and cladding, and between the reflector and cladding where applicable. Thermal radiation is modeled across the entire gap. The gap is not maintained around the full periphery of the fuel in actual operation because the cladding, which will be evacuated during fuel assembly manufacture, will be pushed against the fuel by atmospheric pressure during high-temperature operation. This effect is not relevant neutronically but does have an impact on the thermal analysis. Structural analyses performed by the INL team estimated that 43% of the cladding side wall section would deflect inwards and be in direct contact with the fuel/reflector

blocks. Heat transfer between cladding and fuel/reflector is therefore modelled by assuming both thermal radiation and conduction for the part of the cladding that is in direct contact with graphite.

The effect of can wall deformation was modelled using an anisotropic gas-phase conductivity in the gap between cladding wall and fuel. The conductivity of the gap was set to zero (perfect vacuum) in the transverse direction as well as in the normal (perpendicular to the wall) direction where the can wall is not in contact with the wall. For the case where part of the side cladding wall contacts the fuel element (43%), a high conductivity was used to ensure thermal equilibrium between fuel/cladding. Variation of the cladding thickness due to deformation was neglected.

To summarize the thermal hydraulic analysis, during normal operation there is heat transfer to the the flowing air coolant, which then removes the heat from the core. During the accident scenario it is assumed that there is zero air flow (both blowers are assumed to fail and in addition natural convection is conservatively ignored). In this accident scenario the fuel and cladding are therefore in thermal equilibrium, and the only mode of cooling is via axial conduction (with heat loss radially across the core also conservatively ignored when evaluating the fuel element temperature time-history).

## 3.2 Analyses Assumptions and Parameters

### 3.2.1 Cooling

During normal operation, the reactor is cooled by an induced draft air system that includes two 40-hp turbo-compressors operating in parallel. Each turbo-compressor is rated at 3250 cfm [6]. For the reference TH model, the nominal flow-rate for each turbo-compressor assumes 92% of its 3000 cfm rated capacity. Approximately 90% of the total air flow enters the core (the rest of the flow being diverted to the permanent reflector). Because of the large inlet plenum above the core, it is reasonably assumed that the flow is distributed equally among all assemblies. The majority of the flow that passes through the core, approximately 96%, is distributed to coolant passages formed by the chamfered corners of neighboring assemblies [4]; the remaining 4% passes along the small gaps between assembly sides. During the design basis accident, in which there is an accidental insertion of reactivity, cooling by the filtration/cooling system (F/CS) is assumed to be unavailable, and natural convection is also neglected. Consequently, the only mode of cooling assumed in the fuel assembly during the accident is due to axial conduction (consistent with previous LEU design analysis [2]).

### 3.2.2 Thermal Properties

With exception of the fuel density (which is  $1.85 \text{ g/cm}^3$  for the current design but had a lower assumed value in some previous analysis cases), all other properties such as heat capacity, conductivity, etc. remain the same as for previously-considered LEU design options and base case values [3]. Contact resistance is a measurable quantity that strongly depends on many properties such as contact pressure, surface roughness and temperature. The only currently-available data on contact resistance between graphite surfaces applicable to this analysis are preliminary experiments performed by LANL [21] using B&W compacts; experimental results are shown in Figure 3-2. Contact resistance was measured for two disks in contact with no contact pressure for both as-formed as well as machined surfaces. For cooling time history calculations, contact resistance between graphite blocks varied from  $4 \times 10^{-4} \text{ m}^2 \text{ K W}^{-1}$  (lower bound) to  $5 \times 10^{-3} \text{ m}^2 \text{ K W}^{-1}$  (conservative, upper-bound value). Cooling time histories assuming no contact resistance were analyzed as well for a conservative comparison. For the regions where the cladding is in

direct contact with graphite, a low contact resistance was assumed to ensure equal temperature at that interface.

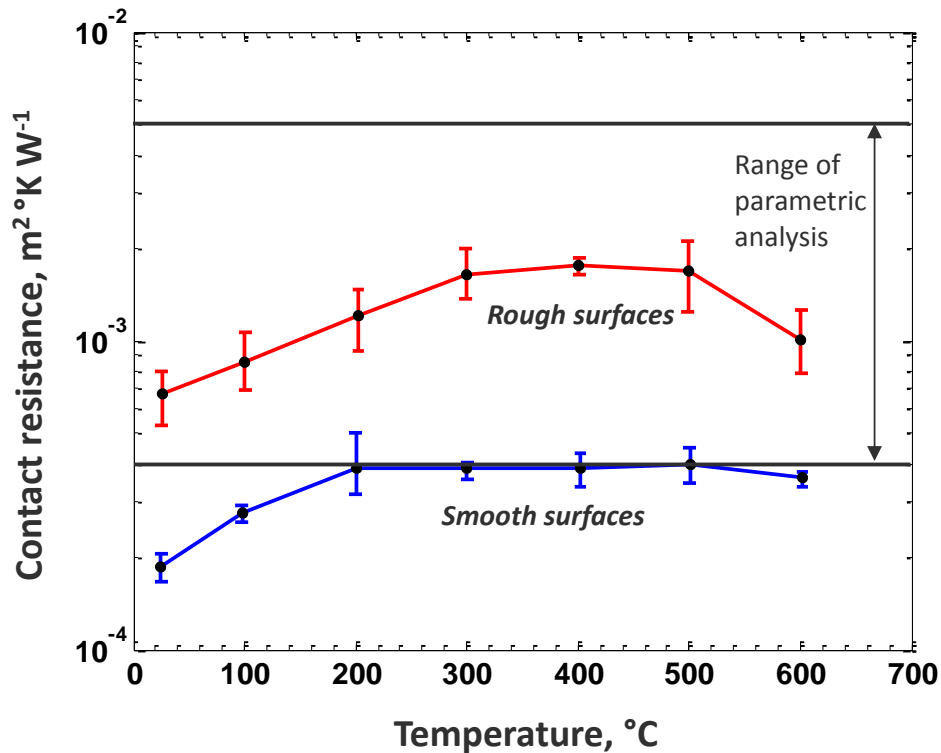


Figure 3-2. Contact Resistance Measured at LANL [21] using two B&W Compacts with no Pressure; measurements Performed for as-formed Surfaces as well as Machined Surfaces.

### 3.2.3 Peak Fuel Temperatures

For normal operation, cooling time histories for shaped transients leading to peak fuel temperatures between 400 – 600 °C were analyzed. This covers a wide range of possible experiments and associated power coupling factors. For the bounding accident case it is assumed that all the available reactivity before a planned experiment is inserted as a step. The accident analysis considered peak fuel temperatures between 700 – 820 °C. As discussed previously, in the HEU core, there is a temperature limit during normal operation (LSSS) of 600°C (operationally applied as a 575°C limit), and an accident scenario temperature limit (SL) of 820°C.

During most typical transients, heat is generated in the fuel nearly adiabatically, with little time for heat transfer from fuel to cladding. The cladding begins to be heated after most of the transient energy has been generated [2]. Figure 3-3 below shows the (MCNP-calculated) LEU axial power profile (normalized to an axial-average of unity) and peak fuel temperature of the hottest fuel assembly as a function of total core energy. The axial profile is non-symmetric due to the partial insertion of the control rods (from the top of the core). This power profile was assumed throughout the analyses outlined in this discussion. The initial temperature profile of the fuel section is established from the total core energy, the energy deposited in the hottest assembly as fraction of total core energy (0.44%), and the MCNP-calculated LEU axial power profile. Thus as an initial condition, all energy is assumed to be deposited

instantaneously in the fuel part of the assembly. For normal operation, the cladding and axial reflectors are assumed to initially be at ambient conditions ( $T=25^{\circ}\text{C}$ ). For added conservatism, the cladding for the accident case scenario is assumed to be in thermal equilibrium with the fuel after the power pulse but before cooldown begins.

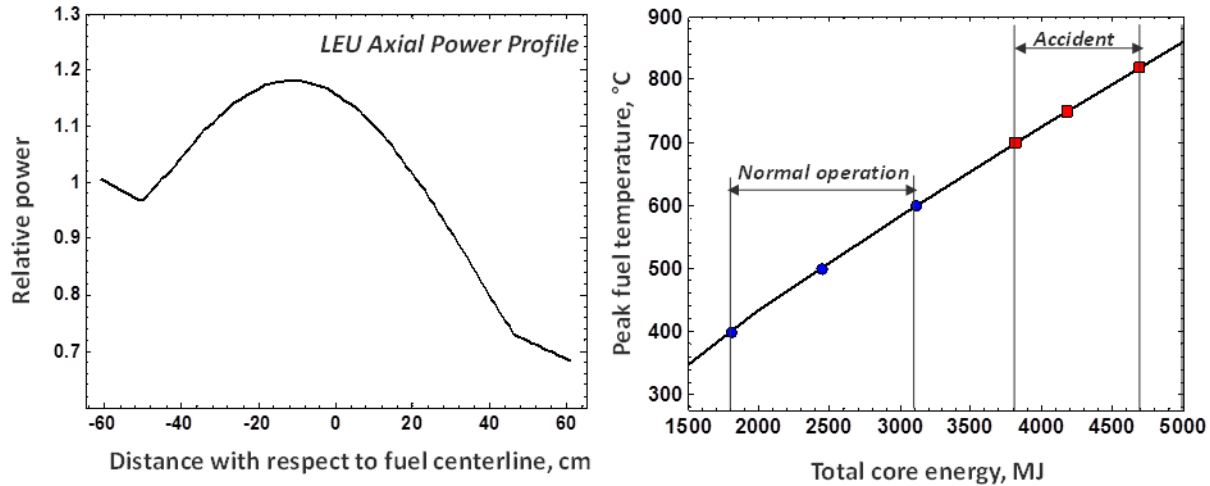


Figure 3-3. LEU Axial Power Profile and Peak Fuel Temperatures as a Function of Total Core Energy; peak Fuel Temperatures Established from the Energy Deposited to the Hottest Assembly.

### 3.2.4 Corrosion Kinetics

For each cooling time history, the cumulative oxidation (or corresponding metal loss) of the cladding was evaluated. This was to demonstrate the relationship between cooling rates and the spatial magnitude of corrosion of the cladding.

The weight gain kinetics of zirconium and its alloys generally fall into two ranges, referred to as pre- and post-transition regimes [22]. During the initial, pre-transition oxidation, the kinetic growth rate is usually controlled by cubic or parabolic kinetics and the reaction progresses by oxygen transport through a growing oxide layer. As long as the growing layer remains protective, solid-state diffusion is the limiting mechanism for zirconium alloy oxidation. In the post-transition regime, during which the oxide scale breaks down, oxidation rates increase and transition to linear kinetics. All rates used for the oxidation kinetics in the following analyses are concerned only with the post-transition regime. Use of such kinetics may be viewed as conservative for periods where the cladding has not yet attained the post-transition region.

The post-transition oxidation kinetics are described by an expression of the following form:

$$\frac{d\Delta W}{dt} = A_0 \times e^{\left(\frac{-E}{RT}\right)} \quad (3.1)$$

where,

$\Delta W$  = Relative cladding weight gain,  $\text{mg cm}^{-2}$

$A_0$  = Post-transition rate constant,  $2.343 \times 10^3 \text{ mg cm}^{-2} \text{ s}^{-1}$

$E$  = Activation energy for the post-transition region,  $129.64 \text{ kJ mol}^{-1}$

$R$  = Universal gas constant,  $8.3144 \text{ kJ mol}^{-1} \text{ K}^{-1}$

The above expression and rate constants represent the post-transition oxidation rates for Zircaloy-2 in air (as provided in the HEU core FSAR, which documents data for Zircaloy-2 as a comparison to the HEU fuel's cladding material, Zircaloy-3). Figure 3-4 below compares the corrosion rates for Zircaloy-2 with corrosion rates in air (post-transition) for Zircaloy-4 [23-25].

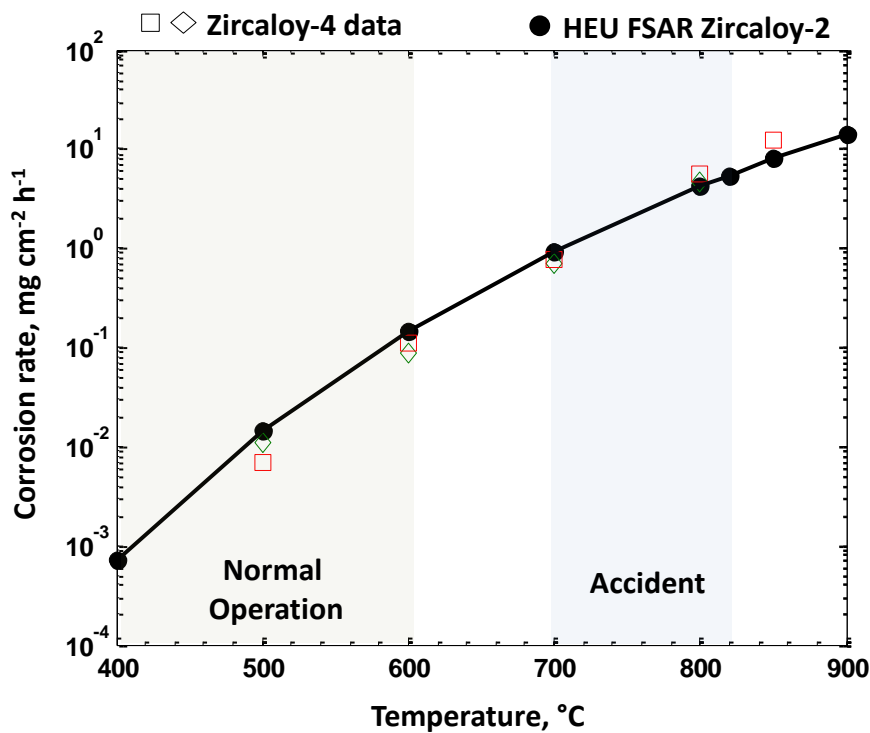


Figure 3-4. Post-transition Corrosion Rates in Air as Function of Temperature, HEU FSAR Zircaloy 2 Rates Compared with Corrosion Rates for Zircaloy-4 (open symbols); Line Corresponds to the Rates as Calculated Using Expression (3.1).

Taking into account the different alloys and protocols used to measure the oxidation rates, the rates for Zircaloy-2 agree well with published data in the literature for Zircaloy-4. For the temperature limits considered in this analyses ( $T < 820 \text{ }^{\circ}\text{C}$ ), use of equation 3.1 should yield reasonable rates for the oxidation of the cladding. However, care should be given when interpreting the laboratory-measured rates for life-cycle analyses relevant to reactor operation, because a) irradiation effects are absent and b) corrosion rates below  $400 \text{ }^{\circ}\text{C}$  are often extrapolated from measurements at higher temperatures due to the very long times required to establish post-transition kinetics.

### 3.3 Results

#### 3.3.1 Normal Operation

Figure 3-5 below shows cooling time histories during normal operation for the case of no contact resistance and with 6000 cfm air cooling flow rate through the reactor. Cooling time histories are calculated for initial peak fuel temperatures between 400-600 °C. It should be noted that the term contact resistance here forth refers only to the resistance between individual fuel blocks and between fuel and reflector regions.

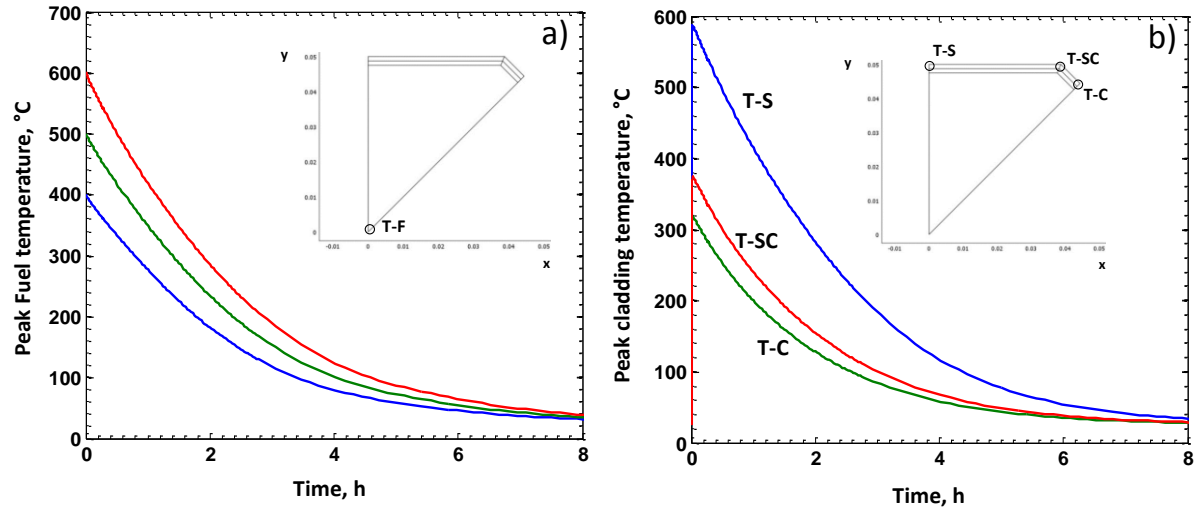


Figure 3-5. Cooling Time Histories for Normal Operation with 6000 cfm of Cooling, a) Peak Fuel Temperatures as function of Cooling Time, Initial Peak Fuel Temperatures of 600 (red), 500 (green) and 400°C (blue), and b) Temperature of the Cladding at Three Different Locations as function of Cooling Time (for 600°C Peak Fuel case).

During the first several hours of cooling, when the temperatures and corresponding temperature gradients remain high, peak fuel temperatures (T-F) are reduced at a higher rate and gradually level off with time. Near-ambient temperatures are obtained after approximately 6 to 8 hours of cooling, depending on the initial temperature of the fuel. Peak temperatures shift axially with time but remain close (~1 to 2 inches) to the location of the axial peak power, as was shown in Figure 3-3, above.

The corresponding peak cladding temperature as a function of cooling time is shown in panel b of Figure 3-5. This plot shows only the results for the case in which the initial peak fuel temperature is 600°C. Here, the temperature is shown at three different locations along the periphery of the cladding, denoted as T-S, T-SC, and T-C respectively (side, side/corner, and corner points). The temperature of the cladding at the side location increases quickly until it reaches thermal equilibrium with the fuel. At that point, the time for that region of the cladding to cool down to near ambient temperature is nearly the same as for the peak fuel temperature. In contrast, the section of the cladding at the corner region (T-SC and T-C), which is where the majority of the cooling occurs, remains substantially cooler. The highest corner cladding temperatures are approximately 200-280 °C lower than the initial peak fuel temperature. Heat flux to the cladding corner is primarily limited by the rate of thermal radiation from the fuel and, to some extent, heat conduction from the side region of the cladding.

Cooling time histories are naturally affected by the amount of flow through the reactor. Reducing the flow to 3000 cfm (one blower in operation versus two) increases the cooling time to 100°C by ~40%, as shown in Figure 3-6.

Reducing the flow rate to 3000 cfm also increases the maximum temperature of the corner section of the cladding by an additional 80-100°C. Regardless of the amount of air flow, contact resistance (CR) had a small effect on cooling times. Even with a conservative value of contact resistance ( $5e-3 \text{ m}^2 \text{ K W}^{-1}$ ), the cooling times increased by less than 10%.

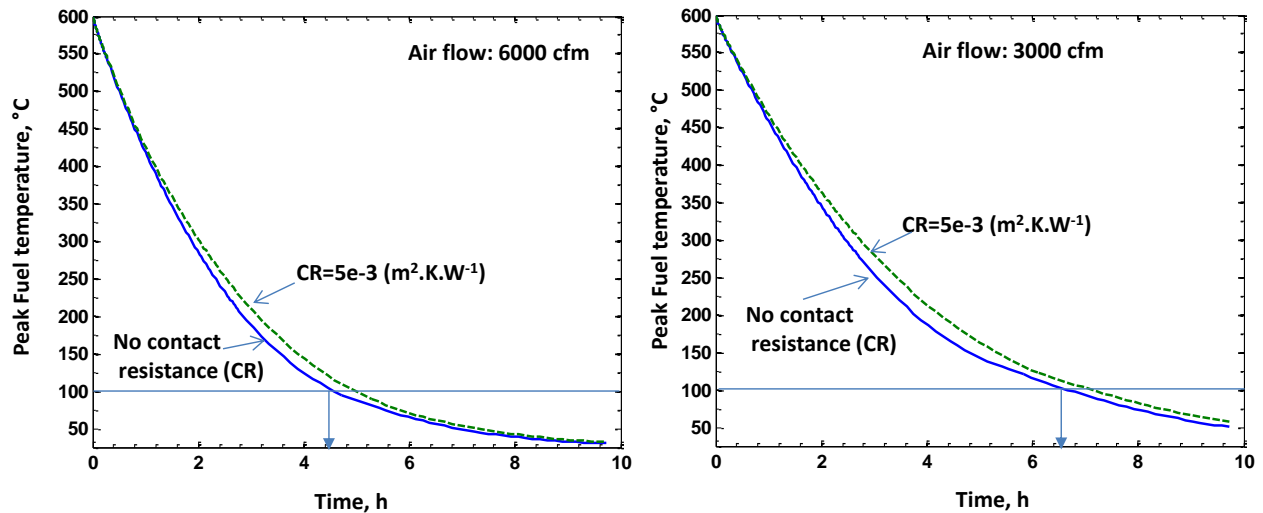


Figure 3-6. Effect of Contact Resistance and Air Flow through the Reactor on Cooling Time Histories; Case Above Shown for a Peak Fuel Temperature of 600 °C.

The amount of oxidation of the cladding will depend on the cumulative temperature-time history that the cladding has experienced. The cumulative loss of metal<sup>2</sup>, i.e. thinning of the cladding, is shown in Figure 3-7 as function of axial distance and initial peak fuel temperature ( $T-F_{max}$ ). For this case, cooling to room temperature was achieved with one blower only (3000 cfm). As also shown schematically in the cross-sectional plots, the metal loss is shown for the side region (T-S) of the cladding. This is the location of the cladding that will exhibit the highest temperatures during cooling. For comparison, the axial temperature profiles of the cladding (T-S) as function of time is also shown in Figure 3-8 (starting from an initial peak fuel temperature,  $T-F_{max}$ , of 600 °C).

Most of the corrosion of the cladding, of course, occurs in the fuel section of the assembly where the cladding is hottest. The metal loss peaks near the fuel mid-plane and decreases rapidly to virtually zero near the reflector region. As shown in Figure 3-8, the cladding at the lower (LR) and upper (UR) reflector regions remains at low temperatures, well below 300 °C, where oxidation rates are negligible. Most of the metal loss in the fuel region of the assembly will occur in the initial stages of cooling when

<sup>2</sup> According to the HEU FSAR, the loss of metal in mils is obtained by multiplying the weight gain of the cladding by 0.176. This is realized from the stoichiometry of the reaction,  $Zr + O_2 \rightarrow ZrO_2$ , and that the weight gain refers to the uptake of oxygen.

temperatures remain high. Once temperatures are below 500 °C, corrosion rates are substantially reduced.

For every 100°C decrease in temperature, corrosion rates are reduced by approximately an order of magnitude. Therefore, as the initial peak fuel temperature is decreased, the metal loss of the cladding follows the expected trend, as shown in Figure 3-7.

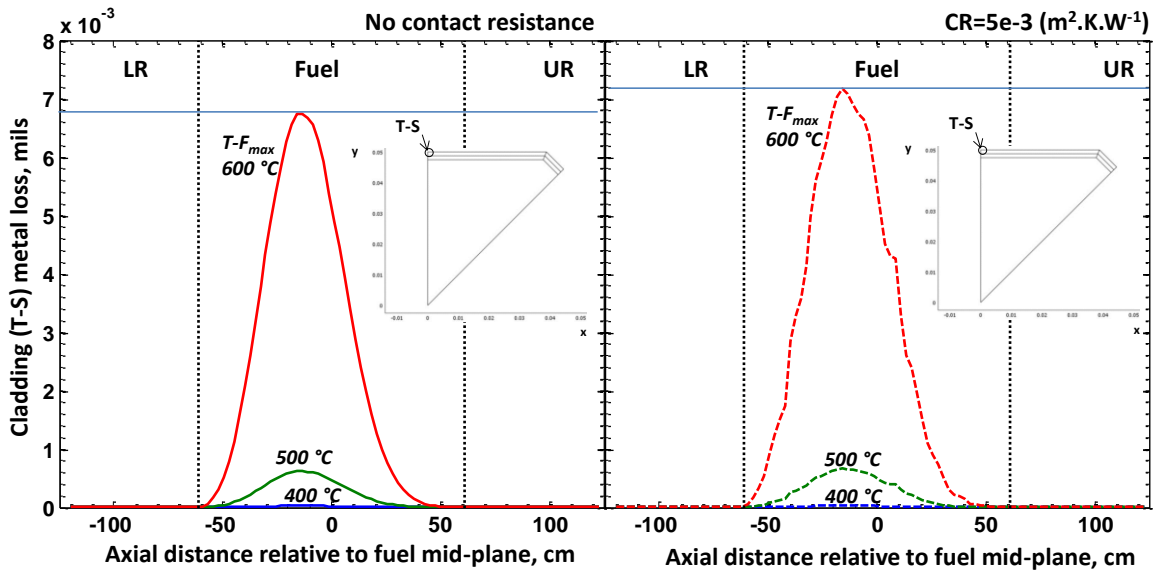


Figure 3-7. Axial Variation of Cladding (T-S) Metal Loss as Function of Peak Fuel Temperature and Contact Resistance; Cooling to Ambient Conditions was Achieved with One Blower in Operation (3000 cfm).

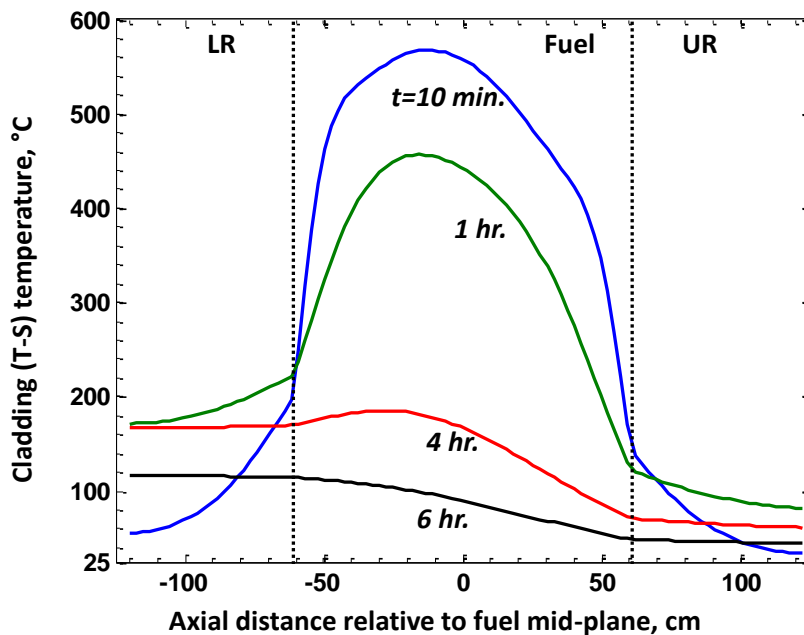


Figure 3-8. Axial Temperature Profiles of the Side Section of the Cladding (T-S) as function of Time, Initial Peak Fuel Temperature = 600 °C, 3000 cfm of Air Cooling through the Reactor.

Since cooling times were found to be insensitive to axial conduction within the fuel if either one or both of the blowers is operating, the total metal loss increased by less than 4% for the most conservative value of contact resistance ( $CR = 5e^{-3} m^2 K W^{-1}$ ).

Figure 3-9 below shows the cross-sectional metal loss of the cladding at the axial location where the peak corrosion has occurred. The corrosion is the result of the temperature profiles developed around the circumference of the cladding. Temperatures are highest at the section of the cladding in contact with fuel and decrease toward the cooling channel region (corner section). The total metal loss in the corner region is almost two orders of magnitude lower than the metal loss in the section in contact with the fuel.

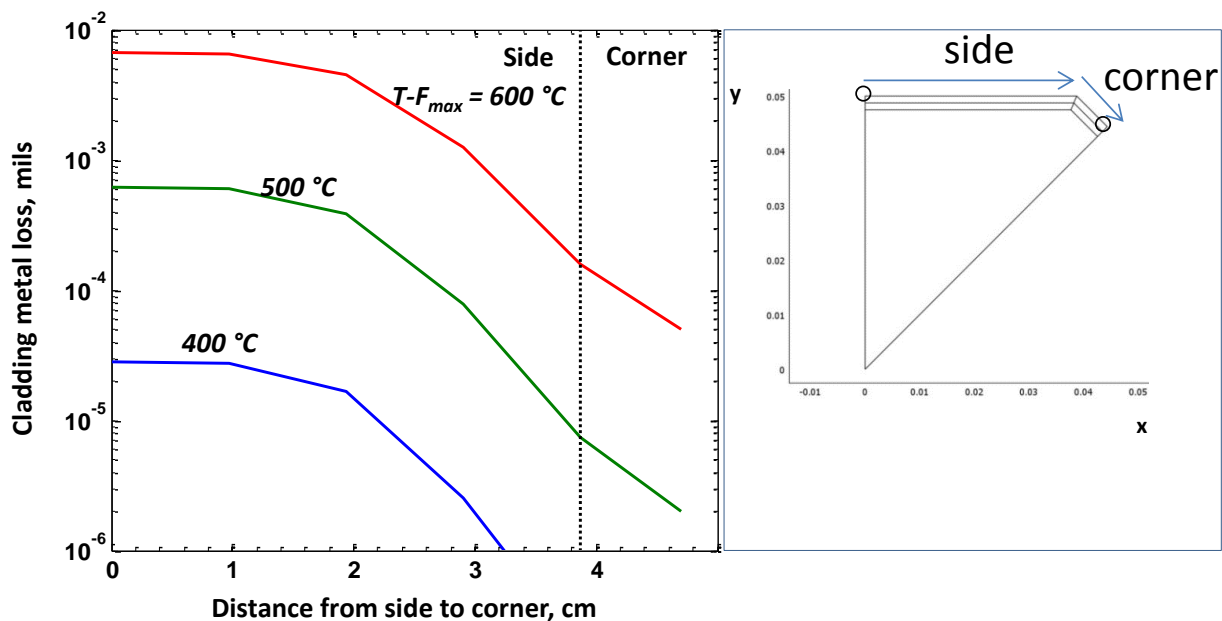


Figure 3-9. Cross-sectional Metal Loss of the Cladding Near the Fuel Mid-plane. Total Metal Loss shown as a function of Initial Peak Fuel Temperature and Cladding Distance, Results Shown when using 3000 cfm of Air Cooling through the Reactor.

The spatial trends of cladding oxidation remain similar when increasing the coolant flow rate to 6000 cfm through the reactor. However, the magnitude of total metal loss is reduced by 40% as compared to Figure 3-9 (3000 cfm of cooling). Transient analyses for constant power operation (120 kW) were also investigated as part of normal operation. In general, since peak temperatures of the cladding remained below 300 °C, corrosion rates were consequently very small. Further detail on core thermal behavior under constant power operation can be found in Appendix B. Total metal loss was high for the case of reactor operation at constant power for 10 h and with one blower in operation. Even then, total corrosion was comparable to the case of a power transient with a peak fuel temperature of 400 °C.

### 3.3.2 Accident Scenario

The accident scenario assumes that all of the reactivity available at the beginning of the planned bounding shaped transient is inserted as a step. The analyses for the cooling time history of the fuel assembly assume no flow conditions, i.e. both cooling blowers fail and the effects of natural convection are conservatively ignored. Furthermore, no heat loss is assumed to occur radially through the core and thus the only mode of cooling is by axial conduction through the assembly. Both ends of the fuel assembly are also assumed to be completely insulated.

On the left panel of Figure 3-10, cooling time histories are shown for the case of no contact resistance and three initial peak fuel temperatures. The highest temperature corresponds to the HEU core Safety Limit, or SL, of 820°C. Since the cladding is assumed to be in thermal equilibrium with the fuel, peak fuel and peak cladding temperatures remain equal to each other. Depending on the initial peak fuel temperature, the cladding will be exposed to temperatures higher than 600°C for three to seven hours. After 24 hours, the temperature will be entirely uniform across the whole fuel assembly.

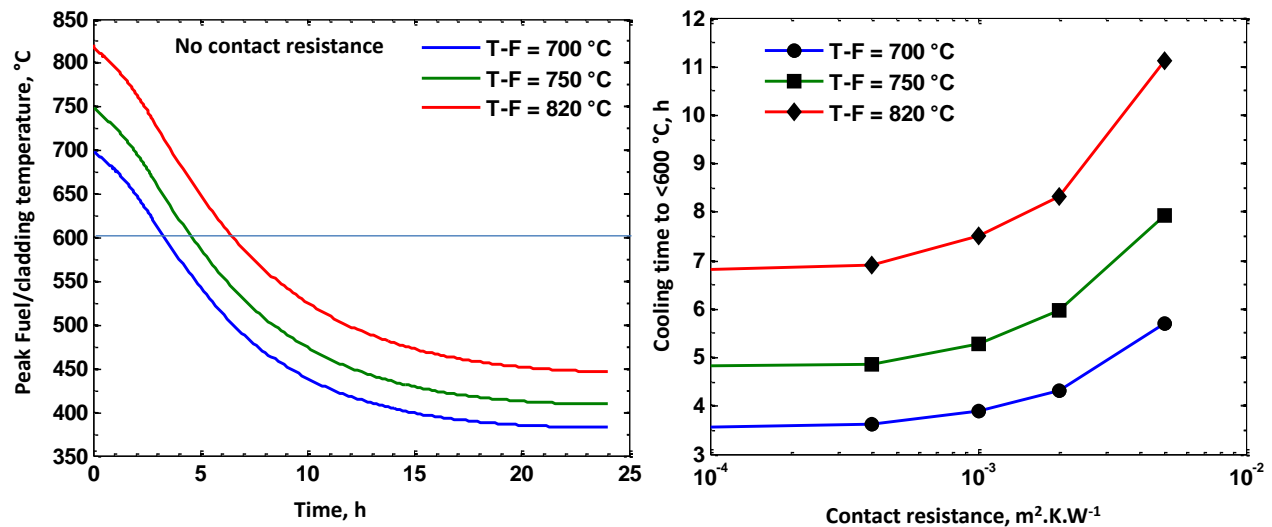


Figure 3-10. Cooling Time Histories for the Accident Case Scenario Assuming No Air Flow, Peak Fuel Temperatures Investigated in the Range of 700-820 °C; Left Panel shows Peak Fuel Temperatures as function of Time Assuming No Contact Resistance, Right Panel shows the Effect of Contact Resistance on Cooling Times to Below 600°C.

The effect of contact resistance between graphite blocks on cooling time to below 600°C is shown in the right panel of Figure 3-10. Irrespective of initial temperature, cooling times start to increase when contact resistances are higher than  $\sim 5e-4 \text{ m}^2 \text{ K W}^{-1}$ . A high contact resistance decreases the heat transferred from the fuel to the reflector section and thus is equivalent to a reduced heat conductivity of the fuel. Figure 3-11 shows the corresponding effective conductivity of the fuel as a function of contact resistance. The range of contact resistances used for the analyses correspond to an effective axial fuel conductivity in the range of 57-95%.

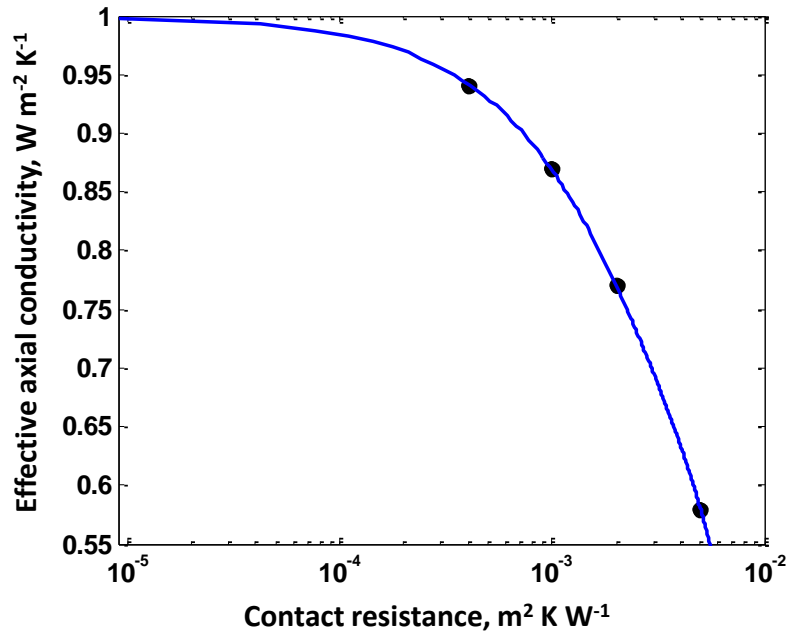


Figure 3-11. Contact Resistance Translated to an Equivalent Effective Axial Conductivity of the Fuel

As in the case with convective cooling, most of the corrosion of the cladding occurs in the fuel section of the assembly. The metal loss peaks near the fuel mid-plane and rapidly falls by three orders of magnitude near the reflector region. In contrast, in the no-air-flow case the entire circumference of the cladding will be at a uniform temperature, and thus the side and corner regions will corrode at the same rate. Figure 3-12 below shows total metal loss of the cladding near the fuel mid-plane, i.e., location of the maximum metal loss. Total metal loss in this case refers to the cumulative loss of the cladding during 24 hours after an accident<sup>3</sup>. As corrosion rates are strongly accelerated at higher temperatures, total metal loss after an accident is sensitive to initial temperature and contact resistance (affecting overall cooling time). For the highest temperature that relates to the HEU core Safety Limit of 820°C, the cladding thickness after such an accident would be reduced by 8 to 14%. This range corresponds to a reduction in effective axial conduction up to approximately 40 %.

<sup>3</sup> Assuming that the fuel assembly does not reject heat to the environment, a temperature of 450 °C (equilibrium temperature of the assembly if the peak temperature is at the Safety Limit) would equate to an additional metal loss of ~0.1 mils/week.

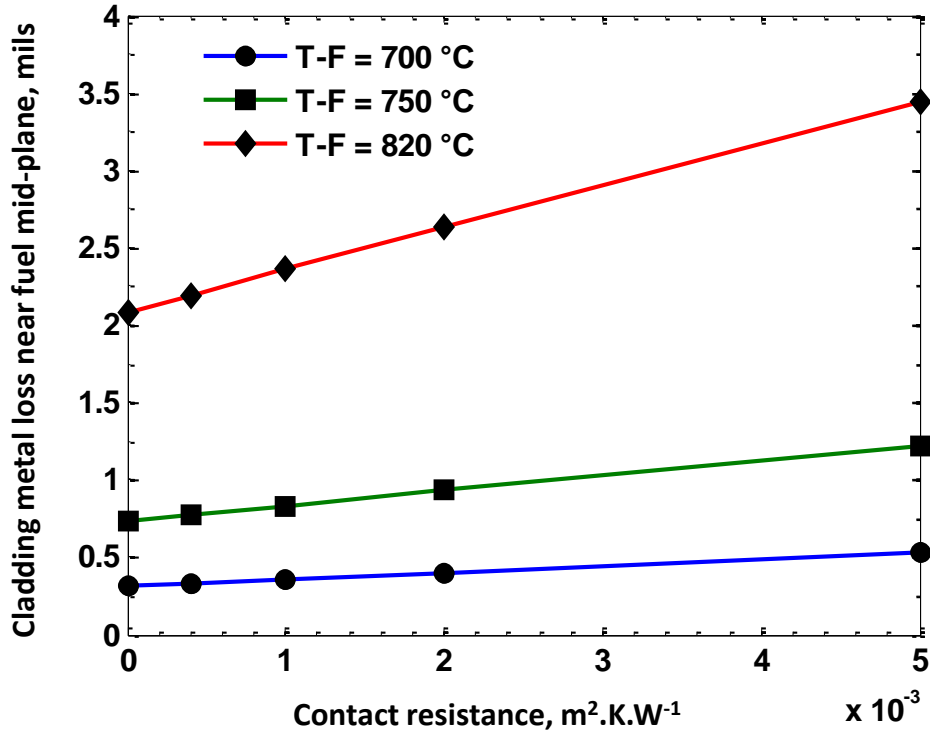


Figure 3-12. Metal Loss of the Cladding Near the Fuel Mid-plane after an Accident (No Air Flow assumed through the Reactor); Total Metal Loss is shown as Function of Initial Peak Fuel Temperature and Contact Resistance.

### 3.4 Summary

Cooling time histories for the current LEU fuel assembly design (conceptual phase) were analyzed during normal operation and accident case scenarios. For the current conceptual design, the height of the fuel block has been limited to approximately four inches according to compaction process limitations. The effect of fuel contact resistance on cooling times was evaluated. Normal operation covered peak fuel temperatures from  $\sim 250^\circ\text{C}$  (during constant power operation) up to  $600^\circ\text{C}$ , the latter reflecting the limit of the most demanding of allowable planned power transients.

During normal operation, cooling times are strongly affected by the coolant flow rate through the reactor. However, contact resistance and hence axial heat conduction within the fuel were shown to cause no significant delay in the cooling time history. The cladding at the corner section of the assembly, where most of the cooling occurs, stayed at much lower temperatures than the side section of the cladding. Due to the non-uniform temperatures developed across the cladding, the total metal loss in the corner region remained almost two orders of magnitude lower than the section in contact with the fuel.

During an accident scenario and with no air cooling, impeding axial heat conduction in the fuel will result in delayed cooling and consequently greater metal loss. Since the entire cross-section of the cladding will be at the same temperature in this scenario, the side and corner region will corrode at the same rate.

## 4 Additional Safety-related Analyses

As minimal design and operational changes are anticipated for the facility's supporting systems (e.g. reactor trip system, filtration/cooling system, etc.), the LEU core must be able to function with the existing supporting systems and must also satisfy acceptable safety limits. Accordingly, bounding safety analyses of coupled core and supporting system performance have been completed during the LEU design process to ensure that safety limitations are not violated. These analyses have spanned neutronic, shielding, and thermal-hydraulic topics that have been identified as having the potential to have reduced safety margins due to conversion to LEU fuel, or are necessary to support the required safety analyses documentation. For all of these analyses, methodologies are utilized that are consistent with, or improved from, those used in analyses for the HEU Final Safety Analysis Report (FSAR) [7].

### 4.1 Previously-performed Bounding Analyses

Numerous safety analyses have been completed during the LEU design process [4] with the objective to perform best estimate, yet bounding, calculations so that these analyses will not need to be repeated as each LEU design phase is completed. Of the analyses completed in this conceptual phase for previous LEU designs, several are still considered bounding for the LEU conceptual design. This includes the analysis of the dose rate at the HEPA filters due to tramp uranium fission products and heating of the radial reflector, both of which are discussed below. Additional analysis details can be found in the previous report [4].

Estimating the dose rate from fission products deposited in or near the HEPA filters as the result of tramp uranium is an extremely complex problem. The key variables are the actual quantity of tramp uranium in the cladding material, the fission history of that material, the trajectory and deposition of the fission products during their ejection from the tramp uranium, and the transport and deposition of the fission products or their daughters in the filtration and cooling system (i.e., the source term). This analysis was completed using the Baseline 2.0 iteration of the LEU core design as a reference and is considered bounding for any core design that exhibits a lower or similar flux, with a similar photon spectrum. The bounding analysis gauged the effects of assumptions on the concentration of tramp uranium in LEU materials and Zr-bearing material that would be used for the fuel and found that dose rates will be similar to or less than those estimated for the HEU core. More importantly, recent insight from INL has indicated that tramp uranium levels in the LEU clad will be several orders of magnitude lower than those found in the HEU clad and therefore are considered negligible.

Heating of the permanent radial reflector was also analyzed for the design basis accident with and without cooling using LEU design Variant 2.1, which had significantly higher core energies (5.59 GJ in the evaluated accident scenario) and temperatures (960°C accident scenario peak fuel temperature) than the current LEU conceptual design. It was found that, given the large mass of the permanent reflector, the reflector is able to absorb a large amount of energy yet remain sufficiently cool. With adequate cooling, the peak temperature of the permanent reflector remains below 60°C for the Variant 2.1 design basis accident core energy. In the absence of cooling, the core and permanent reflector reach a thermal equilibrium temperature of ~160°C. Severe oxidation of the permanent reflector (if any during normal core operation) is highly unlikely, as oxidation rates below 300°C are small, if not negligible. This analysis is considered bounding as it was derived from a power time history for LEU design Variant 2.1, which

exhibited higher core power and temperatures during the characteristic design basis accident than the current conceptual design.

## 4.2 Updated Analysis: Thermal Hydraulic Analysis of Core Support

The following thermal-hydraulic analysis focuses on reevaluating the heating of the core support (grid plate) during a reactivity accident scenario. This information was then provided for structural analysis of the corresponding grid plate distortion. Previous analysis of the grid plate heating and corresponding thermal distortion was completed using the Variant 2.1 iteration of the LEU core design, prior to the establishment of the current conceptual design. Although the Variant 2.1 core had higher peak temperatures than the current LEU conceptual design core, a reassessment was necessary, both because previous calculations were not sufficiently conservative and to obtain results that are more representative of the current reactor configuration.

### 4.2.1 Core Support Model and Assumptions

For all analyses conducted, the half-slotted core loading of the M8 power calibration experiment (M8CAL) is used. Both HEU and LEU fuel element assemblies were evaluated for comparison. For the LEU case, the analyses considered the bounding accident case for a 6.025% $\Delta k/k$  reactivity step insertion that produces a total core energy of 4718 MJ. This is the accident scenario corresponding to  $\frac{PCF_{LEU}}{PCF_{HEU}} = 85\%$ . For comparison, the HEU accident condition considered a total core energy of 4149 MJ (5.95% $\Delta k/k$  pre-transient available reactivity). It is also assumed that the reactor is always convectively cooled by air at flow rates up to the nominal 6000 cfm. The assumption of forced-convection air flow is conservative in the grid plate analysis in that it results in faster heat transfer from the core to the grid plate, consistent with the assumption of no heat transfer from the grid plate to the concrete that supports the grid plate.

A 3D model of the grid plate as shown in Figure 4-1 below was developed in COMSOL®. Figure 4.1 shows the grid plate configuration in the current TREAT core (20 control rods). The model and assumptions have been detailed in a previous report [4] used to analyze previous LEU design options. Briefly, in order to properly analyze the heating of the mild-steel grid plate, the heating due to conduction from supported assemblies was accounted for as well as convection from the air exiting the core and radial reflector. This was done using temperature boundary conditions as a function of time for the grid plate. For example, heat transfer by convection through the perimeter of the grid plate's flow holes and radial slots is treated as a boundary condition.

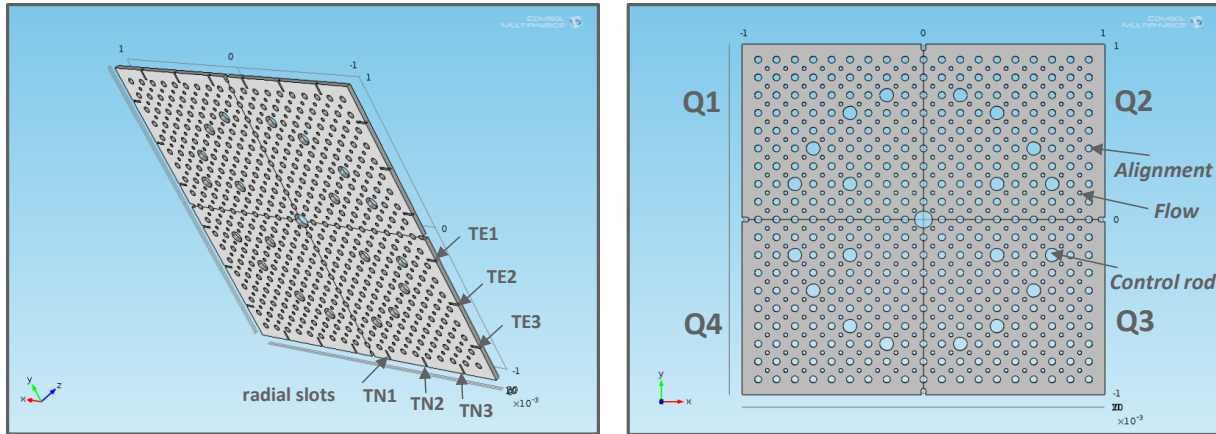


Figure 4-1. Current Grid Plate Configuration for TREAT (without Fuel Alignment Pins)

For each flow channel the gas-phase temperature as a function of time is calculated with a 3D model, described previously, and saved as a look-up table. Knowing the gas-phase temperature entering the flow holes during the transient (via the look-up table), the heat transfer rate to the plate is calculated using established heat-transfer correlations. Similarly, heat by conduction is modeled as an imposed temperature at the top boundary of the plate (at the fuel-assembly alignment pin). The time-temperature history,  $T(t)$ , was evaluated from the lower axial reflector which was calculated with the fuel assembly model.

To reduce computational time, a solution is found for only a quarter of the grid plate, with symmetry being assumed at the boundaries adjacent to other sections. Restricting the model to a quarter symmetry is sufficient for the current analysis. The analysis would be conservative provided that the section analyzed would yield the highest thermal distortion of the plate. Previous analyses considered the north-east section (Q2) of the grid plate, as this section showed both high temperatures as well as the highest temperature gradients during the heating of the plate. Structural analysis, however, showed that the total deformation of the grid plate (and hence total deflection of control rods from their original position) is sensitive to the magnitude of the grid plate temperature. Figure 4.2 below, shows the LEU peak fuel temperature after an accident for the M8CAL core loading. While high temperature gradients are indeed anticipated in section Q2 for the grid plate, section Q3 (south-east section of the core) shows the highest peak-fuel temperatures. Approximately 29% of the total core energy is deposited in section Q3 and will consequently lead to much higher grid plate temperatures (and distortions) than section Q2. Thus, for added conservatism, all re-evaluated calculations of the grid plate now consider the south-east section (Q3) of the core.

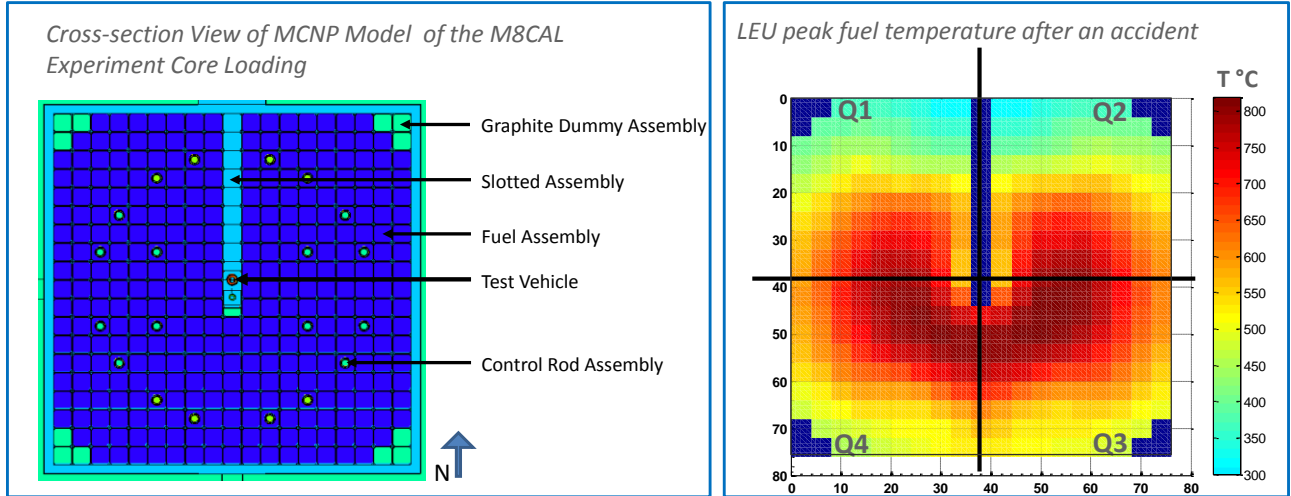


Figure 4-2. M8CAL Half-slotted Core Loading and Corresponding LEU Core Accident Scenario Fuel Temperature Distribution; Peak Temperatures are Highest in South-East (Q3) Region.

#### 4.2.2 Maximum Grid plate Temperatures

The maximum grid plate temperature profiles (Q3) during the accident scenario for both HEU and LEU cores are shown below in Figure 4.3. Given a coolant flow rate of 3000 cfm through the reactor, maximum grid plate temperatures are nearly the same for both cores.

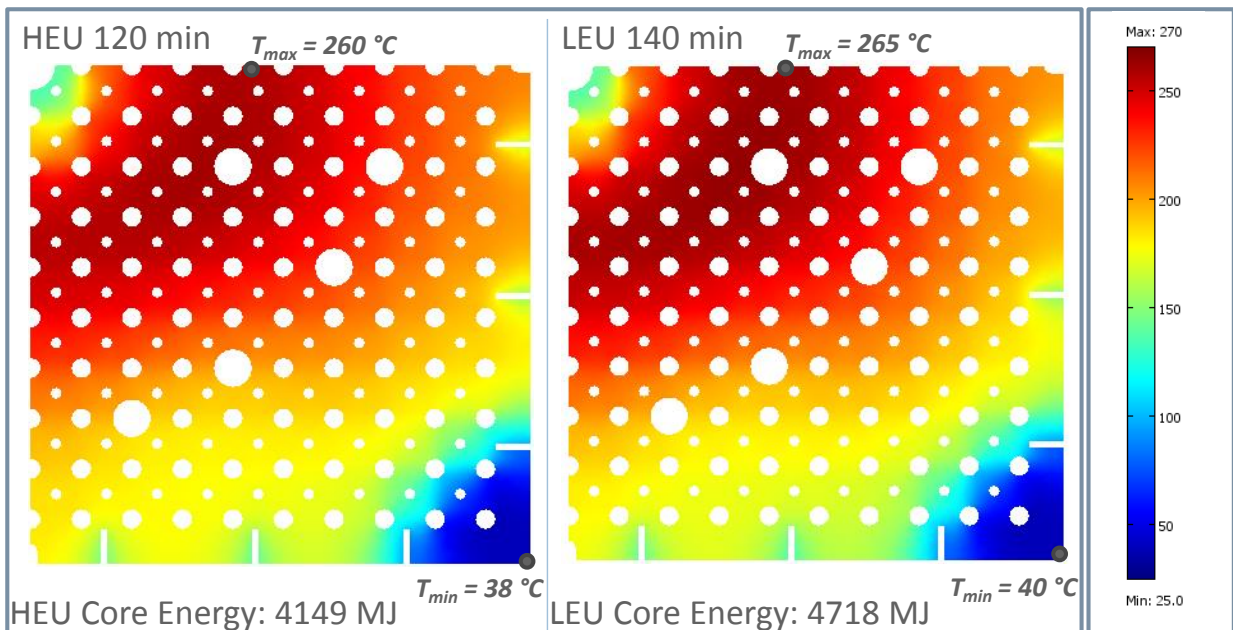


Figure 4-3. Maximum Grid Plate Temperatures After ~2 hours of Cooling after an Accident; Grid Plate Temperature is Nearly the Same for both HEU and LEU Cores.

After approximately two hours of cooling after the accident, a peak grid plate temperature of  $\sim 265^{\circ}\text{C}$  is calculated for the LEU core and  $\sim 260^{\circ}\text{C}$  for the HEU core. The LEU core has a much-higher thermal mass (higher graphite density and graphite volume). Thus, despite the higher core energy obtained for the LEU case, peak fuel temperatures remain slightly lower for the LEU core as compared to the HEU core. The subtle differences in grid plate temperatures are due to more heat being conducted axially in the LEU fuel assemblies, since in the LEU core the fuel and axial reflectors are in contact. In case of the HEU design, on the other hand, axial conduction is impeded due to the  $\frac{1}{4}$ -in evacuated gap between the fuel and axial reflectors.

With 6000 cfm of coolant flow, the maximum temperature was reduced by almost  $50^{\circ}\text{C}$ . However, even with one blower in operation, grid plate temperatures remain well below the  $320^{\circ}\text{C}$  temperature at which control-rod binding from grid plate deflection would occur. The effect of thermal expansion and corresponding bowing of the control rod thimbles is discussed in the following structural analysis section.

### 4.3 Grid Plate Thermal Distortion Analysis

The purpose of this work was to determine if particular accident conditions in the TREAT LEU core could lead to excessive thermal distortion of the grid plate which supports the fuel assemblies. Excessive grid plate distortion could cause the control rods to bind, preventing their operation. Additionally, this analysis sought to determine the maximum-tolerable uniform temperature in the grid plate that would result in a thermal distortion large enough to potentially cause control rod binding. The analysis utilized a finite element model in ANSYS [26] for structural analysis of the grid plate, assuming the bounding value for weight of fuel assemblies, per the Analysis Guide. The non-uniform thermal load for this study was calculated separately in COMSOL<sup>®</sup> [16], as discussed above. The displacement results were then used to determine an angular deflection that occurs at the middle bearing of a control rod guide tube. This angular displacement was then applied to a separate ANSYS beam model of the control rod to calculate deflections, which are compared to the clearances in the guide tube and seal assembly. This method was repeated using a uniform thermal load to determine the maximum tolerable temperature for the grid plate.

#### 4.3.1 Assumptions

This model assumes material properties equivalent to A36 structural steel. The TREAT historical drawings specify mild steel, and Section III of the ASME Boiler and Pressure Vessel Code lists A36 steel as a typical mild steel. Mechanical properties were obtained from the pressure vessel code and are summarized in Table 4-1.

The concrete supporting the grid plate is assumed to undergo no significant change in temperature and thus exhibits no distortion due to thermal loading. The concrete is represented in the ANSYS model with the boundaries shown in Figure 4-4, discussed below. Also, the weight of a single fuel assembly is assumed to be 125 lbs as a simple static load. Mechanical interaction between the two is assumed only insofar as the grid plate forces the bottom of the control rod assembly to be at the same lateral position as the assembly's hole in the grid plate. (During core operation, the fuel assemblies are collectively clamped together at their tops with clamps secured to the concrete shielding of the reactor. On the

other hand, the fuel assemblies may distort during transients, due to lateral temperature gradients across them.)

Table 4-1: Material Properties for A36 Steel

Property	Units	Value
Density	kg/m <sup>3</sup>	7850
Young's Modulus	GPa	200
Poisson's Ratio	-	2.6
Coefficient of Thermal Expansion (CTE)	K <sup>-1</sup>	12.0E-6

### 4.3.2 Non-uniform Thermal Loading

This subsection provides details of the analysis of grid plate deflection in the case of non-uniform thermal loading. This loading is assumed to be the result of a bounding reactivity insertion accident with active cooling (i.e., blowers operating at their nominal capacity). In the case of thermal loading on the grid plate, use of blowers provides the most conservative assessment, since heat will transfer to the grid plate more rapidly via convective heat transfer.

#### 4.3.2.1 Geometry of Grid Plate and Control Rods

The grid plate, shown in Figure 4-4, is supported both by the seal assemblies and the surrounding concrete. The plate rests on the edges of the concrete, which are reinforced with steel. The seal assemblies and the grid plate are bolted together. The grid plate model uses quarter symmetry, and the quarter symmetric model supports 91 fuel assemblies.

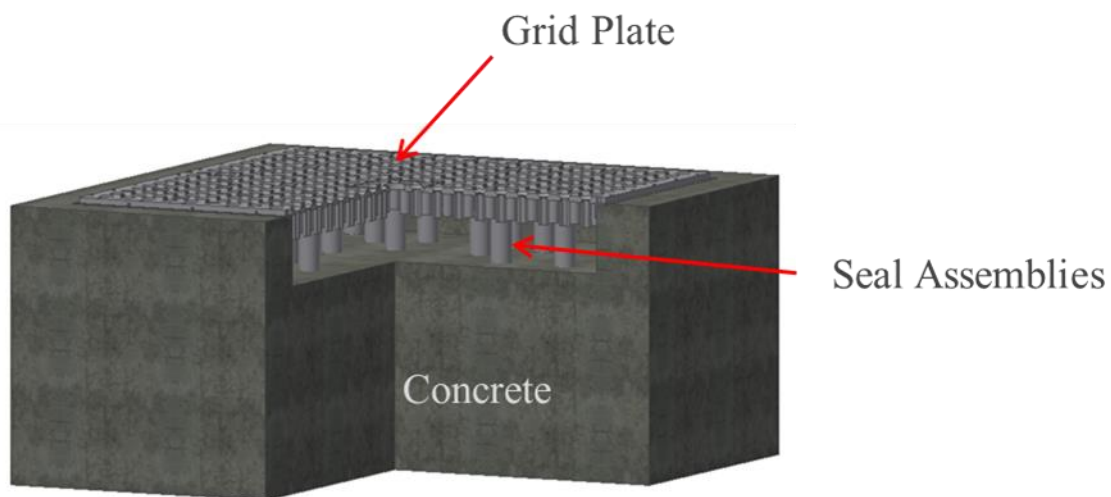


Figure 4-4. Drawing of Grid Plate and Seal Assemblies

The control rod geometry, shown in Figure 4-5, used in the ANSYS model takes into account the outer wall of the control rod, modeled as a simple beam supported at three locations that correspond to the three graphite bearings, shown in red in the figure. The calculated angular displacement will be enforced at the location of the middle bearing.

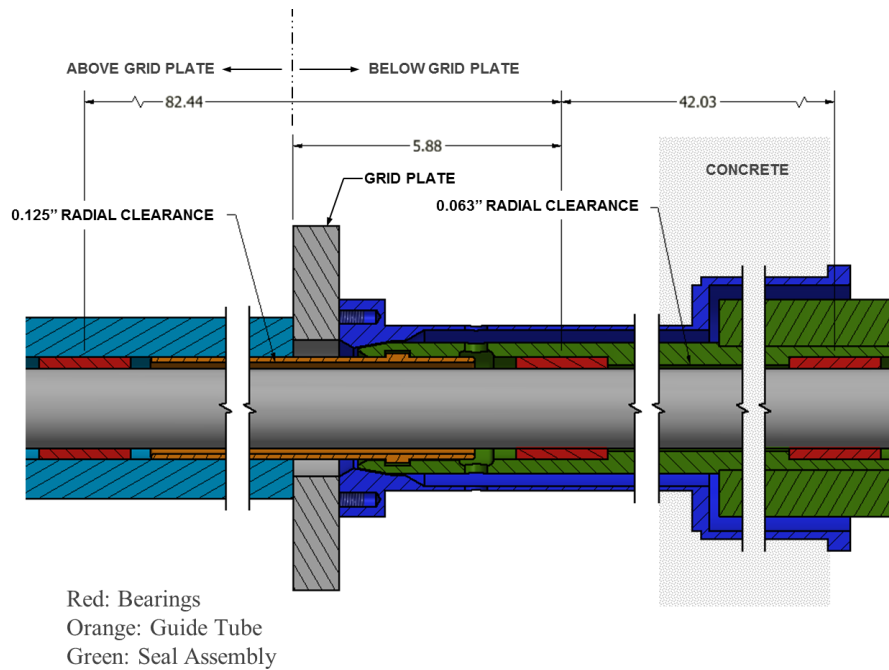


Figure 4-5. Cross-Sectional View of Control Rod Assembly Showing Graphite Bearings (Red)

#### 4.3.2.2 Grid Plate Boundary Conditions

Non-thermal loading of the grid plate is assumed to be the result of the force imposed by the weight of the assemblies and the force resulting from contact with support structures. In the case of the fuel assemblies, it is assumed that each assembly weighs 125 lbs. Compression-only support occurs at the edge of the grid plate, where the grid plate is supported along the edge but is not clamped. Additionally, there are fixed supports in the region of the fuel assemblies, below the surface of the concrete. These loads are shown in the quarter-symmetry drawings in Figure 4-6 a and b, where the load due to the weight of 91 fuel assemblies is shown in panel a, and the loads resulting from the compression and fixed supports are shown in panel b.

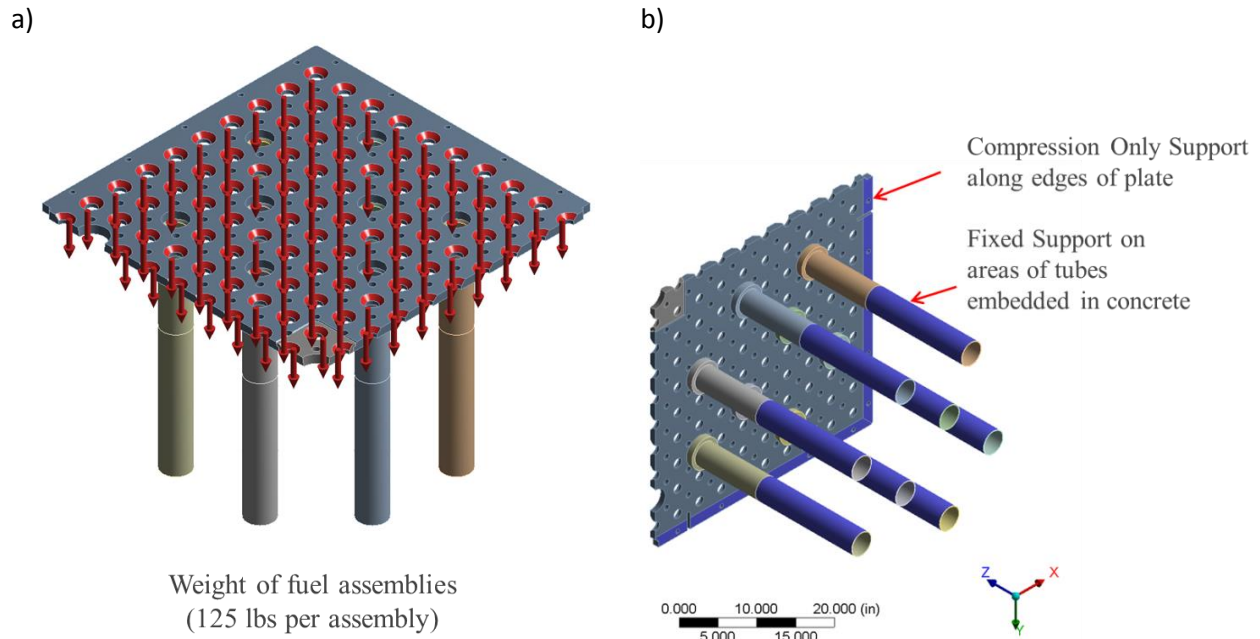


Figure 4-6. Non-thermal Grid Plate Loads in the Quarter Symmetry Model

#### 4.3.2.3 Grid Plate Deflection Due to Non-uniform Thermal Load

The non-uniform grid plate temperature profile (Figure 4-7) used in this structural analysis was generated by a thermal-hydraulic analysis performed with COMSOL®, as described above. Results for the corresponding deflection in the grid plate due to the non-uniform thermal loading are shown in Figure 4-8, below. The total deformation for all directions is shown in panel a), and deformation only in the radial direction with respect to the center of the grid plate is shown in panel b).

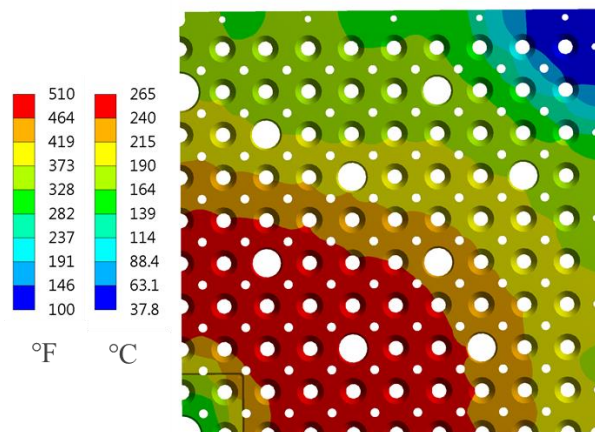


Figure 4-7. Contour Plot of Non-uniform Thermal Loading of the Grid Plate in the LEU Core Design Basis Accident

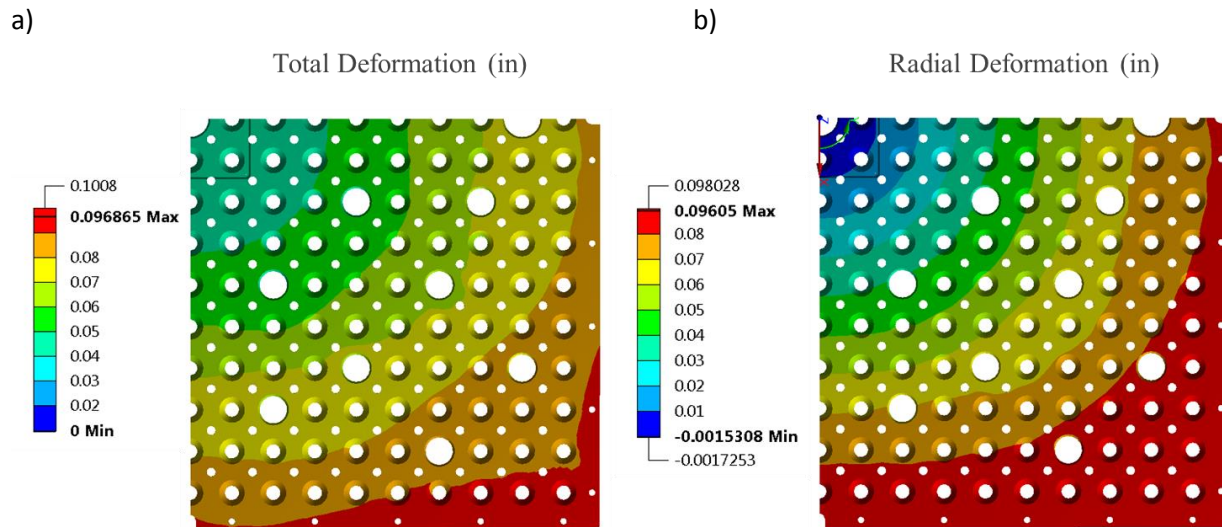


Figure 4-8.. Contour Plots Showing Total (a) and Radial (b) Deformation of the Grid Plate Due to Non-Uniform Thermal Loading

The total deflection from the original position for two control rod positions was also calculated. For a control rod relatively near the axis of symmetry (shown in Figure 4-9, indicated by the lower red circle), the total deflection is 0.0623". This leads to an angular displacement of 0.30° at the middle bearing of the control rod. The displacement angle is calculated as the arctangent of the deflection divided by 12", where 12" is the distance between the grid plate and intersection point of the seal assemblies with concrete. For reference, the deflection at a location further from the axis of symmetry (upper red circle in Figure 4-9) was also assessed, and was found to be 0.085", leading to a total angular displacement of 0.406°. However, this location is not expected to hold a control rod.

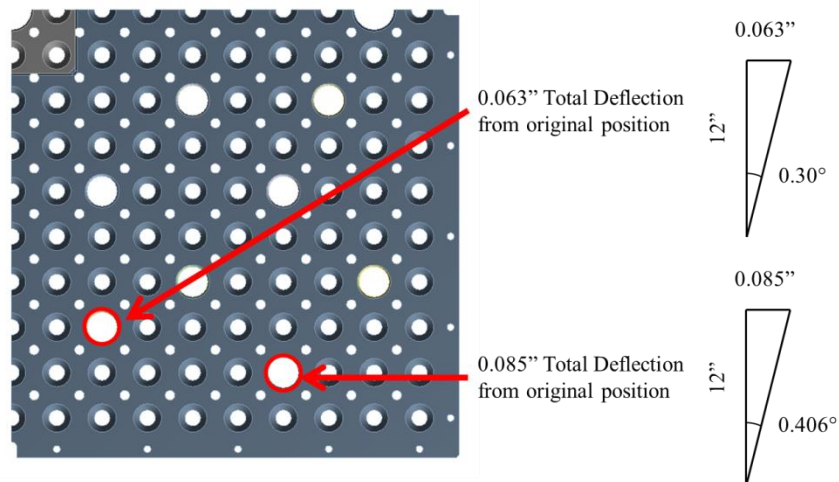


Figure 4-9. Deflection of Control Rod Positions

#### 4.3.2.4 Control Rod Deflection due to Non-uniform Thermal Load

By enforcing an angular displacement of  $0.30^\circ$  at the middle bearing, deflection of the control rod due to non-uniform thermal loading was found to be  $0.0832''$  within the guide tube and  $0.0423''$  within the seal assembly. This deflection is shown in Figure 4-10, below (for the details of the corresponding geometry, please refer to Figure 4-5, above). The clearance in the guide tube is  $0.125''$ , and the clearance in the seal assembly is  $0.063''$ . Therefore, the total deflection in the control rods is not expected to result in loss of control rod functionality.

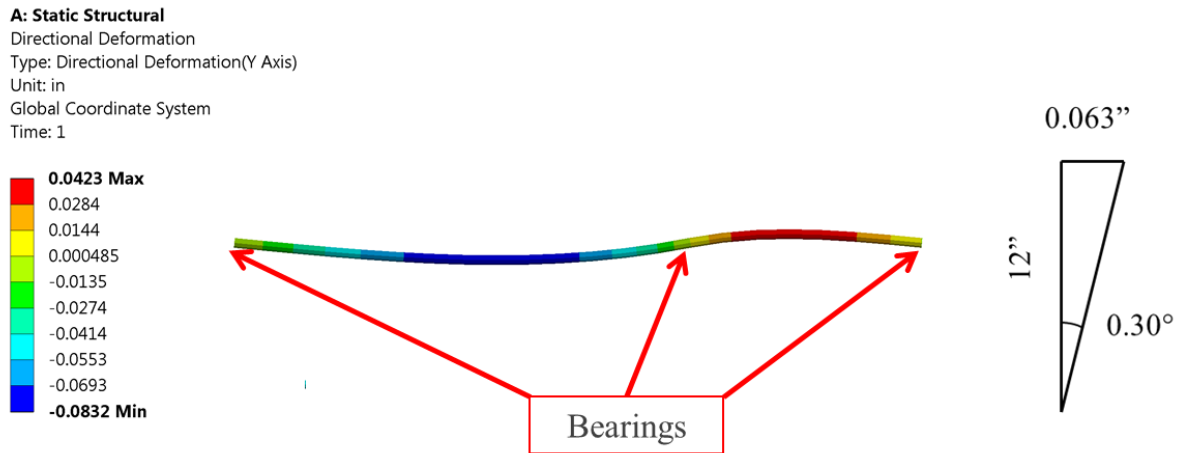


Figure 4-10. Control Rod Deflection (in inches) Resulting from  $0.30^\circ$  Angular Displacement at Middle Bearing

### 4.3.3 Maximum Uniform Temperature

Since the accident scenario used to calculate the thermal loading used in the first analysis did not indicate that the control rods would bind, an additional analysis was performed to determine a maximum uniform thermal load that would cause distortion in the control rods that is equal to or greater than the clearances in the guide tube and seal assembly. The models for both the grid plate and the control rod are the same as in the previous analyses with the exception of a uniform temperature applied to the grid plate. Several iterations of this analysis were performed to obtain the value for the maximum allowable temperature. As discussed in the following subsections, the final maximum grid plate temperature that would yield grid plate deflection sufficient to induce control rod binding was found to be  $320^\circ\text{C}$ .

#### 4.3.3.1 Grid Plate Deflection due to Maximum Uniform Thermal Load

An iterative procedure was used to determine the maximum uniform thermal load required to induce control rod binding from grid plate deflection. For this case, the total deflection of the reference control rod position was found to be  $0.093''$ , resulting in an angular displacement of  $0.443^\circ$  at the middle bearing. A contour plot showing the radial deformation resulting from the uniform grid plate temperature of  $320^\circ\text{C}$  is shown in Figure 4-11a, and the total displacement is shown in Figure 4-11b.

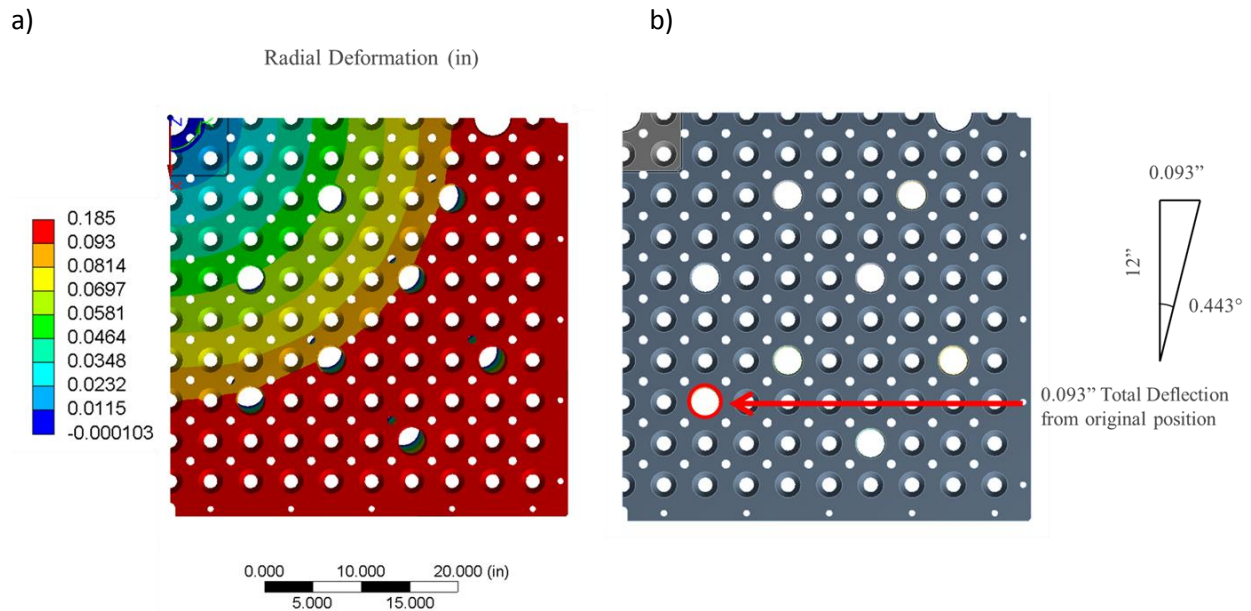


Figure 4-11. Radial Deformation (a) and Total Deflection (b) Resulting From Uniform Thermal Load of 320°C

#### 4.3.3.2 Control Rod Deflection due to Maximum Uniform Thermal Load

By enforcing an angular displacement of 0.443° at the middle bearing, deflection of the control rod due to a uniform thermal loading of 320°C was found to approximately meet or exceed the clearance in the guide tube and seal assembly. As shown in Figure 4-12, the deflection in the guide tube under uniform thermal loading was found to be 0.123", and the deflection in the seal assembly was found to be 0.0624", where the clearances in the guide tube and seal assembly are 0.125" and 0.063", respectively.

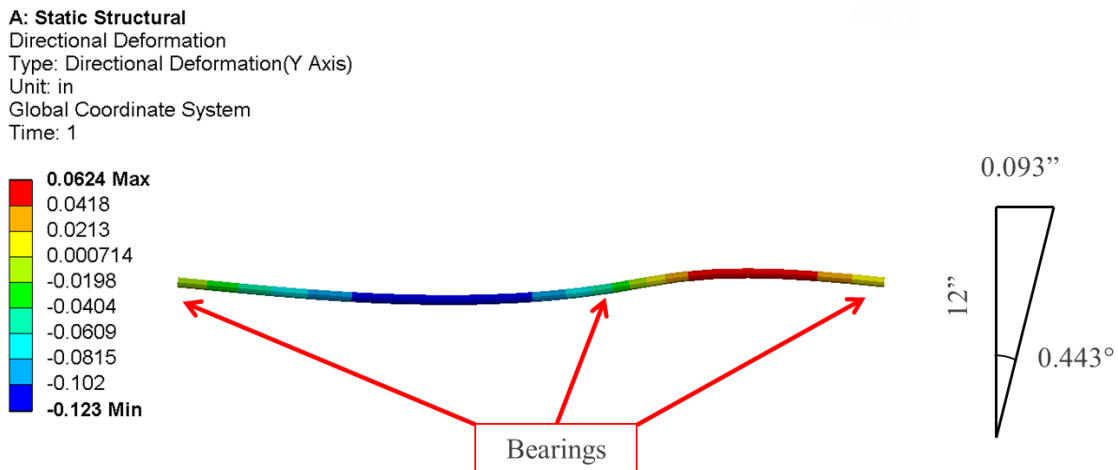


Figure 4-12. Control Rod Deflection Resulting from 0.443° Angular Displacement at Middle Bearing

#### 4.3.3.3 Key Conclusions

Analysis of the control rod deflection for an accident case with an LEU core shows that the control rods will not deflect enough to cause binding with either the guide tube or seal assembly. Analysis of grid plate behavior with a uniform thermal load was completed, demonstrating that a uniform temperature in the grid plate beyond 320°C brings the control rod into contact with the seal assembly and the guide tube. Thermal distortion of the guide tubes was not included in the analysis.

#### 4.4 Updated Analysis: Effect of Effluent Air Temperature on Filtration/Cooling System

The “adiabatic temperature” of the reactor effluent air to the exhaust filtration system (i.e., the temperature assuming no heat loss to components of the filtration and cooling system) was calculated for the reactivity accident scenario for the LEU and HEU cores. This analysis was previously performed for LEU design Variant 2.1, which had significantly higher temperatures than the HEU core. The analysis of the Variant 2.1 LEU core found that nominal flow without use of bypass air from the subpile room would violate the filtration/cooling system temperature limits identified in the HEU FSAR. This analysis has now been repeated for the current LEU core design concept, which has significantly lower temperatures.

Air exits from the reactor below-core plenum chamber via two ~10-in. diameter ducts which lead to the turbo-compressor room [4]. About 13 feet from the plenum, the two ducts and a 9-in. diameter by-pass line join into a 19-in diameter duct leading to the exhaust filters in the compressor room. All flow can be caused to pass through the core (and permanent reflectors), or part of it (up to 3000 cfm) can be caused to by-pass the core by flowing instead from the sub-pile room below the reactor.

The temperature of the reactor effluent air moving to the exhaust filtration system was calculated for the reactivity accident scenario for the LEU and HEU cores (4718 MJ and 4149 MJ, respectively). Scenarios include various flow rates through the reactor (one or two blowers in operation) as well as diverting some flow from the sub-pile room. The reactor effluent refers to the average air temperature exiting the whole core to the point where the flow meets the by-pass flow duct.

The analysis for the LEU core showed that nominal flow without use of bypass air from the sub-pile room will not violate the filtration/cooling system temperature limits (204°C) identified in the HEU FSAR, as shown in Figure 4-13. Using one blower only for cooling (assuming nominal operation at 3000 cfm), peak air temperatures reached ~190°C for the LEU and ~180°C for the HEU. Calculated temperatures are conservative as it is assumed there is no heat loss from the air flow to components (the concrete, control rod thimbles and duct) down-stream of the core leading to the filtration/cooling system. With one blower in operation, passing 2000 cfm through the core and allowing the remainder of the flow to be by-passed, the effluent air temperature is further decreased by an additional 20°C.

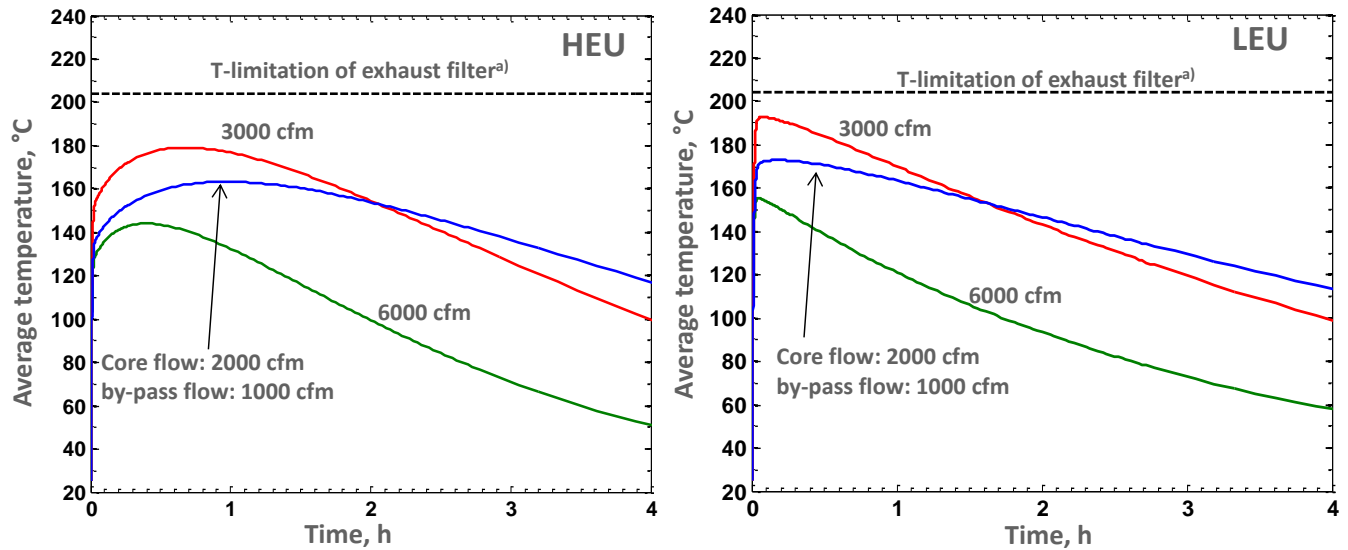


Figure 4-13. Reactor Effluent Air Temperature to the Exhaust Filtration System.

## 4.5 Ongoing and Future Analyses

Currently, several thermal-hydraulic and shielding assessments are being reevaluated to assess the impact of the conceptual LEU design on the various safety metrics. In general, these analyses are being revisited to confirm an increased safety margin due to the improved performance of the current conceptual design (compared to previous LEU designs). The remainder of this subsection provides a description of each ongoing analysis and provides the motivation for reanalysis of each topic. Additional planned safety analyses are also briefly discussed at the end of this section. In general, it is expected that, because the conceptual LEU design exhibits behavior similar to the original HEU core, the results of future analyses for the LEU core will be very similar to those reported for the original HEU core.

### 4.5.1 Heat Transfer from the Experiment to the TREAT Fuel

A qualitative assessment of heat transfer from the test vehicle to adjacent assemblies was included in the previous ancillary analysis work [4]. At that time, an analysis methodology and potentially bounding parameters were prescribed for an LEU core variant that was more thermally demanding (i.e., the core achieved higher temperatures) than the current conceptual design. This topic was not reanalyzed for this report, as it is considered a low-priority item - because the current conceptual design thermal performance is very similar to that of the original HEU core, the results for a given experiment design are expected to be very similar to those of the HEU core. In addition, more detailed information is needed on the anticipated future experiment programs in TREAT in order to estimate bounding experiment designs for this analysis to be performed properly.

### 4.5.2 Source Term Evaluation

Computations of source terms resulting from fuel fission products and cooling-air activation products are being revisited for two reasons. The majority of the preliminary shielding analyses completed in the previous ancillary analysis studies [4] utilized a source term that was calculated using Monte Carlo Burns (MCB) [27], an unsupported code. Recently-implemented software quality assurance procedures require

the use of approved software, which excludes the aforementioned software. Additionally, the source term estimation methodology must be reconfirmed by verifying that HEU results can be reproduced.

In the upcoming preliminary design phase, the necessary shielding analyses will be addressed in detail to confirm no decrease in the safety margin. These analyses include estimation of the dose rate in the hodoscope room, dose rate around the fuel transfer cask, and dose rate above the fuel storage area. The source term reanalysis also includes reassessment of the photon flux profile, which may affect the shielding analyses. Updated shielding calculations were not performed for the current design; however, the LEU conceptual design core is anticipated to operate similar enough to the current HEU core that the differences in dose rates resulting from the use of the two cores will be small with no significant effect on the radiological safety operations of plan personnel.

In the current study, the HEU and LEU source terms have been re-evaluated for the reference conceptual design core (M8CAL), using the bounding operating history prescribed in the HEU core FSAR. This was performed using the code MCODE2.2 [28], which couples MCNP5 [9] and ORIGEN2.2 [29]. The operating power history (similar to that outlined in the HEU FSAR, which assumes a concluding accident-type transient) used in this analysis is indicated in Table 4-2.

**Table 4-2. Operating Power History Used to Evaluate TREAT Core Source Term**

Step	Duration	Unit	Power (W)
1	30	Days	11100
2	90	Days	11100
3	240	Days	11100
4	1	Year	11100
5	3	Years	11100
6	5	Years	11100
7	5	Years	11100
8	5	Years	11100
9	7	Days	0
10	33	Days	122000
11	10	Seconds	600000000

The average fuel discharge composition was obtained from the MCODE2.2 calculation. Based on the mass composition, the activity and photon emission rate were calculated using ORIGEN2.2 [29]. The photon emission rate is summarized in Table 4-3. The LEU and HEU fuel operated at the same power level would yield similar photon emission rates, since approximately the same amount of fission products would be produced.

The ORIGEN2 calculation was performed using the photon library based on UO<sub>2</sub> bremsstrahlung (library file gxuo2brm.lib) [29], which provided conservative results.

Table 4-3. Photon Emission Rate (photons/second) For TREAT Core with HEU and LEU Fuel

Group Average Energy (MeV)	HEU	LEU
1.00E-02	7.64E+17	7.68E+17
2.50E-02	2.92E+17	2.92E+17
3.75E-02	1.41E+17	1.42E+17
5.75E-02	1.84E+17	1.84E+17
8.50E-02	1.34E+17	1.41E+17
1.25E-01	4.12E+17	4.12E+17
2.25E-01	2.03E+18	2.03E+18
3.75E-01	3.55E+17	3.55E+17
5.75E-01	6.75E+17	6.74E+17
8.50E-01	8.60E+17	8.60E+17
1.25E+00	6.91E+17	6.91E+17
1.75E+00	9.77E+16	9.76E+16
2.25E+00	3.68E+16	3.67E+16
2.75E+00	3.65E+16	3.64E+16
3.50E+00	3.24E+16	3.24E+16
5.00E+00	4.60E+16	4.60E+16
7.00E+00	1.71E+15	1.71E+15
9.50E+00	2.00E+11	1.99E+11
<b>Total</b>	6.79E+18	6.80E+18

These preliminary results indicate that the photon distribution and total photon yield do not vary significantly between the original HEU and conceptual LEU cores for a similar core configuration. Because operation of the current conceptual design is very similar to that of the original HEU core, shielding results, which are currently pending, are not expected to vary significantly between the HEU and LEU designs.

#### 4.5.3 Additional Future Ancillary Analyses

In addition to the bounding analyses described in this report, the following safety analyses will be finalized during the preliminary design phase: estimate of dose rates at the periphery of the bioshield and radiography facility; dose rate in the subpile room due to radiation from control rod followers; thermal distortion of control rods due to asymmetric heating; accidental criticality due to flooding (this item was examined previously using an early design variant); and adequacy of the plant protection system. These tasks were described in limited detail in the previous ancillary analysis report [4]. It is anticipated that the HEU models of the TREAT facility will be further refined during the preliminary design phase, after which it will be more constructive to evaluate these additional items.

## 5 UO<sub>2</sub>-graphite Behavior and Fuel Particle Size

Compared to the original HEU TREAT fuel, the prospective LEU TREAT fuel will contain a much higher volume of UO<sub>2</sub> particles. The size distribution of these particles could impact the fuel and reactor performances in the following ways:

- (1) In the case of large particles, there is a concern of overheating the fuel particles during a sharp pulse (reactivity-step) transient, possibly causing the melting of some UO<sub>2</sub> particles. In addition, sufficiently large particles can induce a high thermal resistance in the microscale fuel-matrix system [30], and thus produce a time-lag (defined as the displacement in time between the time-temperature curve for the oxide particle, and the time-temperature curve for its surrounding graphite moderator). This could lead to an increase in the core transient energy generation due to the delay in the temperature reactivity feedback [6].
- (2) In the case of small particles, the particle number density in the fuel is high, leading to a large fission-fragment-damaged region in the fuel with resulting reduction of thermal conductivity. The thermal conductivity degradation could be significant if the average particle size in the fuel is sufficiently small.

Because of the concerns described above about large and small particles, simulations were performed to establish recommended upper and lower limits of particle size for the conceptual design LEU TREAT fuel. These simulations are described below. The results of these analyses will be evaluated in collaboration with the INL and LANL teams to support future decisions regarding the necessary manufacturing specifications and tolerances for particle size and distribution.

### 5.1 Determination of the Upper Limit of UO<sub>2</sub> Particle Size in LEU TREAT Fuel

The maximum temperature of different-sized UO<sub>2</sub> particles for the energy corresponding to a 4.63%Δk/k reactivity step transient in the HEU core was calculated to evaluate the practical upper limit of particle size. This finite element computation using the COMSOL® code [15] is based on a spherical “cell” model proposed by Hetrick [31], in which a spherical UO<sub>2</sub> particle is centered within a spherical volume of graphite matrix, with an assumed radial ratio of 1/8.2 for LEU fuel. For each calculation, one average particle size is used. A detailed description of the model and the thermal properties of both UO<sub>2</sub> and graphite were given in the previous publication on this work [30]. The decrease in thermal conduction due to radiation damage in the graphite at the particle-matrix interface, and its corresponding effect on particle-to-matrix heat transfer, were taken into account in the calculations. An experimental observation has shown that the bulk thermal conductivity of graphite decreased from 41.8 W/(m-K) to a saturated value of ~1.046 W/(m-K) after a fuel burnup of ~60 KWH/cm<sup>3</sup> [32]. To include consideration of the hot spot in the core, different peaking factors (PFs) were taken into account in the simulation. To achieve similar performance as that of the HEU core, the LEU core may need to generate more power (depending on the value of the test sample PCF). Therefore, PFs were also used to compensate for the differences in power generated in HEU and LEU cores. Figure 5-1(a) shows the UO<sub>2</sub> particle center temperature as a function of UO<sub>2</sub> particle diameter in LEU fuel. With the extreme case of PF = 2.0, the temperature of UO<sub>2</sub> fuel particles of sizes of <105 μm in LEU fuel does not exceed the UO<sub>2</sub> melting point (~2,865°C) during the transient.

Another concern is that of the amplitude of the time-lag between the fuel particle and the graphite matrix, which is induced by the thermal resistance in the microscale fuel-matrix system. Previous analysis in the TREAT design summary report [6] used Hetrick’s cell model [31] to calculate the time-lag. In this study, the same analysis was repeated for both HEU and LEU fuels. Figure 5-1(b) shows the time-lag for both HEU and LEU fuels with various sized  $\text{UO}_2$  particles. There is no difference in time-lag for both types of fuels for the same particle size (the two curves overlap.) For 44  $\mu\text{m}$  diameter particles, the time-lag is  $\sim 0.57$  ms for a 5 ms reactor period. If the time-lag for HEU is acceptable, the time-lag for LEU may be considered to be acceptable, depending on other neutron-kinetics parameter values for the two cores. The impact of the time-lag will be evaluated in greater detail in future studies, including incorporation into the transient analyses to assess the effect of delayed reactivity feedback.

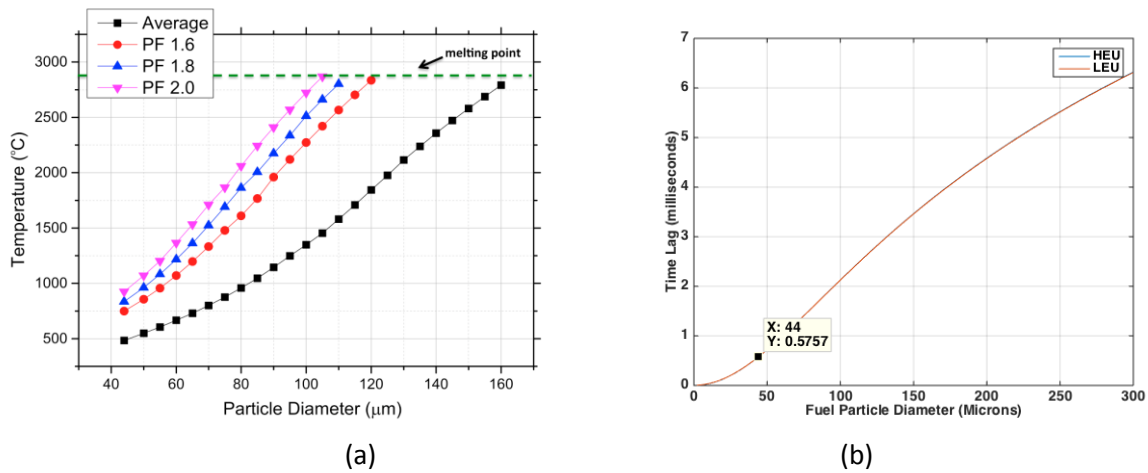


**Figure 5-1. Determination of the Upper Limit of the Fuel Particle Size in LEU TREAT Fuel: (a) The Peak Temperatures of Differently-sized Particles, at the Particle Center, during a 4.63% Reactivity Step Transient (HEU Core), and (b) Calculated Time-lag in HEU and LEU Fuels for Various Sized  $\text{UO}_2$  particles based on Hetrick’s Model [3].**

## 5.2 Determination of the Lower Limit of $\text{UO}_2$ Particle Size in LEU TREAT Fuel

The reactor-radiation induced thermal conductivity degradation of LEU TREAT fuel was computed using a semi-empirical method, which was developed based on the available experimental data of graphite-based dispersion fuels. Figure 5-2 shows the thermal conductivity degradation of LEU TREAT fuels with different sized  $\text{UO}_2$  particles after 1, 3, 10 and 40 years of core operation. The particle size referred to in this discussion is the average particle size within the fuel, and  $K_{unirr}$  and  $K_{irr}^{eff}$  are bulk thermal conductivities before and after irradiation. For average particle size larger than 10  $\mu\text{m}$ , no significant difference was observed in thermal conductivity degradation between the two types of fuels. The bulk thermal conductivity of both fuels decreased  $\sim 50\%$  after usage for 20 years and  $\sim 72\%$  after 40 years. However, if the fuel particle is smaller than 5  $\mu\text{m}$  in the LEU fuel, the thermal conductivity degradation is much more significant than that in the HEU fuel. It should be noted that the neutron radiation damage in graphite can be partially recovered by medium or high temperature ( $> 425^\circ\text{C}$ ) annealing, while fission-fragment damage is very difficult to be recovered. No appreciable recovery was found in the graphite after annealing for 12 hours at  $725^\circ\text{C}$  [33].

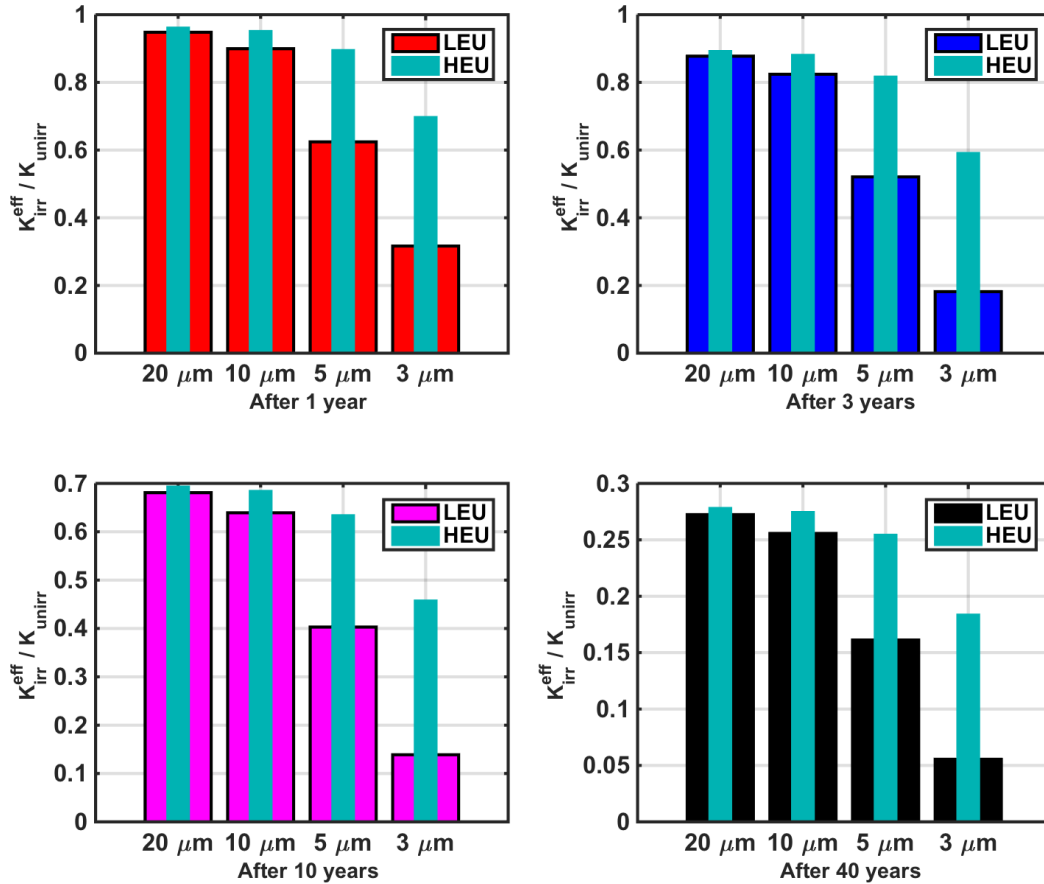


Figure 5-2. The Thermal Conductivity Degradation of LEU TREAT Fuels with Different-sized  $\text{UO}_2$  Particles after 1, 3, 10, and 40 Years; Thermal Conductivity Degradation of the HEU Fuel was calculated to provide a Comparison with the LEU Fuel

## 6 Conclusions

Neutronic and thermal hydraulic simulations were performed in order to evaluate the LEU conceptual design performance under both steady-state and transient conditions, for both normal operation and reactivity insertion accident scenarios. The operating needs of the LEU core will vary based on experiment-specific PCF values. Therefore, these studies did not consider only a single scenario but instead evaluated multiple cases corresponding to the full range of anticipated LEU core operation.

The conceptual design LEU core has PCF's that are similar to those of the HEU core. The PCF is significant for core operation because it dictates the core energy needed for a given experiment – a higher PCF indicates that less core energy is needed for the same test sample TED. The LEU PCF was 97-100% of the HEU PCF for the M8CAL reference core with the test fuel pins and low-enriched monitor wire. Due to the slightly more-thermal neutron-energy spectrum in the LEU core, the LEU-to-HEU PCF ratio decreases for very high absorbing vehicles. For the experiments evaluated in this study, the LEU core PCF values were all at least 95% of the corresponding HEU core PCF values, with the exception of a scenario with an unrealistically high-absorbing experiment vehicle (which had a PCF ratio of 91%). It was also observed

that the LEU-to-HEU core PCF ratio may decrease with increasing core temperature. A wider set of experiments and core conditions will be evaluated in the preliminary phase.

The LEU core energies needed to achieve the same test-sample TEDs as the HEU core result in core temperatures which are comparable to those in the HEU. In general, the higher density of the LEU fuel (relative to the HEU fuel) provides greater thermal mass, which allows the LEU fuel to reach lower peak fuel temperatures for the same core energy (as the HEU core). Similarly, this allows the LEU core to generate more core energy than the HEU core for the same peak fuel temperatures.

The thermal analyses found that during normal operation, cooling times are strongly affected by the coolant flow rate through the reactor. However, contact resistance between graphite blocks and hence axial conduction of heat through the fuel did not significantly prolong the cooldown. The cladding at the corner section of the assembly, where most of the cooling occurs, stayed at much lower temperatures than the side section of the cladding. Due to the non-uniform temperatures developed peripherally around the cladding, the total metal loss in the corner region remained almost two orders of magnitude lower than the section side wall section in contact with the fuel. During an accident scenario and with no air cooling, impeding axial heat conduction in the fuel will result in delayed cooling and consequently a higher metal loss after such an event.

To support the fuel manufacturing studies being performed by INL and LANL, analysis of heat transfer from the fuel  $\text{UO}_2$  to fuel graphite and of changes in fuel conductivity with burnup were also performed. These results will be evaluated along with work being performed by the INL and LANL teams in order to establish fabrication requirements regarding fuel particle size upper and lower limits.

Additional analyses were performed to characterize and evaluate the safety of the converted core. The key focus was a reassessment of the heating of the grid plate (using a more conservative method) and corresponding thermal deflection, for the core energy generated in the design basis accident. This work found that the peak temperature of the grid plate with the LEU core is roughly the same as that of the HEU core case.

The results of the work presented in this study will be evaluated in collaboration with the work which has been performed by INL and LANL for the conversion. These results will support the development of the TREAT conversion project's Conceptual Design Report deliverable.

## References

1. D. Kontogeorgakos, K. Derstine, A. Wright, T. Bauer, and J. Stevens, "Initial Neutronics Analyses for HEU to LEU Fuel Conversion of the Transient Reactor Test Facility (TREAT) at the Idaho National Laboratory", ANL/GTRI/TM-13/4, Argonne National Laboratory, June 2013.
2. H. M. Connaway, D. C. Kontogeorgakos, D. D. Papadimas, and A. E. Wright, "Overview and Current Status of Analyses of Potential LEU Design Concepts for TREAT", Argonne National Laboratory, ANL/RTR-15/9, 2015.
3. D. Papadimas and A.E. Wright, "Thermal Analysis of a TREAT Fuel Assembly," Argonne National Laboratory, ANL/GTRI/TM-14/14, 2014.
4. A. J. Brunett, T. Fei, P. S. Strons, D. D. Papadimas, E. A. Hoffman, D. C. Kontogeorgakos, H. M. Connaway, and A. E. Wright, "Preliminary Results of Ancillary Safety Analyses Supporting TREAT LEU Conversion Activities", Argonne National Laboratory, ANL/RTR/TM-15/10, 2015.
5. D. Kontogeorgakos, H. Connaway, G. Yesilyurt, and A. E. Wright, "Neutronic Analysis of the Minimum Original HEU TREAT Core", ANL/GTRI/TM-14/13, Argonne National Laboratory, April 2014.
6. G. A. Freund, P. Elias, D. R. MacFarlane, and J. D. Geier, "Design Summary Report on the Transient Reactor Test Facility (TREAT)," Argonne National Laboratory, ANL-6034, 1960.
7. Idaho National Laboratory, unpublished information, 2009.
8. W. R. Robinson and T. H. Bauer, "The M8 Power Calibration Experiment (M8CAL)", ANL-IFR-232, Argonne National Laboratory, 1994.
9. X-5 Monte Carlo Team, "MCNP – A General N-Particle Transport Code, Version 5 – Volume I: Overview and Theory", LA-UR-03-1987, Los Alamos National Laboratory, April 2003.
10. K. L. Derstine, T. H. Bauer, D. Kontogeorgakos, and A. E. Wright, "TREKIN/ANL Software Users Guide", ANL/GTRI/TM-13/2, Argonne National Laboratory, February 2013.
11. W. R. Robinson, J. R. Page, and A. E. Wright, "TREAT NPR Calibration Experiment AN-CAL", ANL/NPR-92/11, Argonne National Laboratory, 1992.
12. D. Kontogeorgakos, H. M. Connaway, and A. E. Wright, "TREAT Transient Analysis Benchmarking for the HEU Core", ANL/GTRI/TM-14/11, Argonne National Laboratory, May 2014.
13. D. C. Kontogeorgakos, H. M. Connaway, L. Derstine, A. E. Wright, "Temperature Limited Transient Calculations For The Transient Reactor Test Facility (TREAT) Using MCNP And The Point Kinetics Code TREKIN", ANS MC2015, Nashville, TN, April 19-23, 2015.
14. F. Brown, "The makssf Code with Doppler Broadening", LA-UR-06-7002, Los Alamos National Laboratory, April 2003,
15. R. E. MacFarlane, D. W. Muir, R. M. Boicourt, and A. C. Kahler, "The NJOY Nuclear Data Processing System, Version 2012", LA-UR-12-27079, Los Alamos National Laboratory, February 12, 2015.
16. COMSOL - Multiphysics Modeling and Simulation Software. Version 3.6/4.2/5.1. <http://www.comsol.com>
17. Idaho National Laboratory, "TREAT Low Enriched Uranium Fuel Design Analysis Guide", INL/EXT-15-37074, Idaho National Laboratory, November 2015.

18. D. C. Kontogeorgakos, H. M. Connaway, A. E. Wright, G. Yesilyurt, K. L. Derstine, M. D. DeHart, and S. R. Morrell, "Neutronics Analyses for an LEU Core for TREAT", Transactions of the American Nuclear Society, Vol. 111, pp. 1248-1251, Anaheim, California, November 9-13, 2014.
19. D. C. Kontogeorgakos, H. M. Connaway, and A. E. Wright, "Temperature Dependence of Test Fuel Power Density and Core Energy during Transient Reactor Test Facility (TREAT) Irradiation Experiments", Transactions of the American Nuclear Society, Vol. 112, pp. 363-366, San Antonio, Texas, June 7-11, 2015.
20. F. Brown, Los Alamos National Laboratory, private communication, 2015.
21. E. P. Luther, Los Alamos National Laboratory, private communication, 2015.
22. T. R. Allen, R. J. M. Konings and A. T. Motta, "Corrosion of Zirconium Alloys", Comprehensive Nuclear Materials, Vol 5, pp. 49-68, 2012.
23. K. Natesan and W. K. Soppet, "Air Oxidation Kinetics for Zr-Based Alloys", Argonne National Laboratory, NUREG/CR-6846, ANL-03/32, 2004.
24. C. Duriez, T. Dupont, B. Schmet and F. Enoch, "Zircaloy-4 and M5<sup>®</sup> high Temperature Oxidation and Nitriding in Air", Journal of Nuclear Materials, 380, 30-45, 2008.
25. I. J. Van Rooyen, S. R. Morell, R. K. Jamison, A. L. Crawford, H. T. Hartman III, A. E. Wright, D. C. Kontogeorgakos, D. D. Papadias, H. M. Connaway, G. Yesilyurt and E. P. Luther. "Performance and Fabrication Status of TREAT LEU Conversion Conceptual Design Concepts", RETR 2014 – 35<sup>th</sup> International Meeting on Reduced Enrichment for Research and Test Reactors.
26. ANSYS, Inc., "ANSYS, Version 16.2", ANSYS, Inc., 2015.
27. J. Cetnar, J. Wallenius, and W. Gudowski, "MCB: A Continuous Energy Monte Carlo BurnupSimulation Code, MCB User Manual - V1.0," KTH Royal Institute of Technology, Retrieved from <http://www.neutron.kth.se/research/MCB/MCBmanual.shtml>, 2015.
28. Z. Xu and P. Hejzlar, "MCODE Version 2.2: An MCNP-ORIGEN DEpletion Program", Massachusetts Institute of Technology, MIT-NFC-TR-104, 2008.
29. A. G. Croff, "A User's Manual for the ORIGEN2 Computer Code", Oak Ridge National Laboratory, ORNL/TM-7175, 1980.
30. K. Mo, D. Yun, A. M. Yacout, A. E. Wright, Heat transfer simulations of the UO<sub>2</sub> particle-graphite system in TREAT fuel, Nucl Eng Des, 293 (2015) 313-322.
31. D. L. Hetrick, The Effect of Fuel Particle Size on the Transient Behavior of a Homogeneous Graphite Reactor, NAA-SR-210, North American Aviation, 1953.
32. L. P. Hunter, "Effect of fission recoil fragments on the thermal conductivity of graphite," J. Appl. Phys., 30 (1959), p. 1969.
33. W. P. Eatherly, M. Janes, R.L. Mansfield, B.G. Bourdeau, R.A. Meyer, Physical Properties of Graphite Materials for Special Nuclear Applications, Second United Nations International Conference of the Peaceful Uses of Atomic Energy, 1958.

## Appendix A. Comparison of Temperature-dependent Cross Section Generation with MAKXSf and NJOY2012

The evaluation of the temperature reactivity feedback of the LEU core (as a function of core energy) requires the simulation of the core using temperature-dependent cross sections. In previous analysis these cross-sections were generated using the MCNP utility program MAKXSf, but in the current analysis cross-sections produced with NJOY2012 were used. To support this change, the temperature-dependent cross sections developed with MAKXSf and NJOY2012 were first compared.

MAKXSf uses an equal energy mesh for the interpolation of  $S(\alpha,\beta)$  data at user defined temperatures. The ENDF/B-VII  $S(\alpha,\beta)$  files were constructed by the MCNP developers with the newer version of NJOY, with some data thinning of the elastic scattering data. As a result, the energy meshes in the ENDF/B-VII files generally have different energy meshes for different temperatures, and consequently a different interpolation scheme is needed in MAKXSf [20]. This results in incorrect interpolations for the required temperatures. To demonstrate this, the  $S(\alpha,\beta)$  cross sections at 450K were produced with MAKXSf and NJOY2012 and were compared with the 400K and 500K data that are available in the ENDF/B-VII library for carbon.

The total, elastic, and inelastic cross-sections produced with MAKXSf at the temperature of 450K were compared with the ENDF/B-VII cross sections at 400K and 500K (see Figure A-1, Figure A-2, and Figure A-3). The cross-sections at 450K should lie between the cross-sections at 400K and 500K. However, the elastic cross-sections produced by MAKXSf at 450K are higher than the ENDF/B-VII data at 500K for lower neutron energies.

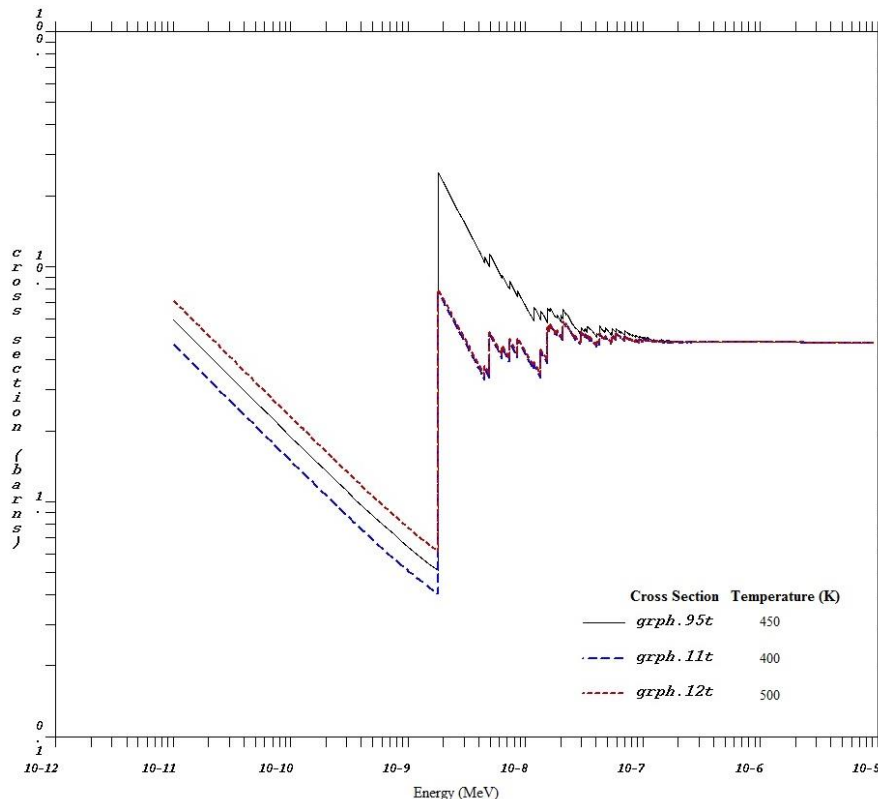


Figure A-1. Carbon  $S(\alpha,\beta)$  Total Cross Section at 400K and 500K from ENDF/B-VII (grph.11t and grph.12t) and at 450K produced by MAKXSf (grph.95t).

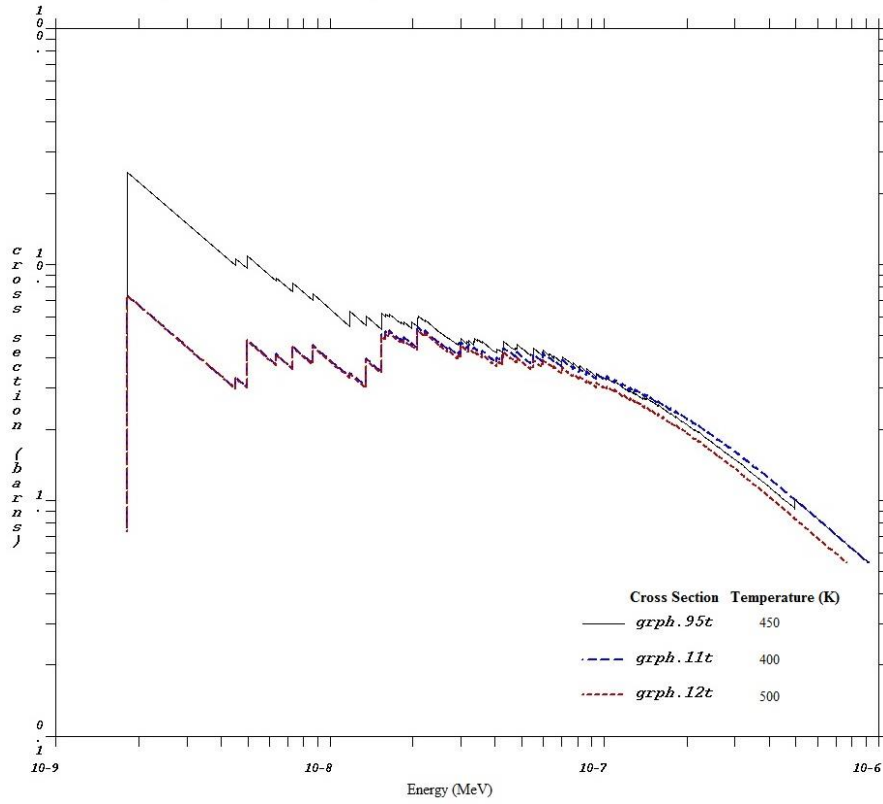


Figure A-2. Carbon  $S(\alpha, \beta)$  Elastic Cross Section at 400K and 500K from ENDF/B-VII (*grph.11t* and *grph.12t*) and at 450K produced by MAKXSF (*grph.95t*).

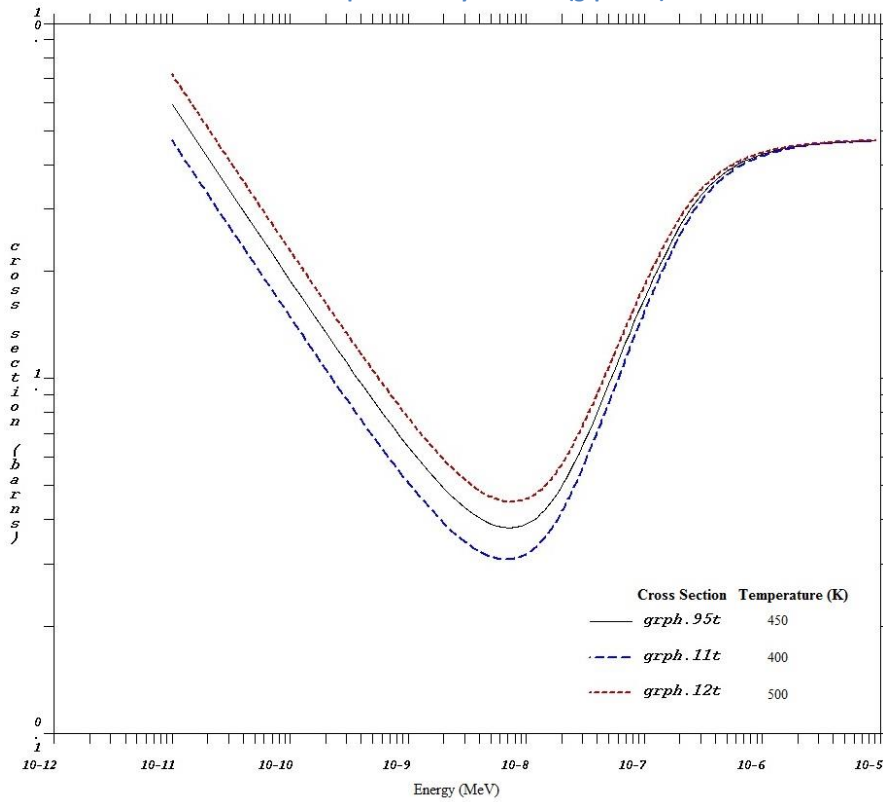


Figure A-3. Carbon  $S(\alpha, \beta)$  Inelastic Cross Section at 400K and 500K from ENDF/B-VII (*grph.11t* and *grph.12t*) and at 450K produced by MAKXSF (*grph.95t*).

This process was then repeated using NJOY2012 - the total, elastic, and inelastic cross sections at 450K that were produced with NJOY2012 were compared with the ENDF/B-VIII cross sections at 400K and 500K (Figure A-4, Figure A-5, and Figure A-6). The NJOY2012 cross-sections at 450K correctly lie between the ENDF/B-VII cross sections at 400K and 500K.

The impact of the differences in the MAKXSF- and NJOY2012-generated cross-sections was evaluated, as described below.

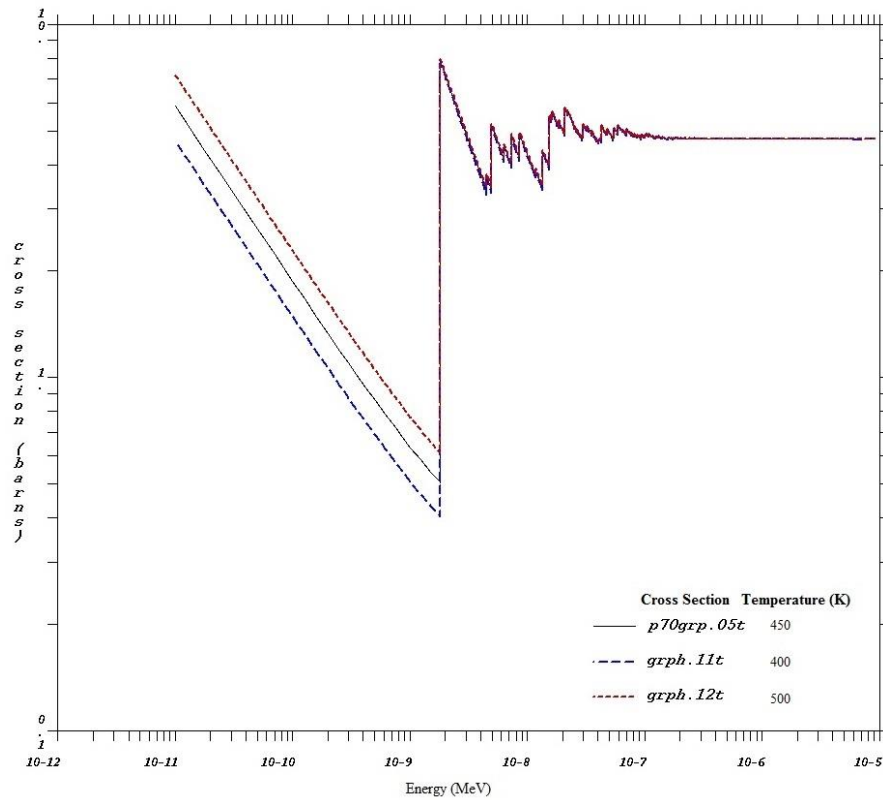


Figure A-4. Carbon  $S(\alpha,\beta)$  Total Cross Section at 400K and 500K from ENDF/B-VII (*grph.11t* and *grph.12t*) and at 450K produced by NJOY2012 (*p70grp.05t*).

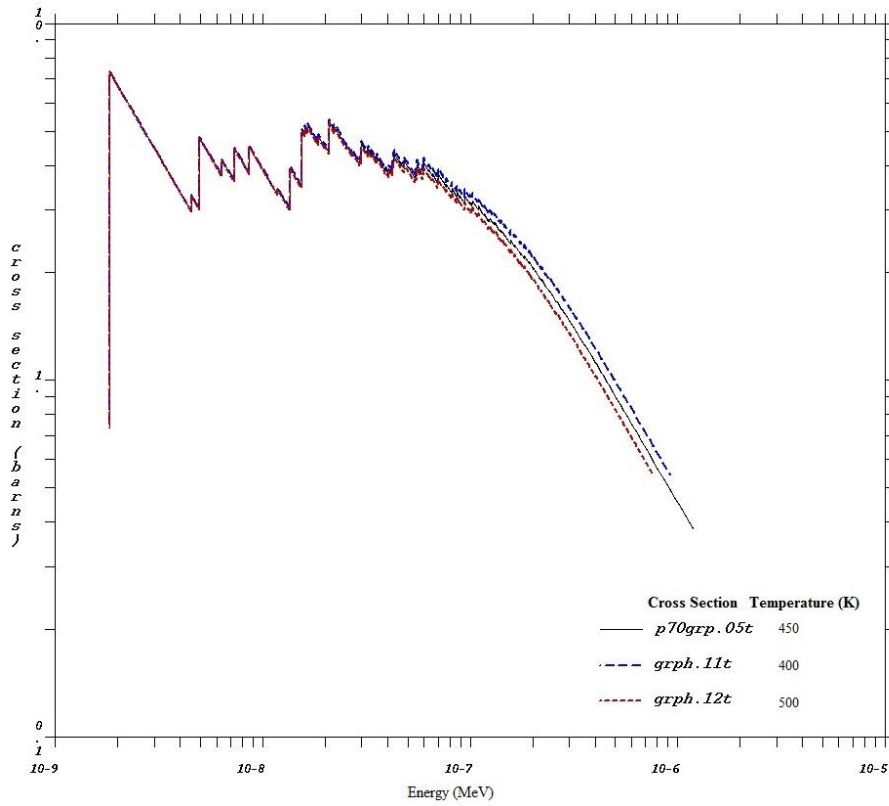


Figure A-5. Carbon S( $\alpha,\beta$ ) Elastic Cross Section at 400K and 500K from ENDF/B-VII (grph.11t and grph.12t) and at 450K produced by NJOY2012 (p70grp.05t).

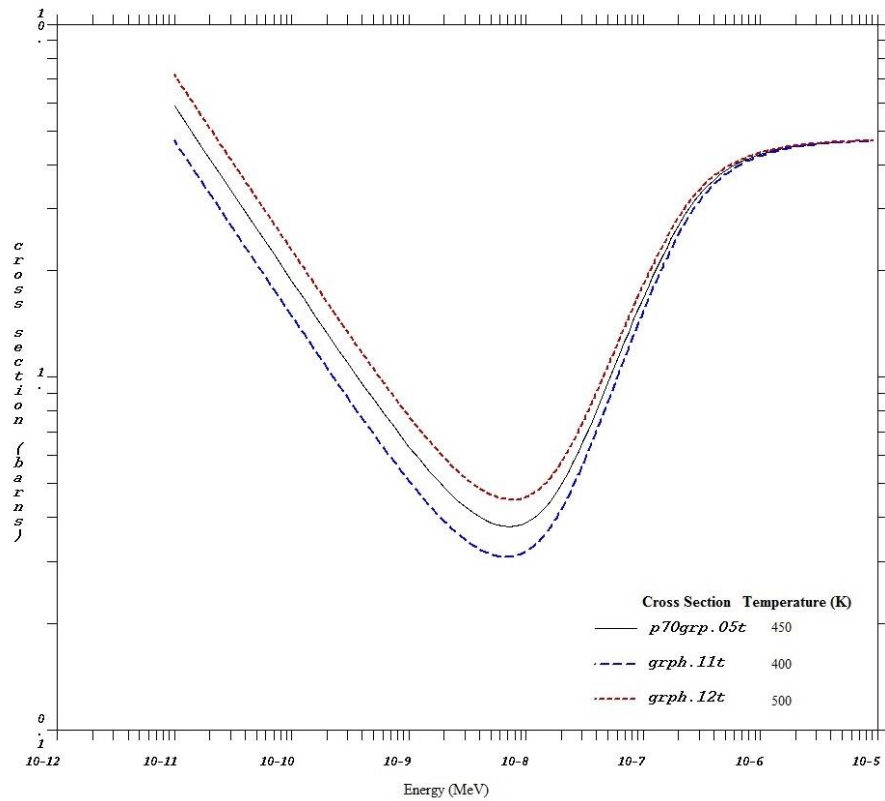


Figure A-6. Carbon S( $\alpha,\beta$ ) Inelastic Cross Section at 400K and 500K from ENDF/B-VII (grph.11t and grph.12t) and at 450K produced by NJOY2012 (p70grp.05t).

To evaluate the impact of the cross-section differences, the temperature reactivity feedback calculations for the LEU core were repeated using both the NJOY2012- and MAKXSf-generated cross-section data. Starting from an initial (cold-core) uniform core temperature distribution of 293.6K, the final fuel assembly temperatures and core temperature distributions were calculated for a series of total core energy depositions ranging from 100 MJ to a maximum of 5000 MJ. For each of these energy steps, the temperature-dependent effective multiplication factor ( $k_{eff}$ ) was calculated using temperature-dependent cross sections (for U-235, U-238, carbon and the associated  $S(\alpha,\beta)$ ) produced with MAKXSf and NJOY2012. Results are presented in Table A-1. The statistical standard deviation of the MCNP-calculated  $k_{eff}$  values was 0.00005 (5 pcm).

**Table A-1. Effective Multiplication Factor ( $k_{eff}$ ) Calculation using Temperature-Dependent Cross Sections Produced with MAKXSf and NJOY2012;  $k_{eff}$  was calculated with MCNP with a Standard Deviation of 5pcm.**

Core Energy (MJ)	$k_{eff}$ w/ MAKXSf	$k_{eff}$ w/ NJOY2012	MAKXSf-NJOY2012 Difference (pcm)
100	1.02661	1.02652	+9
200	1.02192	1.02203	-11
300	1.01732	1.01892	-160
400	1.01329	1.01384	-55
500	1.00960	1.01006	-46
1000	0.99390	0.99454	-64
2000	0.97067	0.97139	-72
3000	0.9531	0.95369	-59
4000	0.93823	0.93908	-85
5000	0.92606	0.93035	-429

The temperature reactivity feedback was calculated as the reactivity change,  $(\frac{1}{k_{HOT}} - \frac{1}{k_{COLD}})$ , where  $k_{cold}$  refers to the cold-core  $k_{eff}$ , which was calculated using the available ENDF/B-VII cross sections at 293.6K. The results are shown in Table A-2. The temperature reactivity feedback values calculated with the NJOY2012-produced cross sections are lower (except for the value corresponding to the 100 MJ total core energy) than those calculated with the MAKXSf-produced cross sections, with a NJOY2012/MAKXSf ratio ranging from 0.90 to 0.99.

Table A-2. Temperature Reactivity Feedback ( $\Delta k/k$ ) with Temperature Dependent Cross Sections Produced with makxsf and NJOY2012.

Core Energy (MJ)	Temperature Reactivity		NJOY2012/MAKXS F
	$\frac{1}{k_{COLD}} - \frac{1}{k_{HOT}}$ w/ MAKXS F	$\frac{1}{k_{COLD}} - \frac{1}{k_{HOT}}$ w/ NJOY2012	
100	-0.60%	-0.61%	1.01
200	-1.05%	-1.04%	0.99
300	-1.49%	-1.33%	0.90
400	-1.88%	-1.83%	0.97
500	-2.24%	-2.20%	0.98
1000	-3.81%	-3.74%	0.98
2000	-6.21%	-6.14%	0.99
3000	-8.11%	-8.05%	0.99
4000	-9.78%	-9.68%	0.99
5000	-11.18%	-10.68%	0.96

Using the above results, the effect of the different temperature reactivity feedback input datasets on the resultant peak core temperatures evaluated by TREKIN was studied by simulating the three historic temperature-limited transients performed in the M8CAL TREAT HEU core. TREKIN does not solve the thermal-hydraulic equations to evaluate temperature; peak temperatures are reported by the code for the TREKIN-calculated core energies, using the user-provided dataset of peak fuel temperature as a function of the total core energy. The results of the TREKIN calculations and the comparison with the measurements (as reported in the core operations worksheets) are summarized in Table A-3.

The temperature reactivity feedback calculated with the NJOY2012-produced cross-sections was lower than that which was calculated with the MAKXS F-produced cross sections. Therefore with the NJOY2012 dataset, TREKIN reported higher peak power and total core energy, and consequently higher peak core temperatures. Specifically TREKIN reports 2% higher peak core temperatures when using the NJOY2012 cross sections.

Table A-3. TREKIN-calculated Peak Core Power, Total Core Energy and Peak Core Temperature using the Temperature Reactivity Feedback with MAKXSf- and NJOY2012-Produced Cross-Sections

Parameter	Measured	TREKIN w/ MAKXSf	TREKIN w/ NJOY2012	MAKXSf/Measured	NJOY2012/Measured
<b><i>#2855 Transient (1.81% reactivity insertion)</i></b>					
Peak Power (MW)	1281	1357	1366	1.06	1.07
Total Energy (MJ)	792	784	815	0.99	1.03
Peak Core Temp (°C)	236	250	257	1.06	1.09
<b><i>#2856 Transient (3.02% reactivity insertion)</i></b>					
Peak Power (MW)	6171	6308	6579	1.02	1.07
Total Energy (MJ)	1572	1536	1577	0.98	1.00
Peak Core Temp (°C)	378	404	412	1.07	1.09
<b><i>#2857 Transient (3.85% reactivity insertion)</i></b>					
Peak Power (MW)	12493	12674	13184	1.01	1.06
Total Energy (MJ)	2265	2167	2217	0.96	0.98
Peak Core Temp (°C)	488	518	527	1.06	1.08

## Appendix B. Steady-state Thermal Hydraulic Analysis

In support of lifecycle corrosion analysis, heating and cooling time histories with corresponding cladding corrosion have been calculated during constant power operation. Analyses considered the following cases:

- 1) Constant power of 120 kW during 2,4,6 and 10 h followed by cooling to ambient temperature
- 2) Air cooling through the reactor using one or two blowers in operation (3000/6000 cfm)
- 3) Contact resistance between graphite blocks varied from 0 to  $5 \times 10^{-3} \text{ m}^2 \text{ K W}^{-1}$
- 4) Ratio of hottest fuel assembly power to total core power: 0.45%

Figure B-1 shows peak fuel temperatures as a function of time during constant power operation. The case shown is when using one blower to cool the reactor (3000 cfm). Peak fuel temperatures gradually increase with time and reach steady-state temperatures of  $\sim 260^\circ\text{C}$  after 10 hours of constant-power operation. Increasing the contact resistance between fuel blocks to a conservative value of  $5 \times 10^{-3} \text{ m}^2 \text{ K W}^{-1}$  causes the steady-state temperatures to increase by approximately  $25^\circ\text{C}$ .

As with the power transients, the trends of the corrosion of the cladding during steady-power operation remain the same, although the magnitude is lower. Most of the corrosion of the cladding occurs in the fuel section of the assembly (fuel), see Figure B-2. The metal loss peaks near the fuel mid-plane and is rapidly reduced to virtually zero near the reflector region. Increasing the contact resistance to  $5 \times 10^{-3} \text{ m}^2 \text{ K W}^{-1}$  more than doubles the amount of corrosion of the cladding. Temperatures are highest at the section of the cladding in contact with fuel and start to decrease as the cooling channel region (corner section) is approached. The total metal loss in the corner region remains over two orders of magnitude lower than in the section in contact with the fuel, Figure B-3.

Figure B-4 summarizes the peak metal loss of the cladding during constant-power operations as a function of coolant air flow rate, time at constant power operation and contact resistance. Time and temperature will naturally affect the cumulative corrosion of the cladding. Corrosion during constant-power operation is more sensitive to variations in flow and contact resistance; this is especially true during longer constant-power operation (6-10 hours). At longer times, especially near steady-state operation, convection and axial conduction both contribute to reduce the fuel temperature. Impeding conductivity of the fuel increases the fuel temperature and consequently the cladding temperature.

While corrosion during constant power is sensitive to fuel conductivity, the magnitude of corrosion needs to be put in perspective. Given the most extreme case (10 hours of operation at 120 kW, 3000 cfm of air-cooling through the reactor and conservative contact resistance between fuel blocks) the maximum metal loss is on the order of  $\sim 1 \times 10^{-6}$  mils. Assuming a fuel assembly life-cycle of 40 years, the amount of constant power operation is unlikely to contribute much to the total corrosion of the cladding.

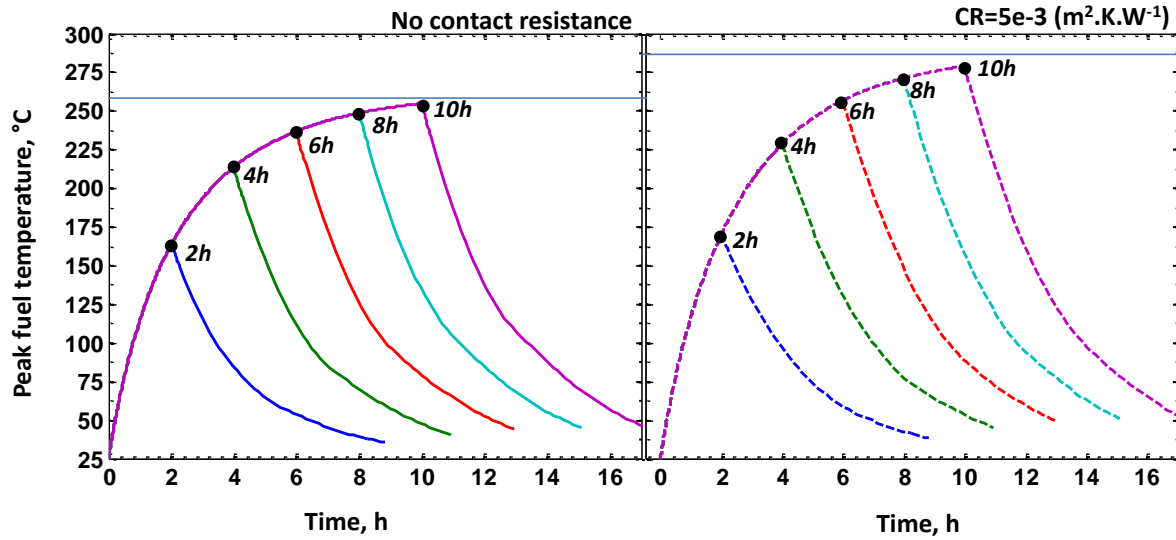


Figure B-1. Constant power operation (120 kW) as function of time followed by cooling to near ambient temperature. Cases shown with 3000 cfm air cooling through the reactor. Left plot: no contact resistance. Right plot: contact resistance (CR) between graphite blocks of  $5e-3 \text{ m}^2 \text{ K W}^{-1}$

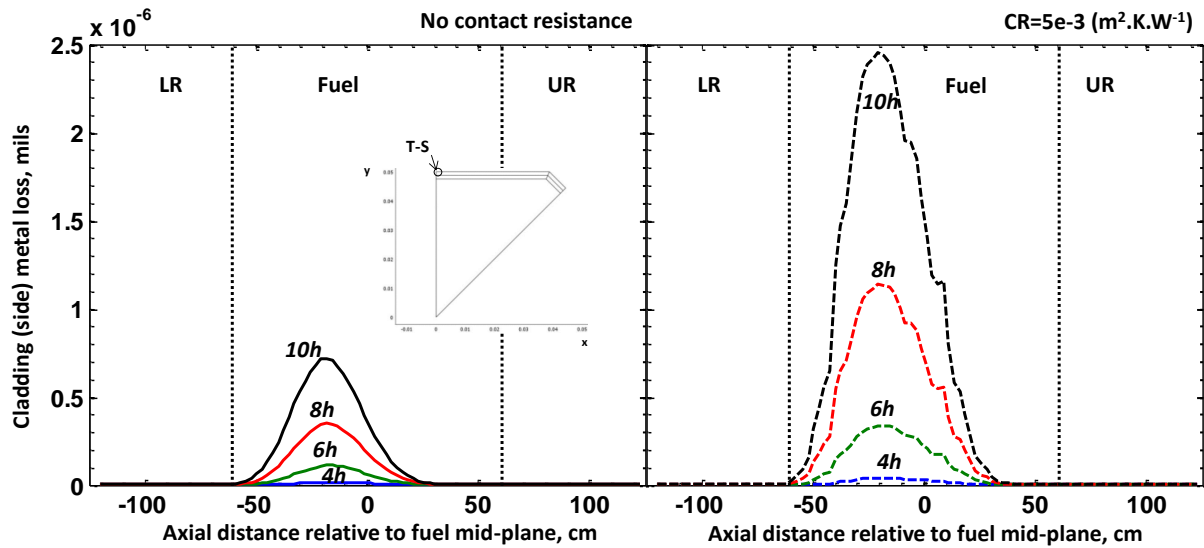


Figure B-2. Axial Variation of Cladding (T-S) Metal loss as Function of Peak Fuel Temperature and Contact Resistance (as Indicated above Axis, Numerical Values of Metal Loss are Multiplied by  $1E-6$ ; Cooling to Ambient Conditions Achieved with One Blower in Operation (3000 cfm).

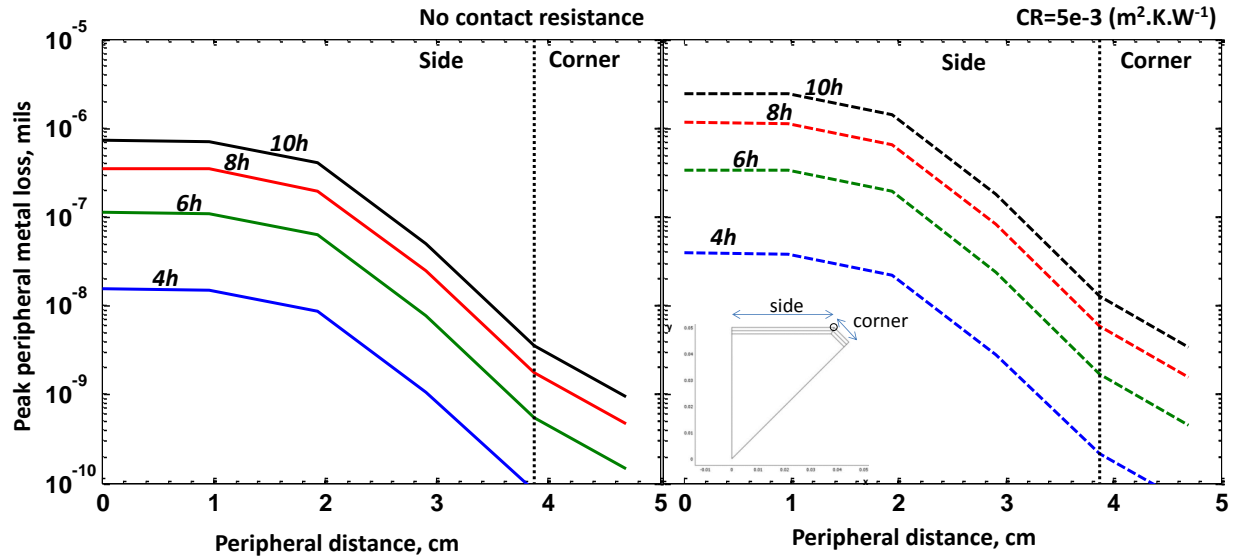


Figure B-3. Cross-sectional Metal Loss of the cladding near the fuel mid-plane. Total metal loss is shown as a function of time during constant power operation. Results shown when using 3000 cfm of air cooling through the reactor.

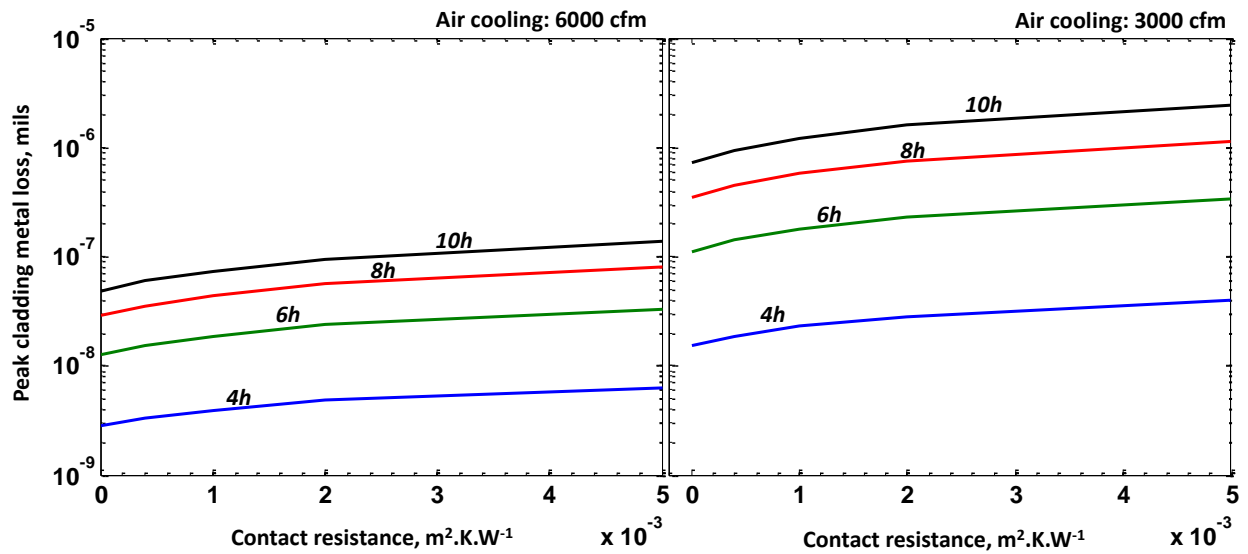


Figure B-4. Maximum metal loss of the cladding during constant power operation. Effect of air flow through the reactor and contact resistance.



## **Nuclear Engineering Division**

Argonne National Laboratory  
9700 South Cass Avenue, Bldg. 208  
Argonne, IL 60439-4842

[www.anl.gov](http://www.anl.gov)



Argonne National Laboratory is a U.S. Department of Energy  
laboratory managed by UChicago Argonne, LLC